The Thesis Committee for Lindsay A. Hull
Certifies that this is the approved version of the following thesis:

Experimental Testing of a Steel Gravity Frame with a Composite Floor under Interior Column Loss

APPROVED BY
SUPERVISING COMMITTEE:

Michael Engelhardt, Supervisor

Eric Williamson

Experimental Testing of a Steel Gravity Frame with a Composite Floor under Interior Column Loss

by

Lindsay A. Hull, BSCE

Thesis

Presented to the Faculty of the Graduate School of

The University of Texas at Austin

in Partial Fulfillment

of the Requirements

for the Degree of

Master of Science in Engineering

The University of Texas at Austin

May 2013

Acknowledgements

This material is based upon work supported by the Science & Technology Directorate, U.S. Department of Homeland Security under Award Number: 2010-ST-108-000014. The author thanks the Department of Homeland Security (DHS) for their support of this research program. The views and conclusions contained in this document are those of the author and should not be interpreted as necessarily representing official policies, either expressed or implied, of the U.S. Department of Homeland Security.

Special thanks go to Dr. Engelhardt for all of his support over the past two years. Thank you for inviting me to participate in this research project and for encouraging my involvement with the first year engineering course as a teaching assistant. I've learned so much from these two challenges and thoroughly enjoyed working with you. Thanks also to Dr. Williamson for his helpful guidance. Your leadership and knowledge have been invaluable to the progress of this project.

Thank you to the rest of the research team: Michalis Hadjioannou, Sean Donahue, and George Moutsanidis. I'm grateful for all of your hard work and for your persistence in finally forcing the specimen to failure. Thanks to all of the staff at Ferguson Lab, particularly Eric Schell and Mike Wason for teaching me how to handle the finicky data acquisition equipment.

Finally, thanks to my family and all my friends, here in Austin and across the country. Thank you for believing in me and for keeping me mostly sane these past two years. I couldn't have gotten this far without your love and humor.

May 3, 2013

Abstract

Experimental Testing of a Steel Gravity Frame with a Composite Floor under Interior Column Loss

Lindsay A. Hull, MSE

The University of Texas at Austin, 2013

Supervisor: Michael Engelhardt

Progressive collapse research aims to characterize and quantify the behavior of different structural systems in events of extreme local damage caused by bombings to improve the performance of targeted structures and to protect occupants. The focus of the research program described herein is the performance of steel gravity frame structures with composite floor systems in column loss scenarios. The goal of the project is to contribute to the development of rational design guidelines for progressive collapse resistance and to assess any potential weaknesses in current design standards.

This thesis presents the results of a series of tests performed on a steel frame structure with simple framing connections and a composite floor slab under interior

column loss. The specimen was designed and constructed in accordance with typical design practices and was subjected to increasing uniform floor loads after static removal of the central column. No significant structural damage was observed up to a load equivalent to the ultimate gravity design load. Further testing was performed after the deliberate reduction of the capacity of the steel framing connections, ultimately resulting in total collapse of the specimen.

Table of Contents

List of Tables

List of Figures

CHAPTER 1

Introduction

1.1 OVERVIEW

This thesis describes the results of one testing sequence performed as part of a larger research program on progressive collapse resistance of buildings. The program was conducted by a team including researchers at The University of Texas at Austin, Imperial College, and the consulting firms of Walter P. Moore, and Protection Engineering Consultants. The primary focus of the research was an experimental and analytical investigation of the progressive collapse resistance of steel gravity frames with composite floor systems.

Progressive collapse is defined as the disproportionate failure of a structure after localized damage by the American Society of Civil Engineers Standard *Minimum Design Loads for Buildings and Other Structures* (ASCE 7-10). The ability of a structure to redistribute gravity loads after the damage of individual structural elements is a measure of its structural integrity. Progressive collapse is considered an extreme event, much like an earthquake, where the design objective is protection of the occupants rather than prevention of structural damage. Reserve strength of steel frame structures against progressive collapse can come from several sources that include intrinsic conservatism in the initial design, additional strength from serviceability-based design, capabilities for inelastic behavior and redistribution of internal forces, and development of catenary

action in beams and membrane floor system, among others. Material and geometric nonlinearity and dynamic behavior must be assessed for an accurate estimate of progressive collapse resistance.

The demand for deeper understanding of progressive collapse resistance results from historical events that demonstrate the consequences of poor structural integrity. In the UK, the collapse of the Ronan Point Apartments in 1968 after a gas stove explosion prompted an industry-wide discussion of progressive collapse. After investigation of the structural deficiencies of Ronan Point Apartments and significant research into the subject of progressive collapse, the British government adopted minimum guidelines for structural robustness and blast resistance (Pearson 2005). In 1993, the Oklahoma City bombing destroyed critical structural elements of the Alfred P. Murrah building, resulting in total collapse of a large portion of the structure. Engineers estimate that a majority of the fatalities in the bombing resulted from the building collapse (Corley 1998). The destruction of the World Trade Center towers on September 11, 2001, raised questions in the structural engineering community of how such an event could be mitigated (Newland 2002). These events have illustrated the need for engineers to consider how to improve structural performance after extreme occurrences of localized damage.

The test presented in this thesis consisted of pseudo-static interior column removal and uniform distributed loading of a steel frame with a composite floor designed at approximately half-scale. All steel framing connections were simple; shear tabs and double angles were used. The floor system consisted of corrugated steel decking with a

lightly reinforced concrete slab with shear studs provided along the lengths of the beams for partial composite action. Four separate tests were carried out on a single specimen until complete structural collapse was achieved.

1.2 RESEARCH PROJECT OBJECTIVES

The larger progressive collapse project, of which this thesis is a part, had a number of objectives and tasks. The first task was a literature review of previous research on progressive collapse of steel structures as well as past work on the development of membrane action in floor systems.

A second major task was developing and carrying out an experimental testing program to assess the progressive collapse resistance of composite floor systems in steel gravity frame structures. The purpose of the testing program was to observe the system behavior and capacity in the occurrence of column loss. The experimenters hoped to characterize the resistance mechanism and to identify critical elements responsible for ultimate failure.

The test frame was designed to accommodate a 2-bay by 2-bay composite floor system with structural steel framing for static column removal in multiple configurations. The construction of this test frame allows for testing of interior columns, perimeter columns along each axis, and corner columns.

A third major task in this project is the development of computational models to study progressive collapse in steel gravity framing. This includes the development of

detailed three-dimensional finite element models. The experimental program was intended to provide data to validate the models. The validated models can then be used to explore a wider range of issues related to the behavior of steel gravity framing during column loss scenarios.

The computational portion of the research project, as led by Imperial College, consists of the development of sophisticated finite element models that successfully predict the behavior observed in physical testing. This process is iterative; computer models are used to estimate the expected behavior of the test specimens and then modified based on the data collected. Individual components of the structure, such as the structural steel connections, are also modeled under progressive collapse loading scenarios and evaluated based on available experimental data.

The final goal of this project is to contribute to a broader understanding of progressive collapse phenomena in steel gravity framing, and to develop improved analytical tools, modeling criteria, and design approaches for progressive collapse that will lead to safer buildings.

The results of various portions and tasks of this larger program will be documented in a series of MS theses and PhD dissertations in the near future. This thesis documents a part of the experimental portion of this project.

1.3 RECENT RESEARCH ON PROGRESSIVE COLLAPSE OF STEEL GRAVITY FRAMING SYSTEMS

1.3.1 General

Several past studies have investigated issues related to the behavior of steel gravity framing under column loss scenarios. Issues that have been studied include the behavior of steel beam-to-column simple framing connections subjected to forces and deformations resulting from column loss, development of catenary action in beams, development of membrane action in floor systems, and others. Some key past studies are briefly described below.

1.3.1 Computational Studies

Substantial computational modeling has been performed investigating the behavior of steel frame structures in progressive collapse. Izzudin et al. (2008) used an energy-based approach to determine the structural response in a nonlinear static analysis and then to compute the dynamic magnification. The system failure was defined by the failure of a single connection based on the assessment of the ductility demand. Sadek et al. (2008) and Main and Sadek (2012) conducted an extensive series of computational studies on progressive collapse of steel gravity systems. Analysis of prototypical structural designs indicated that the systems have significant reserve strength but are prone to failure under the full progressive collapse design load, particularly in cases without lateral restraint from neighboring bays. The failure mode of the steel framing

connections was found to be particularly critical in determining the system ductility. The ultimate failure criterion was defined by the erosion of the shell elements representing the floor slab.

Alashker et al. (2010) performed a computational study investigating the progressive collapse resistance of steel frame structures with composite floor systems and shear tab connections. Particular attention was given to the impact of dynamic loading effects and the contribution of different elements to the system capacity. This research built upon previous work accomplished by Sadek et al. (2008), Foley et al. (2006) and Astaneh-Asl et al. (2001). Models were validated against experimental data from a variety of projects that provided data on certain components of the specimen, such as the concrete slab behavior.

The study by Alashker et al. (2010) concluded that collapse would be triggered by failure of the steel decking. The response of the structure to column push-down loading and uniform floor loading were compared. Under uniform floor loading, the structure was able to develop greater resistance after the failure of the steel framing connections through membrane action. As a result, the most significant contribution to resistance was the thickness of the steel decking. Modeling of both static and dynamic column loss resulted in a calculated dynamic impact factor of approximately 1.3.

1.3.2 Experimental Studies

Studies carried out by Chen et al. at Tongji University in Shanghai (2012) included physical testing of a two-story steel frame structure with a composite floor system in accordance with Chinese building codes and finite element modeling of the observed behavior. The experiment consisted of dynamic removal of a perimeter column. The structure was preloaded and the beams and columns were instrumented with strain gages to measure the change in load distribution after the column removal. The structure did not collapse during testing and strain gage data suggests that no yielding occurred in the steel framing.

Two nonlinear dynamic finite element models were developed for the test specimen: one with bare steel framing and one incorporating the concrete floor slab and steel decking. The first model overestimated the observed deformation by a very large margin while the second one more closely matched the experimental results. Although this test did not provide any guidance on the controlling failure mechanism, it clearly demonstrated the importance of the floor system in progressive collapse resistance.

In an experiment carried out by Song and Sezen at Ohio State University (2009), four perimeter columns were sequentially removed from a steel frame structure without causing collapse. The building was constructed in 1951. Elastic-static and dynamic nonlinear analyses of the demand to capacity ratio of each element indicated that the majority of the structure met the requirements of the General Services Administration

(GSA) published in 2003. No additional loading was performed and the behavior of the floor system was not investigated.

1.3.3 Summary

Significant work has been done in the field of computational analysis for progressive collapse behavior, but little experimental data exists to validate the modeling results. In particular, researchers have made different assumptions of the failure criteria for the system and the action of the composite floor slab within the structure. The actual distribution of load, development of membrane action, and collapse sequence are largely untested.

1.4 CURRENT DESIGN METHODOLOGY (2009)

The Unified Facilities Criteria [Department of Defense (DOD) 2009] provides a set of design guidelines to mitigate progressive collapse for new construction. Three different methods are presented for use in different risk levels and with varying levels of computational demand.

The Tie Force method does not explicitly model the load bearing mechanism of a structure after column removal, but prescribes a minimum level of reserve strength to transfer loads to undamaged areas. The implied mechanism in the Tie Force method is catenary and tension membrane resistance. The UFC 2009 has been updated to allow engineers to include tying forces in the floor system, acknowledging the significant level of resistance available in membrane action. Horizontal tie forces can only be carried in

beams and girders if the members and their connections can be shown to withstand a nominal rotation.

In the Alternate Path method defined in the UFC, the structure may be analyzed for set progressive collapse scenarios using a linear static model, a nonlinear static model, or a nonlinear dynamic model. In this method, structural components are designated as either force or deformation controlled. Force controlled elements are limited by the lower bound material strength. Deformation controlled elements are limited by a maximum allowable inelastic deformation before failure. A computer analysis is performed for each selected localized damage scenario, such as the interior column loss investigated in this thesis. All components must survive the column removal without exceeding their acceptance criteria.

Elements designated as secondary components may be excluded from models but must be checked for allowable deformation to prevent fracture. The deformation criteria for secondary elements are less stringent because they are assumed to carry no load and must only provide continuity.

A dynamic increase factor is used to account for the amplified forces experienced in the structure during dynamic response. The structure must be able to equilibrate after reaching its maximum deflected position. The increase factors provided in the UFC design code are derived from computer modeling that compares capacities observed under dynamic and static column removal and are directly related to the inelastic

behavior of the material. For steel frame structures, the dynamic increase factor is generally around 1.3 to 1.5.

The third design method allowed by the UFC guidelines is Enhanced Local Resistance. Critical structural elements are explicitly designed for extreme load events such as blast or vehicle impact. This research program is only concerned with the structural behavior after a critical element has been destroyed.

1.5 THESIS SCOPE AND ORGANIZATION

The scope of this thesis consists of documentation of the construction and testing of a single specimen within the research program described above. The associated work was carried out at The University of Texas at Austin from January 2012 to May 2013. A 2-bay by 2-bay specimen was constructed with typical structural steel framing and composite floor design. The test consisted of pseudo-static removal of the interior column and uniform distributed floor loading.

Four separate tests of the specimen were completed before the specimen collapsed. The structure experienced little to no damage in the first test after the loading capacity of the experimental setup had been reached. The first test also experienced significant problems with data collection. The loading was repeated in a second test and the specimen again sustained the maximum applicable load without failure. The third and fourth tests incorporated weakening of the steel framing connections for the purpose of

inducing greater deformation in the structure. Total structural collapse occurred during the fourth test.

Chapter two contains an account of the experimental set up and design. A detailed description of the test specimen, including the structural steel framing and connections, the composite floor system, and the external reaction frame, is provided. The loading system and instrumentation plan are also documented here.

The procedures and observations made during the course of testing are described in chapter three. This chapter contains important information defining the state of the specimen at different stages of testing and the measurements being recorded by the instrumentation.

Chapter four presents all data collected during the four tests leading up to the structural collapse. A load-deflection curve was constructed from the data in each test with respect to the displacement of the column being removed. Additional data was used to evaluate the rigid body rotation of the steel members, and the flexural stress in the girders and the restraining frame. Photographs of damage sustained by the test specimen during the collapse are also included here.

The purpose of this thesis is to provide clear documentation of the methodology used in this test and the observed results. Preliminary evaluation of the behavior recorded during this test is included. More detailed modeling and analysis of the test results is

beyond the scope of this thesis and will be included in subsequent theses and dissertations on this project.

CHAPTER 2

Experimental Setup and Specimen Design

2.1 TEST SPECIMEN DESIGN

This chapter provides a description of the test specimen, the experimental setup, the loading system, and instrumentation. Further details of the specimen design and experimental setup are also provided in an upcoming thesis by Donahue (2013).

The test specimen geometry was defined by practical constraints of the experimental set up. A full scale structure would have exceeded the available budget for this project. The research team chose to design a steel gravity frame structure with approximately 15-foot bays and secondary floor beams at the midspan of each bay. Corrugated steel decking with a cast in place slab was designed for composite behavior with the structural steel members. Lateral restraint and system stability was provided by an external test frame.

The following terminology will be used to define different components of the structure throughout this thesis:

Primary beams: horizontal members framing east to west supported directly on columns

Secondary beams: horizontal members (east to west) framing into girders

Girders: horizontal members framing north to south, supported directly on columns and supporting secondary beams

Ring beam: large, heavy beams installed around the outside of the frame to provide vertical and lateral restraint to floor system

Test specimen: consisting of the primary and secondary beams, the girders, the column, and the composite floor system

Test frame: consisting of the ring beam, the outer columns, and additional structural components designed to provide system stability

The specimen was designed to strength and serviceability requirements at the given geometry rather than being scaled down directly from a typical size. The following loads and load combinations were considered in the specimen design and the tests.

Table 1: Test Specimen Design Loads

Dead Load	DL	75 psf
Live Load	LL	50 psf
Ultimate Gravity Load	1.6LL + 1.2DL	170 psf
Progressive Collapse Design Load	0.5LL + 1.2DL	115 psf
Amplified PC Design Load	1.33(0.5LL + 1.2DL)	155 psf

The progressive collapse design loads are listed above to provide a comparison point with the measured capacity of the structure during testing. No explicit design or detailing for progressive collapse resistance was performed for this test specimen.

Engineers at Walter P. Moore assisted in the design process by providing a prototype building design using their office's standard details. Further detail on the criteria and procedures used in design can be found in the upcoming thesis by Donahue (2013).

2.1.1 Structural Steel Framing Members

All test specimen framing members were specified to be of ASTM A992 steel. The beams, girders, and columns were all designed with wide flange structural steel members.

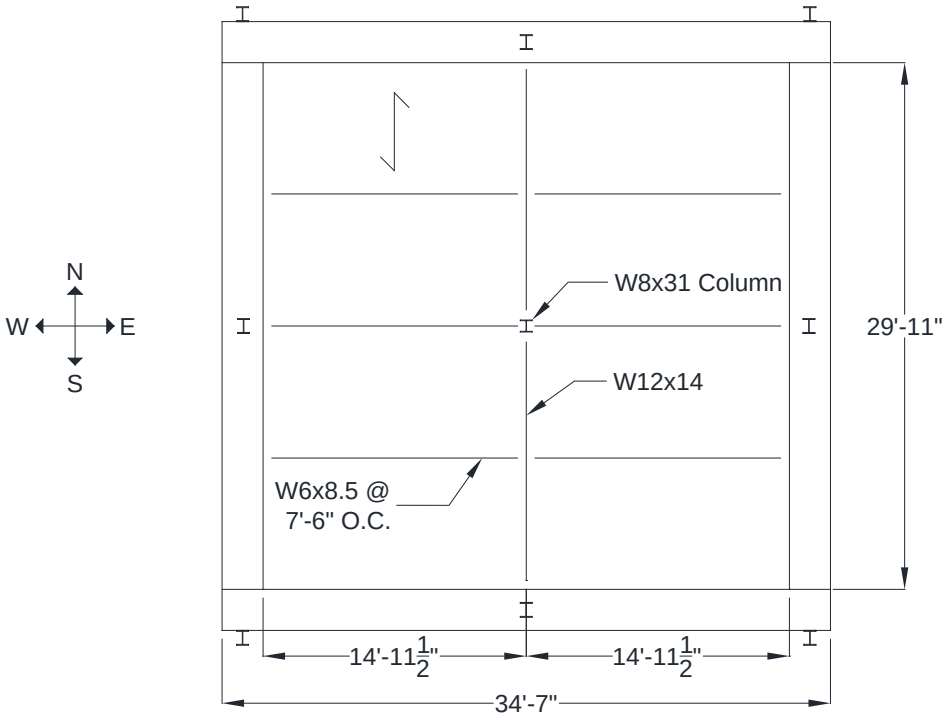

Figure 2-1: Plan View of Test Specimen

The layout of the members is shown in Figure 2-1. The W12x14 girders span north to south on the specimen, with secondary beams framing in at midspan. The corrugated steel decking spans 7.5 ft. north to south between the W6x8.5 beams. The exact dimensions of the test specimen are 29’-11” by 29’-11”. All beams and girders were connected directly to the ring beam at the perimeter of the specimen.

A W8x31 section was used for the central column. The column extended 18’-6” up from the bottom of the floor system with lateral bracing at 8 feet. The self-weight of the column may be considered a point load of 575 pounds at the center of the floor system. The column base was supported on an actuator directly below the steel framing connections.

Figure 2-2: Interior Column Connection

Figure 2-2 shows the temporary steel shoring used to support the central connection during the construction and instrumentation process. This was removed during testing and the base plate on the central column was connected to a long-stroke linear actuator to simulate static column removal.

Simple framing connections were used for all framing members in the floor system. The primary beams and girders were attached using double angles at each end. The secondary beams were connected to both the girder and the ring beam with shear tabs. All angles and plates were specified to be of ASTM A36 steel.

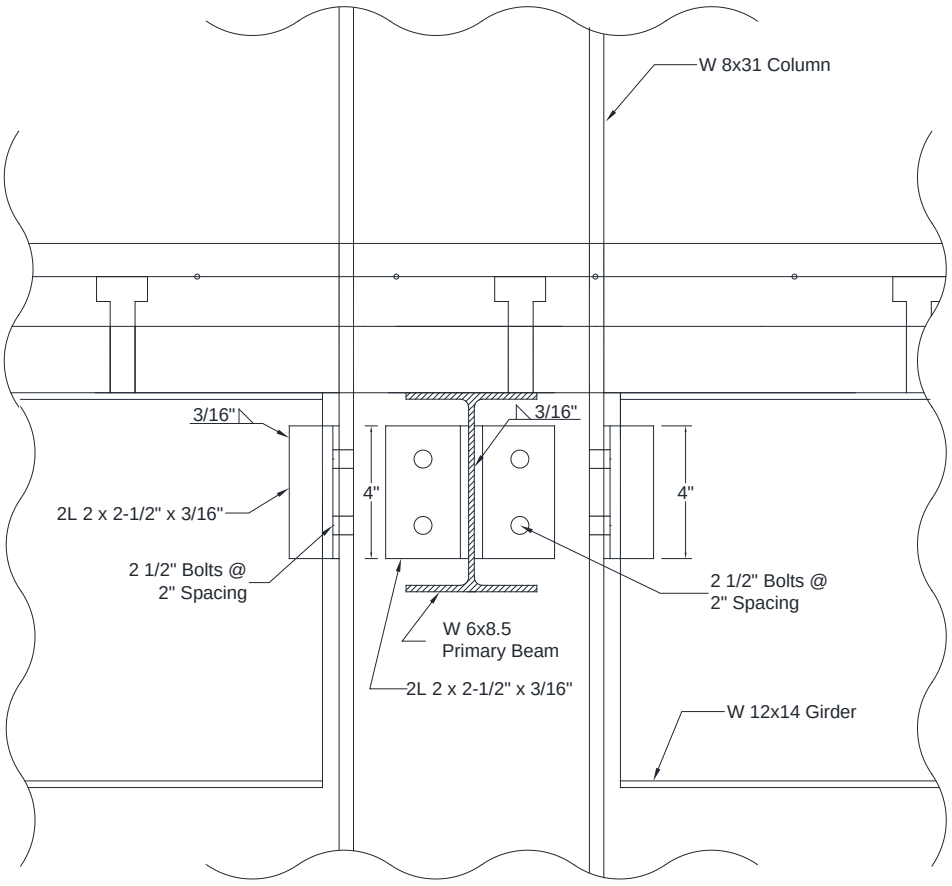

Figure 2-3: Beam to Column Double Angle Connection

Figure 2-3 shows the detail used for the double angle connections of the primary beams and girders to the central column. The angles were welded to the beams and girders using 3/16” fillet welds with E70 electrodes and were subsequently bolted to the column. Two ASTM A325 bolts were used for each angle. The same connection detail was used to connect the primary beams and girders to the ring beam except for the substitution of L3 x 2-1/2 x 3/16” angles for those shown in Figure 2-3.

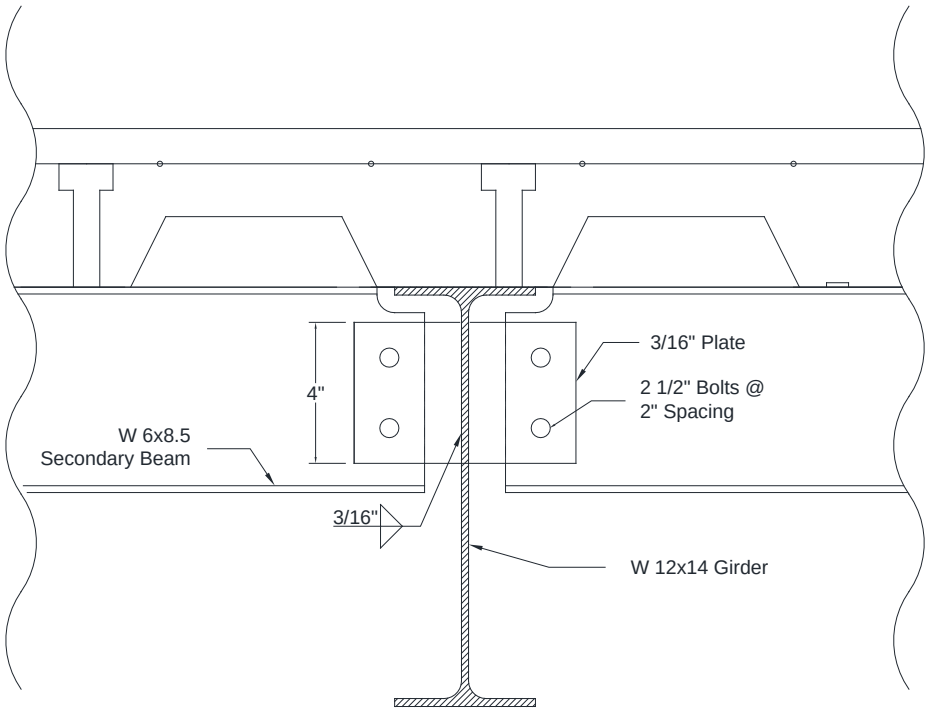

Figure 2-4: Secondary Beam to Girder Shear Tab Connection

Figure 2-4 depicts the shear tab connection for the secondary beams. The same detail was used for the connection of the secondary beams to the ring beam. The top flange of the secondary beams was coped at the connections to provide clearance for the girder in accordance with standard practice.

2.1.2 Composite Floor System

The composite floor system consisted of 22-gage 2-inch composite steel floor decking with 4.5” inches of concrete measured from the bottom of the rib. The concrete compressive strength was specified as 3.5 ksi. Concrete was cast on July 3, 2012. The

concrete was placed with no shoring for the floor system. Substantial sagging was noted in the floor beams and decking and may have required the placement of extra concrete.

Welded wire reinforcement was used to provide temperature and shrinkage resistance. On the recommendation of the practicing structural engineer on the research team, extra reinforcing bars were included along the main girder and on the east and west perimeter of the floor system to prevent cracking. Short #3 bars were placed a 12” spacing transverse to the girder along its entire length. Identical reinforcement was included along the perimeter of the floor. Figures 2-5 and 2-5 show the details of the floor system.

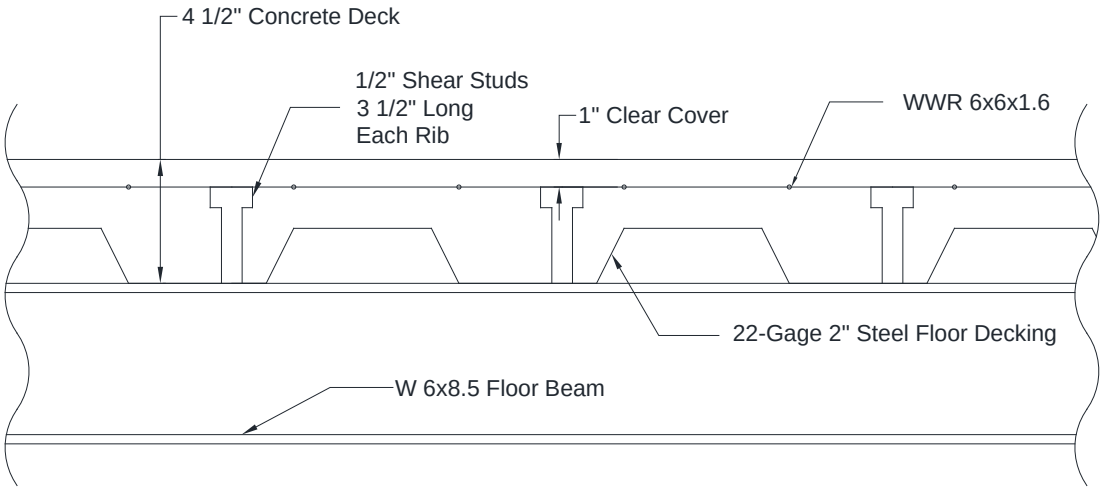

Figure 2-5: Composite Floor Detail over Floor Beam

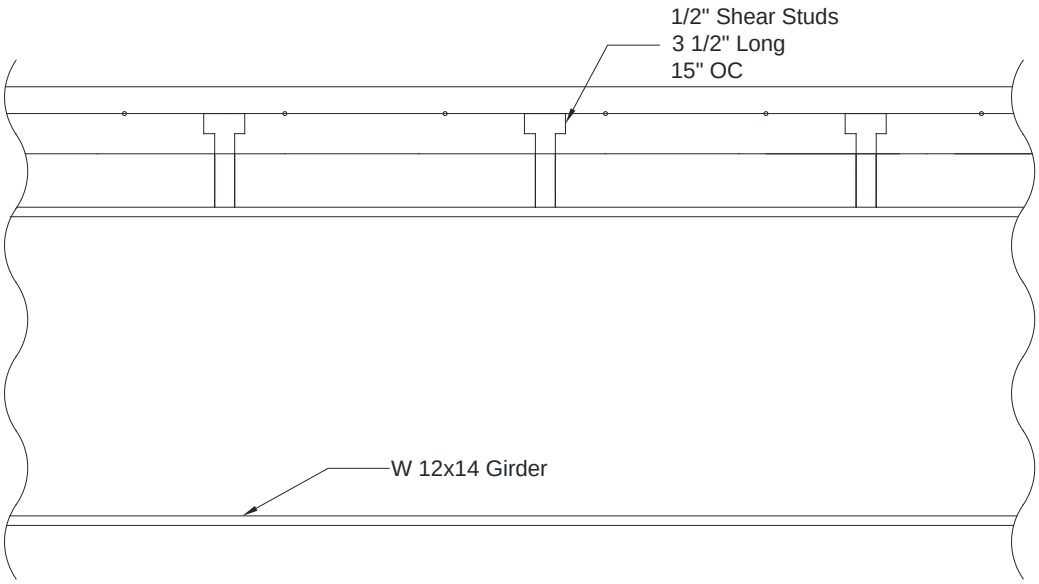

Figure 2-6: Composite Floor Detail over Girder

A longitudinal seam ran along the top flange of the primary beams. Due to the small size of the structural steel framing, a 4” overlap was required at this seam to provide sufficient attachment to the beam for each sheet. The shear studs along these beams were welded directly through both sheets. This detail is not standard in construction practices and the effect it may have on the resistance of floor system is unknown. The placement of the longitudinal seam can be seen in Figure 2-7.

Figure 2-7: Longitudinal Seam over Primary Beam

The strips of corrugated decking were 3 feet in width and all side laps were attached with self-drilling screws. The steel deck was attached to the framing members with self-drilling screws to hold the decking in place until the shear studs were installed. Along the beams, shear studs were welded at each low flute, resulting in approximately 12 inch spacing. The shear studs were placed at 15 inch spacing along the length of the girders and 12 inch spacing along the ring beam. Threaded rods were used in the place of some shear studs on the ring beam to ease the demolition process. All shear studs were ½" diameter, 3 ½" long, with 1" of clear cover.

2.1.3 External Test Frame

To model in an approximate manner the boundary conditions at the edges of the test specimen, a heavy steel ring beam was attached along the four outer edges of the specimen. The heavy ring beam is visible in this photo.

Figure 2-8: External Test Frame before Construction of Test Specimen

Each beam of the ring beam assembly was placed on its weak axis to resist horizontal flexure. Steel plates of ½" thickness were welded to the top and bottom of each beam to form closed sections. As seen in Figure 2-8, the north and south ring beams extended beyond the outer edge of the east and west beams.

Figure 2-9: Ring Beam Corner Detail

Figure 2-9 shows the west ring beam framing into the south ring beam. Steel gusset plates were used to provide lateral and vertical restraint to the ends of each ring beam. The fixity at the ends of the north and south beams differs from that of the east and west beams because of the layout of this detail.

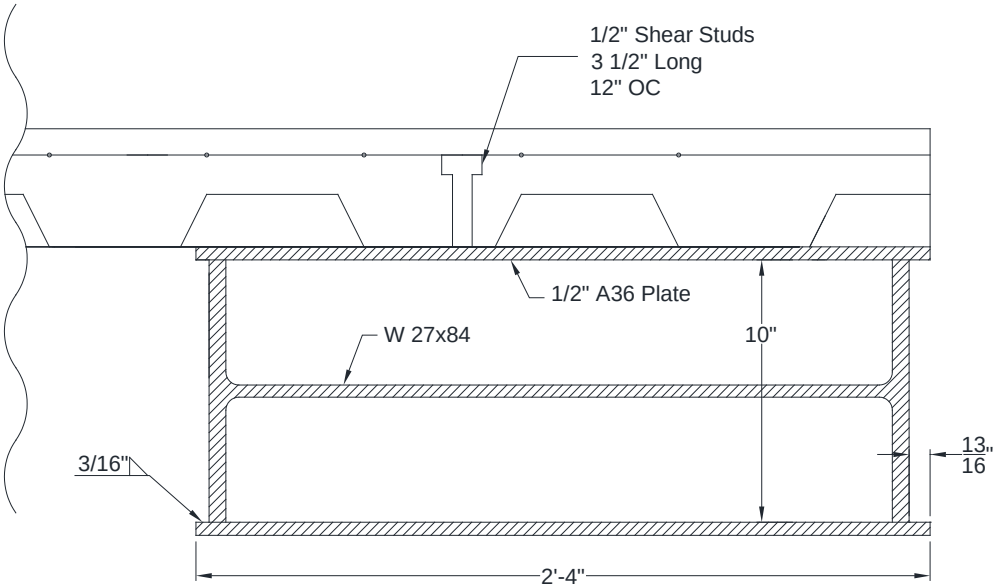

Figure 2-10: East/West Ring Beam Cross Section

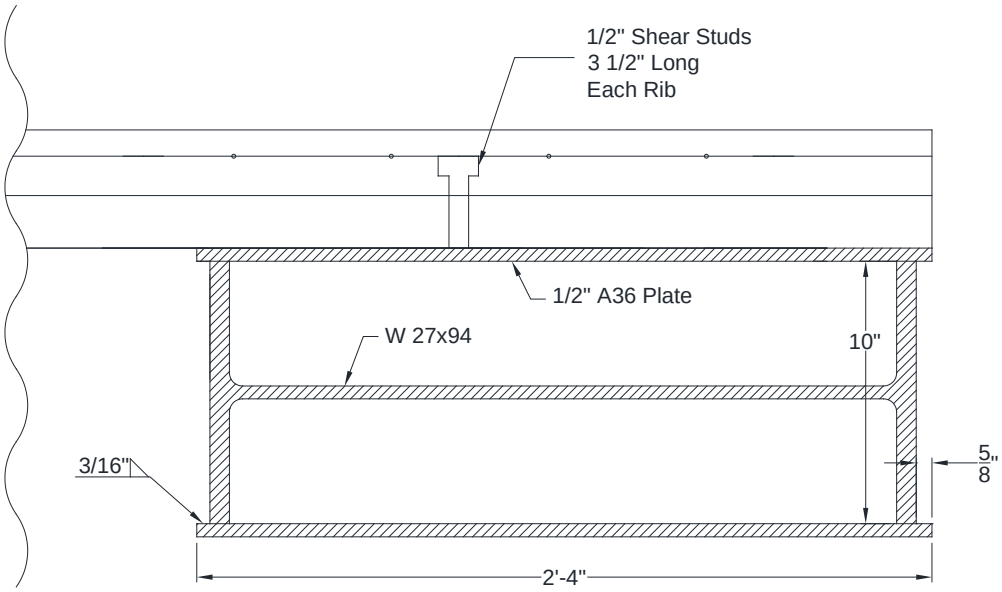

Figure 2-11: North/South Ring Beam Cross Section

Figure 2-10 shows the cross section of the ring beam at the east and west boundaries of the structure. Figure 2-11 shows the cross section of the ring beam at the north and south boundaries. The only significant difference is the use of a heavier section at the north and south boundaries where the corrugated decking is supported.

While the restraining beam could not be designed to match the behavior of adjacent bays in an actual structure, the stresses and deformation of the beams were monitored during testing to approximate the demand that would be placed on such floor systems. The beams and girders of the test specimen framed directly into the ring beams with connections described in section 2.1.1. The composite floor was attached to the restraining beams using one row of shear studs at 12" spacing on each beam. Slip between the floor system and the ring beam was considered particularly significant to the behavior of the specimen. The intersection of the decking with the ring beam was marked with paint to visually monitor slip behavior during testing.

Figure 2-12: Painted Decking-Ring Beam Attachment

The remainder of the external test frame was designed to isolate the behavior of the test specimen floor system. A high factor of safety was used for all external columns and connections to ensure that any collapse would occur due to failures within the test specimen. Substantial stability analysis was performed to evaluate the safety of the test setup. Torsional or sway modes of failure were considered highly undesirable, particularly as substantial dead load was being applied at an elevation of 15 feet off the ground. The design of the structural anchorage, external columns, and bracing is discussed in greater detail in Donahue (2013).

2.2 LOADING SYSTEM DESIGN

The loading system design accounted for two different stages of testing. First, the central column would be removed. The research team chose to apply the progressive collapse design load of 115 psf to the structure before simulating column loss. This would force the structure to redistribute forces as support was removed from the floor system. The unamplified progressive collapse design load was considered a baseline test for the structural robustness of the test specimen. The self-weight of the structure accounted for an initial load of 50 psf.

If the structure survived the column removal with the unamplified progressive collapse load, the researchers intended to continue loading the structure until collapse to find the ultimate capacity of the structure. The loading system needed to include a mechanism for increasing the floor load such that weight remained reasonably evenly

distributed over the 30 foot by 30 foot area. The distributed load would also have to be measured with reasonable accuracy throughout the loading process. The researchers determined that the maximum load they should reasonably accommodate in the loading system design was the ultimate gravity load of 170 psf. The chosen solution was the construction of plywood buckets with a layer of concrete for initial loading and the capacity to hold several inches of water for additional loading.

Figure 2-13: Plywood-Concrete Loading Buckets

Figure 2-13 depicts the plywood-concrete buckets constructed for loading the test specimen. Waterproof sheeting was used to line the buckets before the concrete was poured. Each bucket contains six inches of concrete to apply an initial loading approximately equal to the progressive collapse design load. Rebar connects the buckets in 2x2 units so that they may be placed on the slab four at a time. The plywood siding, with its waterproof lining, can contain a maximum of 18 inches of water as superimposed load.

Figure 2-14: Loading Water Supply and Irrigation System

A large temporary pool contained the water supply for the loading process. PVC piping (Figure 2-14) was used to create an irrigation system that distributed water equally into each individual bucket.

Figure 2-15: Loading System at Capacity

Figure 2-15 shows the concrete buckets placed on top of the slab and fully loaded with water from the irrigation system.

A total of 64 individual buckets, or sixteen 2x2 units, were used. The spacing between each individual bucket was approximately 10 inches. This spacing prevented the buckets from coming into contact and contributing any resistance to floor deformation. The separation of the water load into so many distinct units also prevented substantial redistribution of weight based on sagging in the floor system. Although each bucket would tilt slightly as the floor deformed, the water stayed essentially uniformly distributed.

Each 2x2 unit was weighed before being placed on the specimen for a precise measurement of initial loading. The range of loads capable of being applied using this system is described in Table 2.

Table 2: Applied Loads

Self-weight of structure	$SW_{structure}$	60 psf
Self-weight of loading buckets	$SW_{buckets}$	60 psf
Maximum water loading	LL_{water}	60 psf
Initial loading	$SW_{structure} + SW_{buckets}$	120 psf
Maximum loading	$SW_{structure} + SW_{buckets} + LL_{water}$	180 psf

The loads in the table have been reduced to account for the total area of the floor system as compared to the area covered by the buckets. This normalization realistically approximates the way the load is carried by the structure.

2.3 TEST SPECIMEN INSTRUMENTATION

The instrumentation was selected to endure substantial exposure and resist damage. Since the test specimen was outdoors and the test sequence included water loading, the researchers anticipated that the equipment could be subject to damaging conditions. The primary concern was keeping the instrumentation running accurately throughout the duration of the test. It was also considered a priority to protect the equipment in the case of total structural collapse for use in future tests. The rate of data acquisition used throughout all testing was 1 Hz.

2.3.1 Load Measurements

A 50 kip load cell was attached to the actuator such that it would measure the total load from the column base supported by the actuator. The load cell tare value was measured when the actuator was fully disengaged from the column base. After the column removal simulation was completed, the load cell could no longer be used for load measurements.

The additional loading was performed using an irrigation system that distributed water equally into the loading buckets resting on the floor.

Figure 2-16: Loading System Flow Meters

Two pumps were needed to load the system at a rate of approximately 0.7 psf per minute, resulting in a total time of about an hour and a half to fully fill the buckets. Flow meters were connected directly to the pumps to measure the total volume of water distributed into the irrigation system as shown in Figure 2-16.

2.3.2 Vertical Displacement Measurements

Linear potentiometers with a maximum capacity of 62 inches were placed on each beam and girder at their midpoints. At the central connection, linear potentiometers with a 125 inch stroke were located at the end of each beam framing in and at each edge, north and south, of the base of the column. All potentiometers rested on the slab beneath the structure. The cables were fully extended and connected to the appropriate member using wire that was attached to a bracket glued to the bottom of each beam.

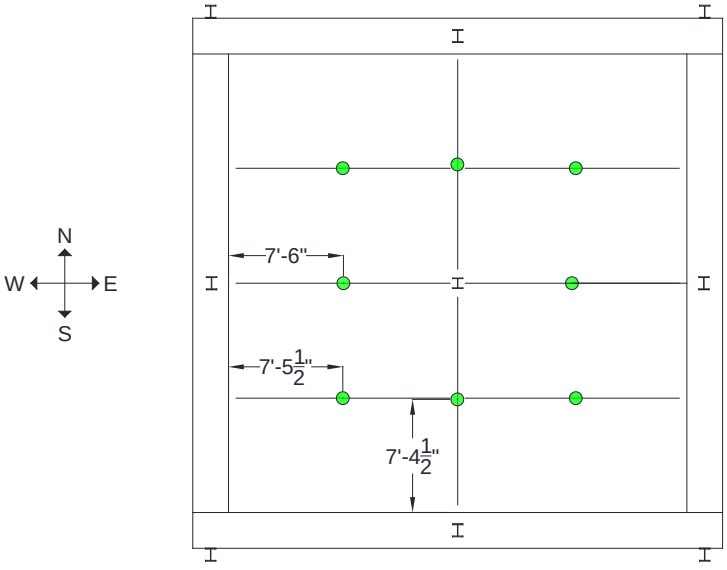

Figure 2-17: Plan View of Vertical Linear Potentiometers

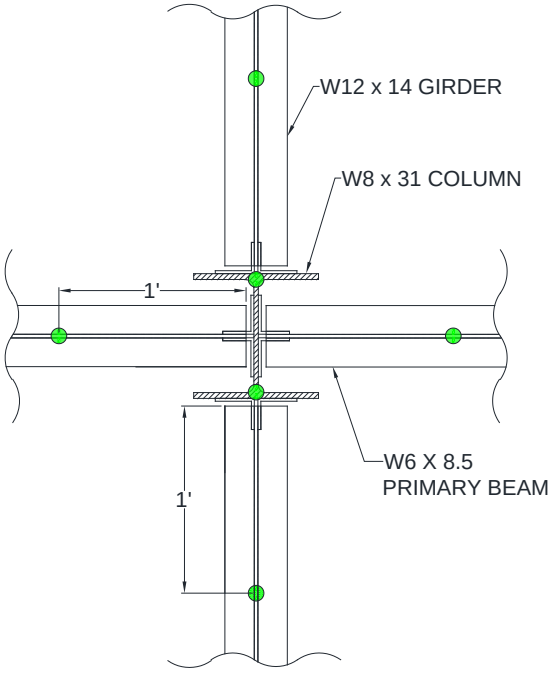

Figure 2-18: Vertical Linear Potentiometers at Central Connection

The locations where vertical displacements were measured near the column are shown in Figure 2-18. The vertical linear potentiometers attached to the beams and girders framing into the columns were set back 12 inches from the end of each member to provide adequate spacing for the instruments on the slab below. Two potentiometers were attached to the column to measure an average displacement of the column base. The instrument locations are shown on Figure 2-18 at the midpoint of the column flanges to show that the two potentiometers were located at the north and south edges of the column. The potentiometers were actually connected to steel plates added to provide clearance from the actuator, as seen in Figure 2-19.

Figure 2-19: Steel Plate Extensions for Column Displacement Measurements

2.3.3 Horizontal Displacement Measurements

Smaller linear potentiometers with a 7 inch stroke were attached to the top and bottom of the web of each beam and girder framing into the column. The cables were extended approximately an inch and connected to the side of the column using wire

attached to magnets. Magnets were used to prevent destruction of the string pots in the case of structural collapse, where the 7” stroke would likely be exceeded. The precise horizontal projection of the cable was established with a laser in order to place the magnet in the proper location.

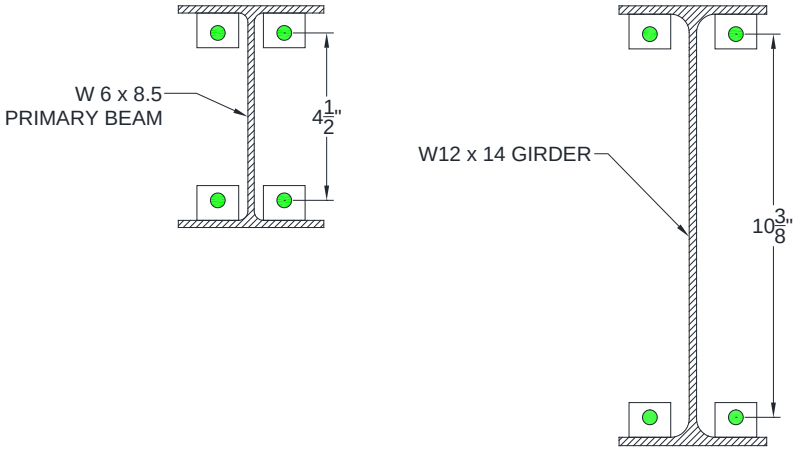

Figure 2-20: Location of Horizontal Linear Potentiometers

Four linear potentiometers were attached to the web of each member framing into the interior column to measure the rotation and net horizontal separation of the beams from the column. The location of the instruments is shown in Figure 2-20. The vertical spacing of the instruments was maximized to enhance the accuracy of calculated rotations. The use of linear potentiometers on both sides of the web provided redundancy in data acquisition and allowed for the observation of any unexpected out-of-plane rotations. The installed linear potentiometers can be seen in Figure 2-19.

2.3.4 Girder Strain Gages

The main girders, spanning north to south on the test specimen, were instrumented at their midpoints with strain gages. Eight strain gages were used on each girder to measure the strain profile of the girder at the midpoint. Figure 2-21 is a photo showing the gages attached to the girder.

Figure 2-21: Strain Gages on Girder

The strain gages were offset eight inches from the beam connection to avoid localized stress concentrations at the beam-to-girder connection. For both girders, the offset was towards the perimeter of the specimen. Protective coatings were used to account for outdoor exposure and prevent the loss of bond between the gauge and the steel. The location of the gages on the girder cross-section is shown in Figure 2-22.

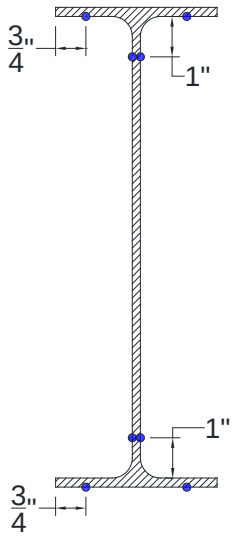

Figure 2-22: Location of Girder Strain Gages

These strain gages were intended to permit calculation of bending moment and axial force in the girder in the elastic range.

2.3.5 Ring Beam Strain Gages

Strain gages were placed on the ring beam to provide an estimate of the vertical and horizontal moments induced in the beam. Four strain gages were placed at each section to define the strain profile on both axes. The midpoint and both ends of each individual beam were instrumented for a total of 48 strain gages. The specific layout of the strain gages is shown in Figure 2-23.

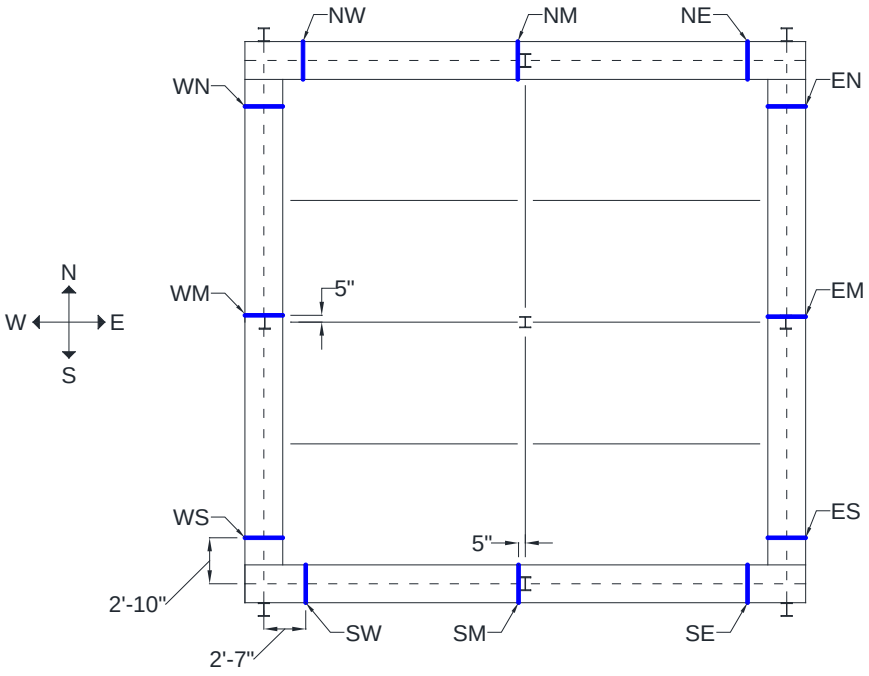

Figure 2-23: Plan View of Ring Beam Strain Gage Locations

The strain gage groups are labeled based on their location: the first letter corresponds to the location of the beam and the second letter designates the strain gage location on this beam. For example, EN represents the group of strain gages at the north end of the east ring beam. In data analysis, the strain gages were grouped in accordance with the symmetry of the structure. Further discussion of the methods used to analyze the strain gage measurements is provided later in this thesis.

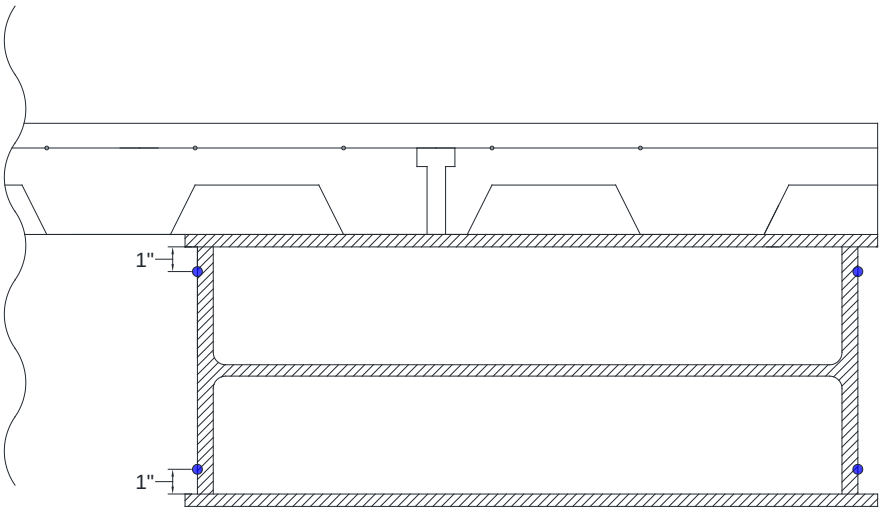

Figure 2-24: Section View of Ring Beam Strain Gage Locations

At each ring beam section that was instrumented, four gages were attached to measure longitudinal strain as shown in Figure 2-24. The locations of these gages were labeled Inside Top, Inside Bottom, Outside Top, and Outside Bottom. The strain measurements could be used to calculate values of both vertical and lateral flexure in the ring beams.

CHAPTER 3

Test Procedures and Observations

3.1 OVERVIEW

This chapter describes procedures used for conducting tests on the test specimen, and also provides some general observations of specimen performance during testing. More detailed observations and data analysis are presented in the next chapter.

A series of four tests were performed on this test specimen before total collapse occurred. Changes were made between tests to improve data acquisition and weaken the structure based on the judgment of the research team. The testing program for this specimen is summarized below:

- Test 1
  - Interior column removal
  - Superimposed distributed loading
- Test 2
  - Repeat superimposed loading with improved data collection
- Test 3
  - Remove nuts from bolts in beam-column connections to eliminate tension resistance
  - Repeat superimposed loading
- Test 4
  - Remove bolts from all steel framing connections to isolate composite floor system resistance
  - Repeat superimposed loading

3.2 TEST 1

The first test of Specimen 1 was carried out July 31 to August 1, 2012. Data acquisition was activated in the morning before any load was applied to the structure. Each instrument was zeroed in its position under the self-weight of the structure with the central column fully supported. The tare value for the load cell measured before the actuator was engaged was input by hand at this point to measure the full reaction at the base of the interior column. A crane was used to lift each load unit, consisting of four connected buckets, and place it on the slab. Certain units had to be pushed towards the middle of the slab using a forklift to avoid interference with the bracing above the test frame. The actuator remained fully engaged during the initial loading process. The superimposed load of the buckets, prior to filling with water, resulted in a deflection of approximately 0.1 inches at the midpoint of each of the secondary beams.

Figure 3-1: Placement of Loading Buckets on Test Specimen

The column loss simulation began at 2:30 pm, a few hours after the progressive collapse design load had been placed on the structure. The hydraulic actuator supporting the central column base was slowly lowered until fully disengaged from the specimen. The rate of lowering was regulated by the operator of the hydraulic pump. The actuator was fully disengaged from the specimen after 35 minutes and the resulting deflection was 2.1 inches. No damage was observed during this process. The specimen was observed to carry the full progressive collapse design load upon the static removal of central column.

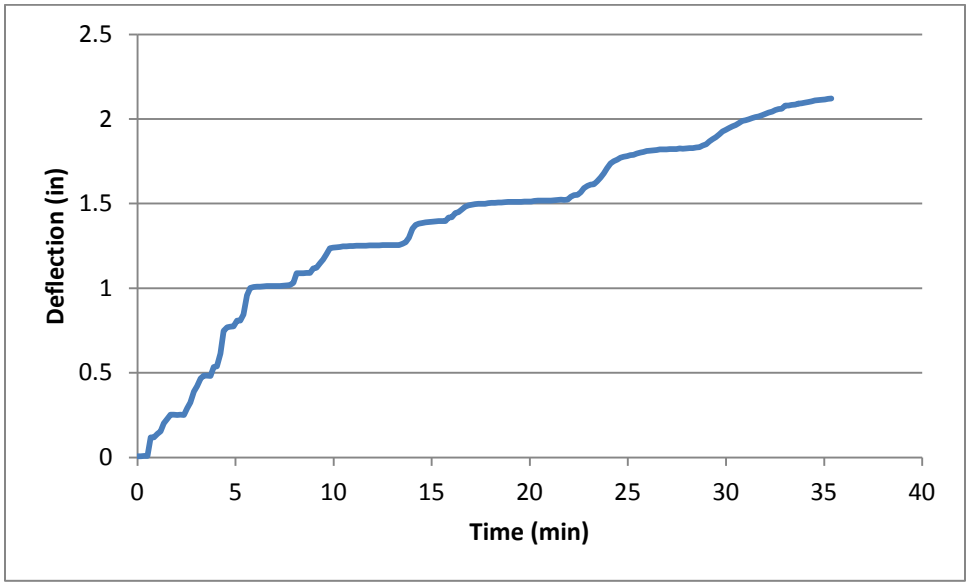

Figure 3-2: Rate of Static Column Removal

Figure 3-2 shows a plot of vertical column deflection versus time while the actuator was being lowered. The lowering of the actuator was occasionally paused to allow the structure to equilibrate. As the load on the column decreased rapidly for only small displacements, the column was lowered more slowly until the actuator was fully disengaged.

The next step in the testing procedure was the addition of load through an irrigation system pumping water into each bucket on the slab. Due to problems with the pumps, this phase was delayed until the next day. To avoid disrupting the test sequence, the specimen was left loaded and unsupported at the central column. All instrumentation remained running and team members took shifts monitoring the structure throughout the night. No major changes were observed, but the floor continued to creep under the applied load. In the 17 hours between test stages, the deflection increased from 2.1 inches to 2.5 inches. The rate of observed creep is discussed further later in this thesis.

Before testing started back up, minor changes were made to the instrumentation to improve data collection and reduce potential damage to the instruments in the case of a structural collapse. The magnets used to connect the horizontal linear potentiometers to the central column had slipped when water leaked through the connection. These were replaced in their original position. The vertical linear potentiometers at the midpoints of each beam were removed as they did not have sufficient protection to survive a potential collapse.

After the pump system had been repaired, additional loading commenced through the pumping of water into each of the buckets. The intermittent performance of the two pumps led to some irregularity in the distribution of water between buckets on the north and south sides of the slab. Substantial leakage of water from the buckets was also observed throughout the course of loading. As a result, the total load on the slab at any point during this stage of the test is uncertain. After two hours, it was observed that the buckets had either reached their full capacity or were leaking too extensively to bear additional load. The final displacement of the central connection under the maximum applied load was 4.5 inches. No damage was observed to any component of the specimen, floor system or framing connections.

Figure 3-3: View of Loading Buckets at Completion of Test 1

It can be seen in Figure 3-3 that some buckets have reached their full capacity and are beginning to overflow while the water level in others is several inches below the top.

The buckets were stored outdoors in the months before testing and the waterproof lining in some buckets was damaged by the exposure, resulting in the problems with leakage.

The research team decided to preserve the test specimen while further testing procedures were discussed. The actuator was raised until it engaged with the base of the central column in its deflected position. The floor system was not pushed up by the actuator, but simply held in place. The water was removed from the buckets in the following days and shoring was built to temporarily support the floor system.

3.3 TEST 2

The second test was performed on September 20, 2012. Improvements were made to the plywood loading buckets to decrease the leaking and additional protection was applied to the instrumentation located at the central connection. Preliminary observations of the data from the first test indicated that the superimposed distributed load measurements were highly uncertain and several instruments malfunctioned after getting wet. The purpose of the second test was to repeat the same testing procedures for the superimposed loading and collect more reliable data.

All loading buckets were empty at the beginning of testing. The actuator supporting the central connection was raised until the pressure in the hydraulic ram approached the maximum safe level. At this point, the vertical displacement of the central connection from its initial, fully supported position was 3 inches. All instrumentation was zeroed in this position. The load cell was not functioning, so no data was collected for

compressive load on the central column while the actuator was still engaged. After zeroing all of the instrumentation, the actuator was disengaged and testing began with the addition of distributed load.

Figure 3-4: Specimen before Test 2

Figure 3-4 shows the condition of the test specimen before the start of Test 2. The vertical linear potentiometers were covered with waterproof sheeting to prevent water damage. The three-inch initial deflection was measured with the actuator engaged to its maximum safe pressure. Before loading began, the actuator was fully retracted and the floor system was allowed to equilibrate. The deflection of the unsupported floor before water was pumped into the loading buckets was 3.2 inches.

The pumps ran from 9:30 am until 11 am when the buckets reached their capacity. The maximum load due to water in the buckets was approximately 60 psf during this test and the resulting additional deflection during loading was 1 inch. The total displacement

from the initial, fully supported position was therefore 4.3 inches. This maximum deflection is actually lower than the deflection measured at the end of Test 1, although the maximum load applied in Test 2 was most likely higher than Test 1. This observation is discussed further later in this thesis.

Figure 3-5: View of Loading Buckets a Completion of Test 2

Figure 3-5 shows the loading buckets at the end of the second test. The added waterproofing resulted in substantially improved water retention in the loading system. The water appears to be evenly distributed between buckets and the maximum load measurement matches the estimated load for the full buckets.

Data acquisition was run for 2 hours after loading was completed with the full load applied to observe any additional deformation under sustained load. The final position of the central column when data acquisition was disconnected was 4.4 inches from the initial, fully supported location. No physical damage was observed. The actuator

was reengaged with the bottom of the central column and shoring was placed under the floor system to protect the specimen between tests.

3.4 TEST 3

For the third test of this specimen, the research team chose to weaken the structure to try to force structural collapse. As no significant damage was observed in the previous two tests, the researchers were interested in observing the behavior of the structure once it reached a stage of distress. To this end, the nuts were removed from the bolts at all connections of the beams and girders to the central column except two of the bolts on the beams. Removing the nuts from the bolts at these connections allowed the connections to still transfer shear, but limited their ability to transfer moment or tension. Figure 3-6 shows the girder-to-column connection after removal of the nuts.

Figure 3-6 - Girder-Column Connection with Nuts Removed

The third test took place on September 25, 2012. The test was initiated by a similar procedure used in the second test, with no water in the loading buckets. The actuator was pushed up against the bottom of the central column. In this test, the floor system was raised back up to a higher initial position without exceeding the maximum safe pressure in the hydraulic ram. The vertical displacement from the initial position of the slab was only 1.25 inches as compared to 3 inches for the second test. Possible reasons for this change are discussed later. All instrumentation was zeroed at this time so subsequent measurements were taken from this position. The actuator was then lowered until it was disengaged from the structure. The central connection deflected 2.7 inches during this process, before additional loading was applied. The position of the center of the floor slab was therefore a total of approximately 4 inches below the initial, fully supported location.

The pumps for the water loading system were started at 9:00 am and ran until water was observed overflowing from the buckets at 10:40 am. The central connection deflected an additional 2 inches under the total applied water load of 60 psf for a final displacement of 6 inches from the initial position of the floor slab. No physical damage was observed on the specimen. The structure was left unsupported and fully loaded to observe any time-dependent behavior. The floor deflected an additional inch in the first ten minutes after loading was stopped, after which creep slowed dramatically. After three and a half hours, the central connection reached a total displacement of 7.4 inches

without any components failing. The structure was stabilized by reengaging the actuator and replacing the shoring towers until the next test.

Figure 3-7 - Central Connection during Test 3

Figure 3-7 shows how little separation occurred between the angles and the column despite the removal of the nuts. The beam and girder rotations measured in each test are discussed in the next chapter.

3.5 TEST 4

For the fourth test on the original specimen, the researchers chose to weaken the framing connections further to increase the demand on the floor system. The nuts and bolts were removed from all connections such that stresses could only be transferred into the steel framing members through the decking. Since the beams were not connected to the central column base, the actuator could not be used to push the floor back up into its

initial position. All instrumentation was zeroed with the actuator engaged at a displacement from the initial floor level of 6.06 inches. The floor deflected an additional 0.25 inches after the actuator was lowered entirely and before water loading began at 9 am on October 4, 2012.

Figure 3-8 - Test Specimen before Test 4

Figure 3-8 shows the structure just before water loading began for Test 4. The actuator has already been fully retracted and the floor system can be seen visibly sagging in the center.

The water loading proceeded as in the previous tests and no distinct changes in behavior were observed as the floor reached higher displacements. Researchers on site began to hear substantial cracking and creaking sounds in the minutes before collapse. At 10:10 am, with a distributed water load of approximately 40 psf and a total displacement of 15.5 inches, the floor system collapsed. Observers agreed that failure seemed to be

initiated by tear out at a longitudinal seam of the corrugated steel decking. Collapse was essentially instantaneous after this failure.

Figure 3-9 - Central Connection during Test 4

Figure 3-9 shows a photo taken only minutes before the final collapse. The rotation of the framing members at the central connection indicates the high level of displacement. The beams appear to be undergoing primarily rigid body motion. The proportion of rigid body motion and flexural deformation is investigated further in Chapter 4 using the data collected by beam instrumentation.

Figure 3-10 - Test Specimen after Collapse
a) Facing East
b) Facing North

Figure 3-10 shows the structure after total collapse. The lack of damage to the corrugated steel decking suggests that it failed along the longitudinal seam. Close examination of the video footage of the failure supports this interpretation. In Figure 3-10a, the steel decking appears to have torn along a side lap during collapse. The secondary beams can be seen hanging from the steel decking in Figure 3-10b.

Upon completion of Test 4, the specimen was removed by a professional demolition company. Portions of the specimen were saved, however, to allow material testing.

CHAPTER 4

Experimental Results and Analysis

4.1 OVERVIEW

This chapter presents the data collected in the four tests on this specimen. All data was initially plotted by the author. Measurements that were far outside the range of values observed by equivalent instrumentation were eliminated from data analysis. For example, if a sudden jump was observed in one of the linear potentiometers attached to the column base but not the other, the jump was eliminated from data analysis as invalid. Details are provided for each graph on which instruments have been removed from analysis.

4.2 LOAD-DISPLACEMENT OBSERVATIONS

This section presents the load-displacement relation observed in all four tests. The displacements presented in this section were measured at the base of the column and are computed using an average of the two linear potentiometers attached to the base of the column. Superimposed load over time was calculated assuming that all water discharged through the pumps was applied as uniform load over the floor system. The total weight of water discharged was divided by the total loading time to find a constant load rate. Thus, the load at a given deflection measurement directly corresponds to the elapsed loading time.

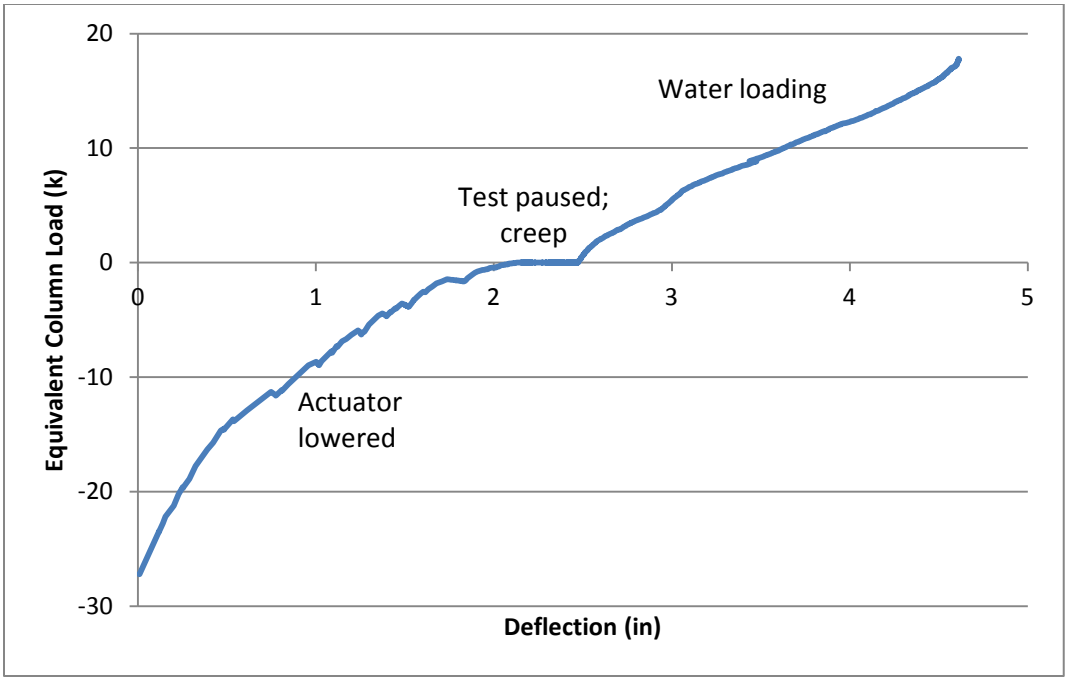

Figure 4-1: Summary of Test 1

Figure 4-1 depicts the deflection at the midpoint of the floor system through the different stages of testing for Test 1. Negative load corresponds to the load supported on the actuator as it was lowered. Positive load corresponds to estimated water load that would be carried by the central column if it were in place. The equivalent column load due to water loading was calculated using a 15 foot by 15 foot tributary area. Static column removal lasted 45 minutes. Creep under the sustained load after support was removed was observed over 17 hours. Superimposed loading using the irrigation system took 2 hours.

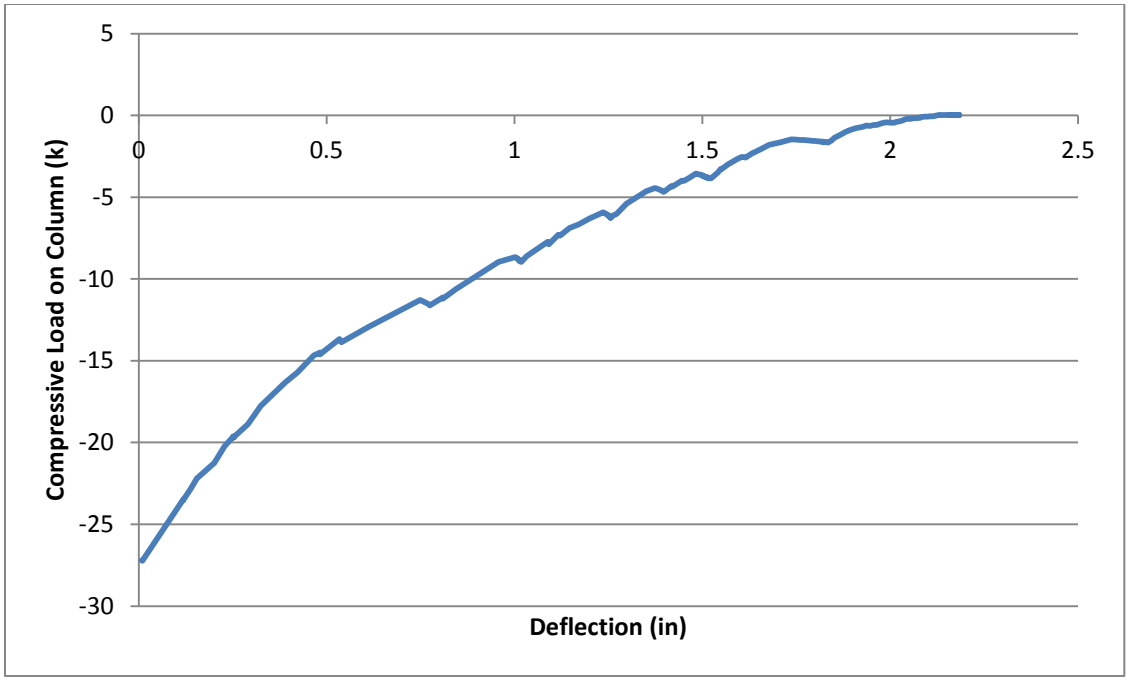

Figure 4-2: Load-Deflection Curve during Static Column Removal

Figure 4-2 shows the load-deflection relationship during the removal of the column. Unloading was not smooth over time due to manual operation of the hydraulic ram. The data shows a clear nonlinear trend, possibly due to initial cracking in the concrete and/or nonlinear response of the beam and girder end connections. The load measured at the central column before unloading began agrees reasonably well with the load on the floor system given a 15 foot by 15 foot tributary area with a uniform load of 120 psf. This indicates that the distribution of forces within the structure resembles the response expected from a simple tributary area approach. The total deformation that occurred within the floor system upon complete removal of the central support was 2.15 inches.

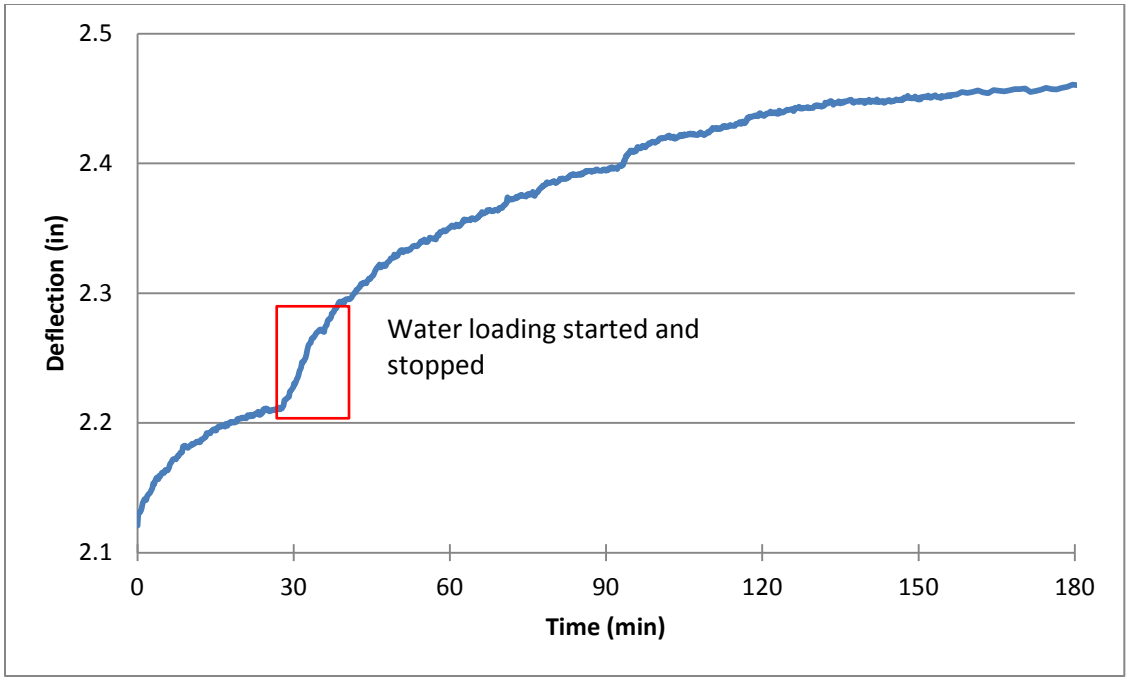

Figure 4-3: Test 1 Creep - First 3 Hours

Figure 4-3 shows the deflection that occurred in the three hours after column removal in Test 1. The unsupported structure continued to deflect for the first three hours after the actuator was disengaged. The creep began to level out after the first thirty minutes, but the irrigation system was turned on and approximately 4 psf of water load was applied before the pumps began to malfunction. The effect of this small load can be seen in Figure 4-3 as further movement is triggered in the structure. An additional 15% deflection was observed over this time frame.

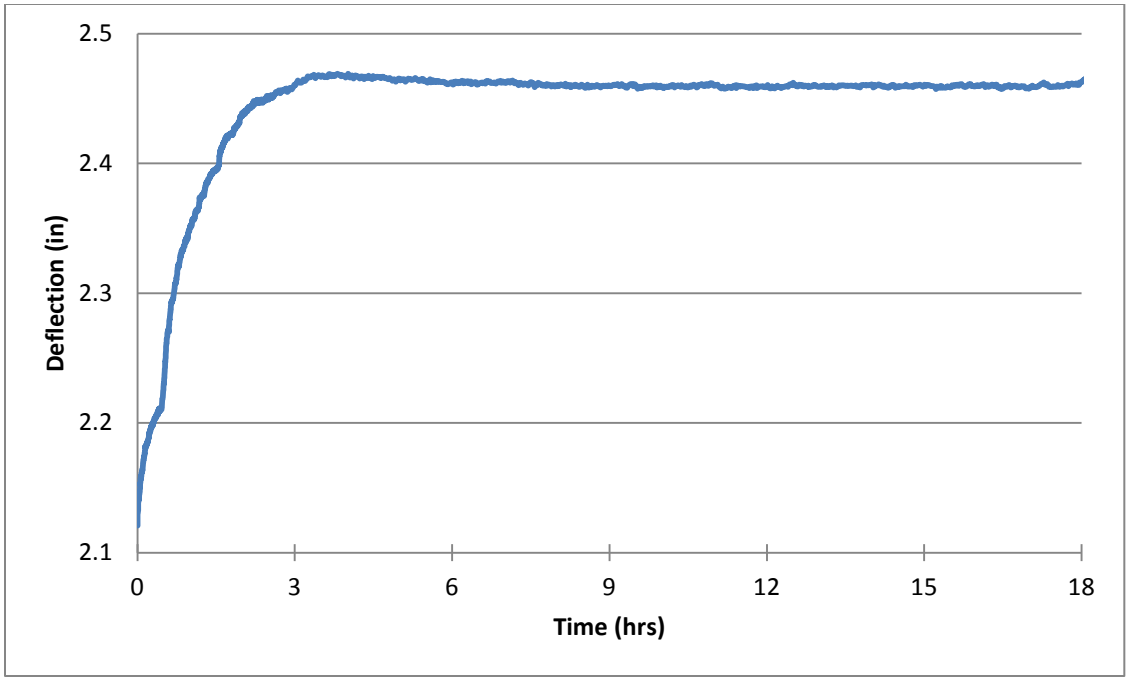

Figure 4-4: Test 1 Creep

Figure 4-4 shows the column deflection versus time for the 18 hours that the specimen was left unsupported without added load. After the first three hours, the deflection no longer increased, and the structure maintained a consistent displacement of 2.46 inches until loading began the next morning. The fact that the specimen continued to deflect under constant load may be of significance in actual building emergency events. If a building is damaged in an event but does not immediately collapse, there may be a concern that collapse may occur minutes or even hours later. For this specimen, the structure stabilized after about 3 hours. It is unclear if this same stabilization would occur in an actual structure.

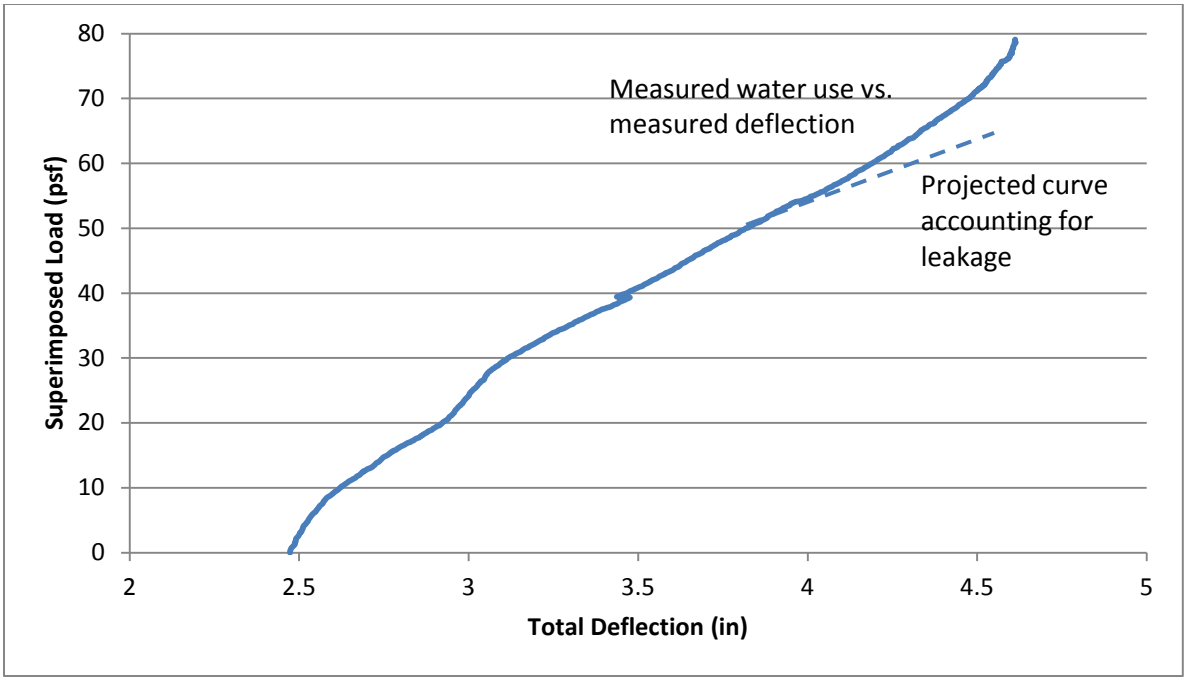

Figure 4-5: Test 1 Superimposed Loading

Figure 4-5 shows the load-deflection relationship observed during the water loading in Test 1. The measured curve of load versus observed deflection shows the irregularities resulting from problems with test procedures. The total weight of water discharged during testing was divided by the total loading time and the floor slab area to find a uniform load rate over time. In Test 1, neither the loading rate over time nor the distribution of load over the area of the specimen was uniform due to pump failures and leakage. The superimposed load is therefore likely overestimated for each measured deflection. Near the end of the test, this effect is particularly pronounced as the system appears to gain stiffness. In reality, the load rate was decreasing during this time range as a greater percentage of the water discharged into the system was lost due to overflowing and leakage. The dotted line visually approximates a continuation of the trend seen at

lower loading levels to eliminate the effect of the overestimation of load. Based on the design of the loading system, the maximum load that could be contained in the buckets is closer to 60 psf. The calculation of an applied load of 80 psf is therefore considered unrealistic.

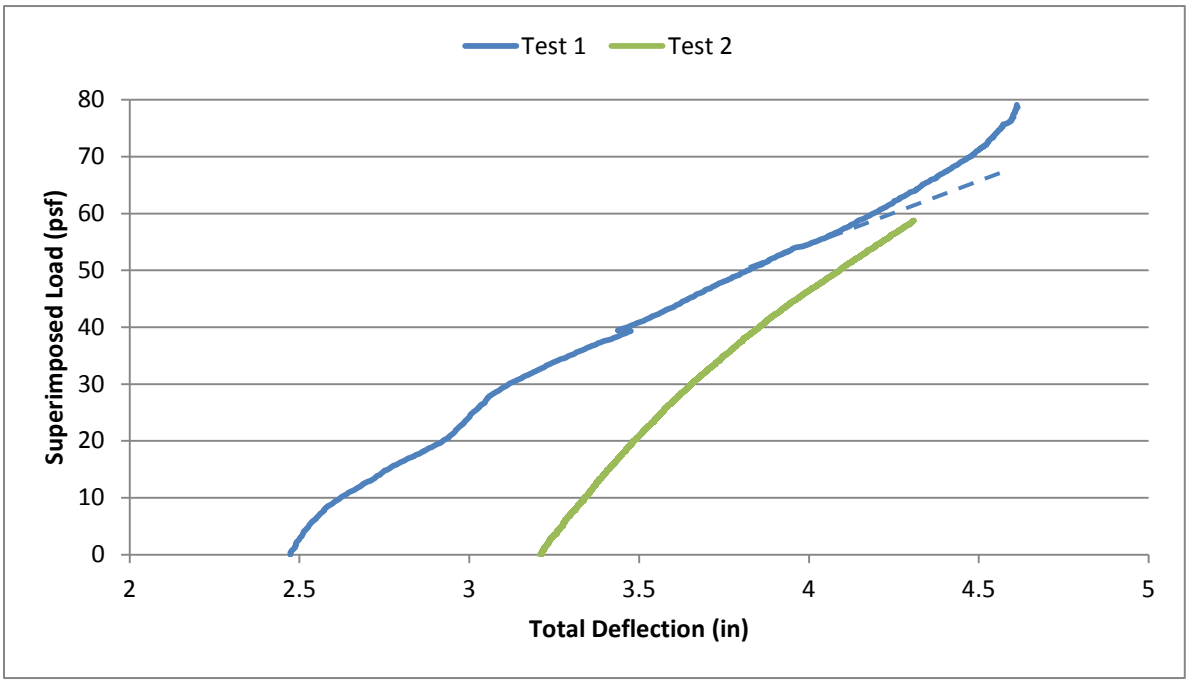

Figure 4-6: Comparison of Load-Deflection Measurements in Tests 1 and 2

Figure 4-6 shows the load-deflection relationships in Tests 1 and 2 during the water loading. After the actuator was disengaged from the column base in Test 2, the floor system equilibrated at a displacement of 3.21 inches. The structure did not elastically rebound to the 2.46 inch displacement observed at the same load level in Test 1, suggesting the development of damage to the specimen in Test 1. The load-deflection trend is much clearer in this test due to improved data collection. The stiffness in this test is noticeably higher. Despite starting at a higher initial displacement, under the maximum

applied loading the structure does not reach the maximum displacement observed in Test 1. The increase in stiffness was not expected, but may possibly be due to a geometric stiffness contribution in Test 2 resulting from the higher initial deflection at the beginning of water loading in this test.

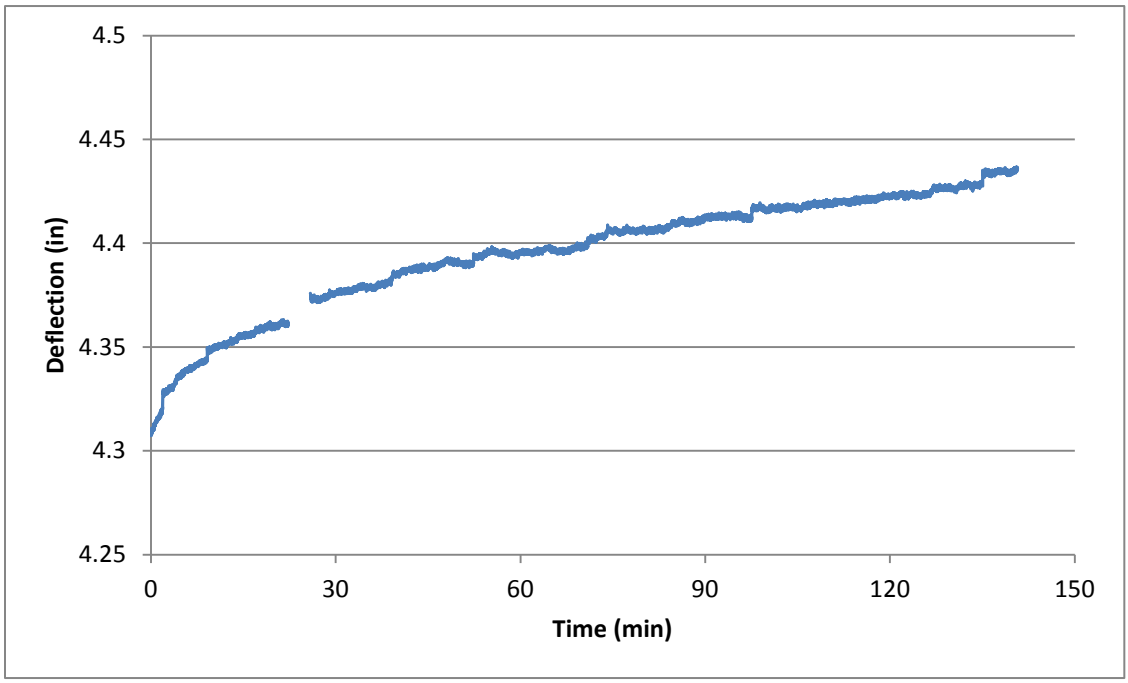

Figure 4-7: Test 2 Deflection under Sustained Load of 180 psf

Figure 4-7 shows the measured deflection versus time after the full water load was applied in Test 2. Data acquisition was left running for 3 hours after loading ceased. The amount of additional deflection was relatively small, but the structure did continue to creep at a steady rate during this time period. The maximum observed deformation was 4.44 inches. An unexplained spike in the data at 22 minutes was removed from the data plotted above. Because the spike occurred in only one of the two instruments used to

measure deflection of the column base, it is considered invalid and the trend continues smoothly after this point.

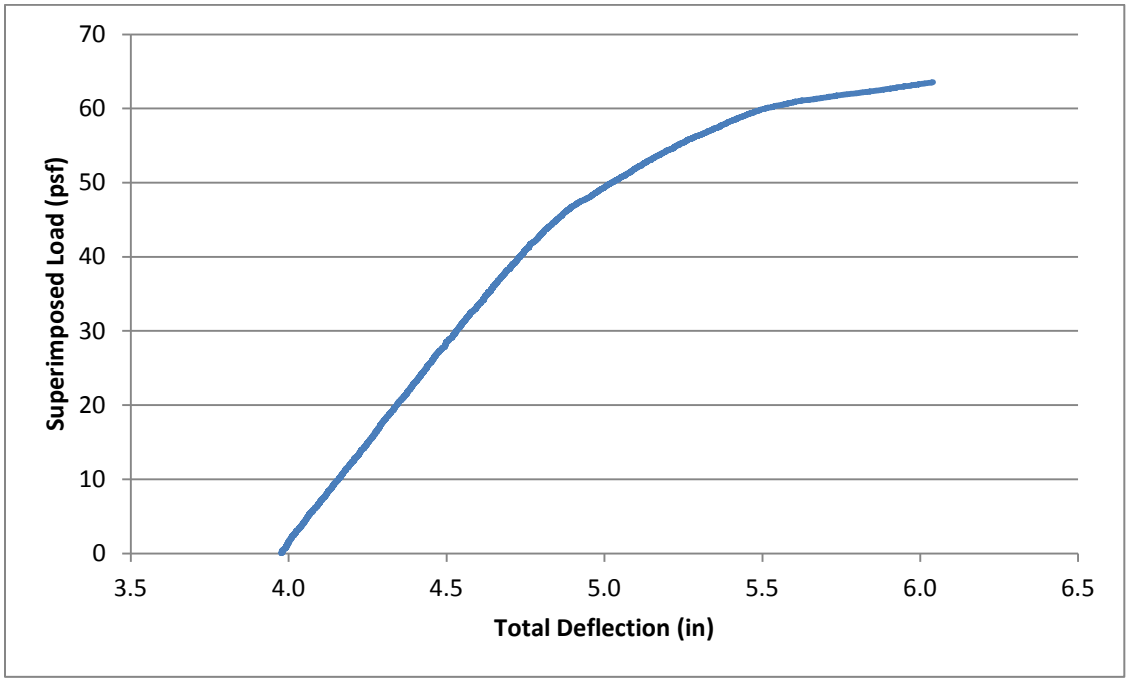

Figure 4-8: Test 3 Superimposed Loading

Figure 4-8 shows the load-deflection relationship measured under water loading during Test 3. In the third test, with the nuts removed from bolts at the central connection, the actuator was raised to a higher position without exceeding the maximum allowable pressure on the actuator. The lack of tensile capacity at the connections appears to have reduced the overall stiffness of the system. After the support at the central column was fully removed, the deflection reached 4 inches. The load-deflection rate remained reasonably linear for the first 40 psf of applied load with a stiffness only slightly lower than that measured in Test 2. The system clearly begins to soften around a load of 50 psf,

corresponding to a total load of 170 psf. However, the loading system reached its full capacity without any substantial damage or component failures within the structure.

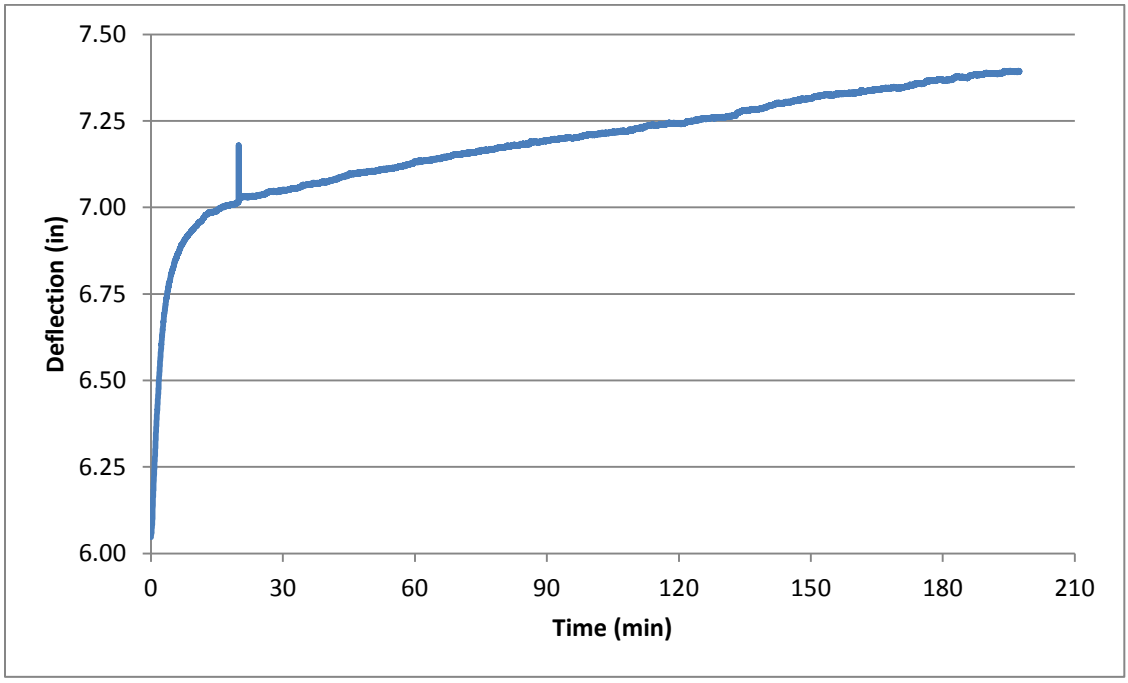

Figure 4-9: Test 3 Deflection under Sustained Load of 180 psf

Figure 4-9 shows the deflection at the total load of 180 psf versus time in the third test. After the maximum load was reached, the structure continued to deform at a steady rate for approximately ten minutes. For the following 3.5 hours that the structure remained loaded, additional deflection occurred at the column at a significantly decreased rate.

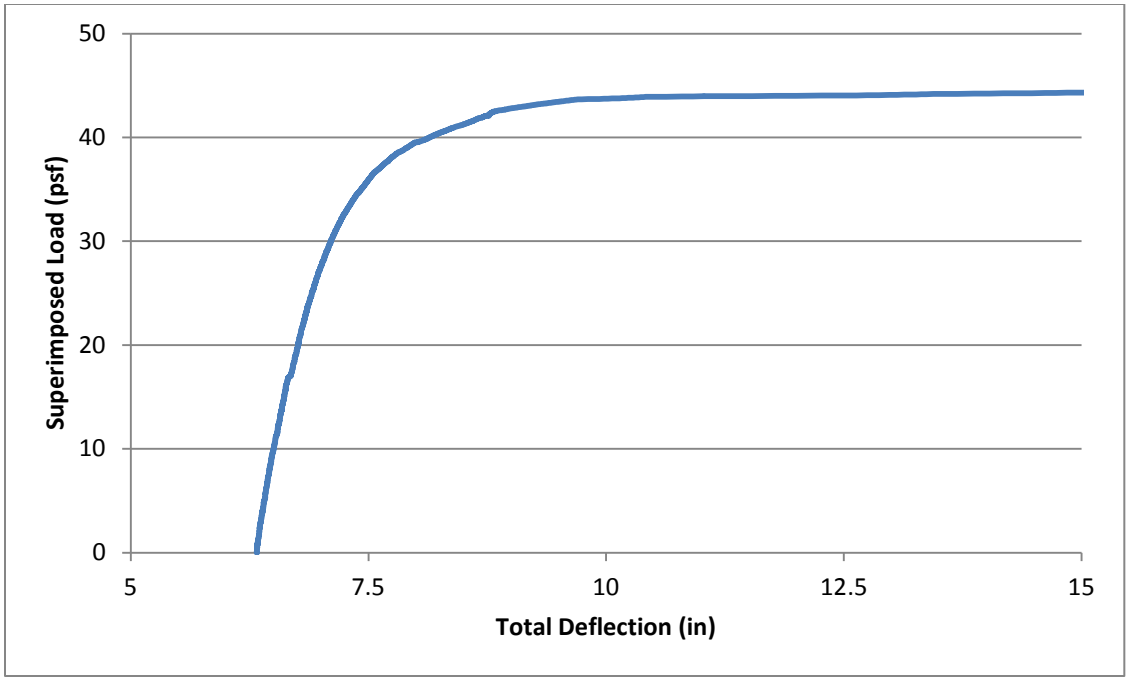

Figure 4-10: Test 4 Superimposed Loading

Figure 4-10 shows the deflection versus applied water load in Test 4. After the nuts and bolts were removed from the structural steel framing connections, the structure sagged to a deflection of 6.32 inches before additional water loading was applied. The floor system deformed at a steady rate for 1 inch of deflection over 35 psf of superimposed load before substantial softening began.

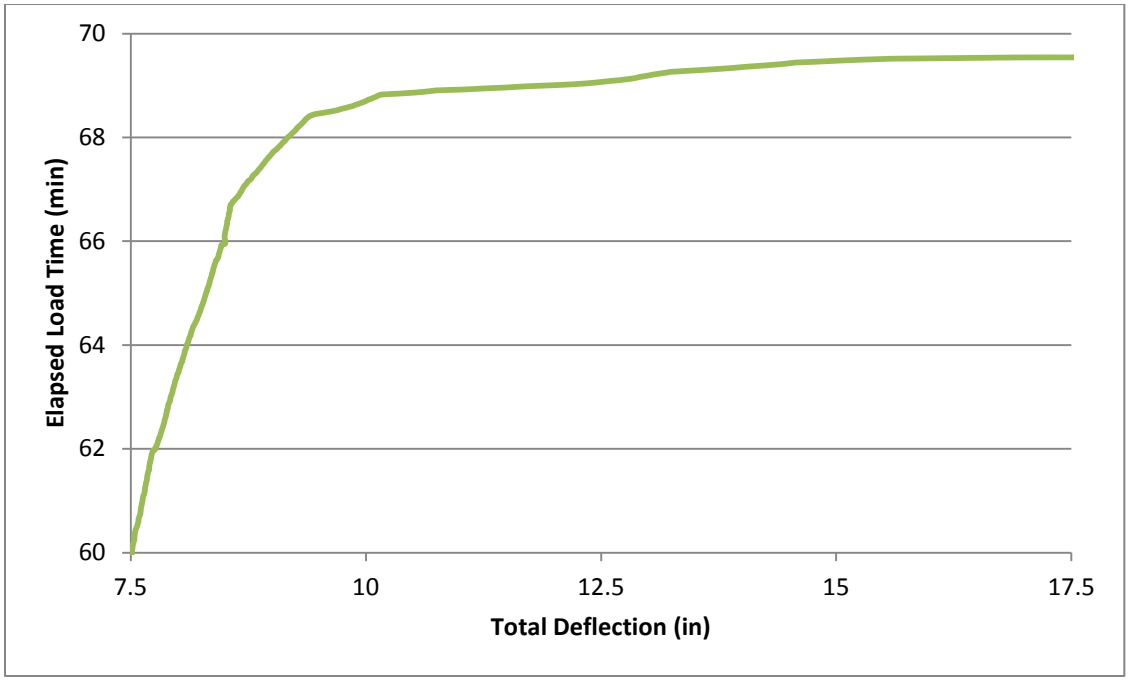

Figure 4-11: Test 4 Deflection vs. Time before Collapse

Figure 4-11 depicts the deflection of the specimen versus time in the last ten minutes before collapse. In these ten minutes, the structure deformed an additional ten inches. The softening began at a total deflection of about 7.5 inches and an applied load of 35 psf. Although the loading continued, the high rate of deformation over time indicates that the structure was unable to reach static equilibrium at these higher loads.

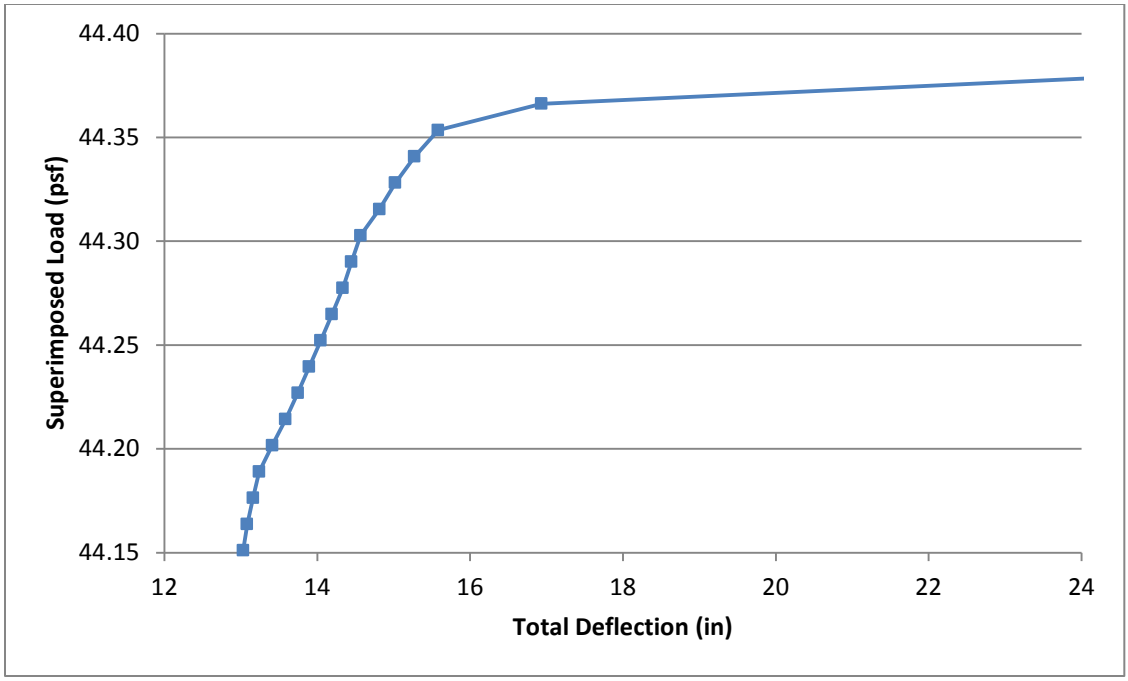

Figure 4-12: Failure of Test Specimen

Figure 4-12 shows the measured deflection versus load in the final seconds before collapse. The data points shown in the plot are one second apart. The floor system continued to deform at a steady rate until the deflection reached 15.6 inches. At this point, the structure collapsed. The superimposed load at the time of failure was 44.3 psf, but the actual failure load may be closer to 35 psf based on the rapid movement of the structure during this period of loading. Water was being pumped onto the structure continuously through the time of collapse; the high rate of displacement over time suggests that the structure was unable to stabilize under the additional load. The total collapse load of the floor specimen with no connections in the steel framing may be approximated as 155 psf including the self-weight of the specimen and the loading buckets.

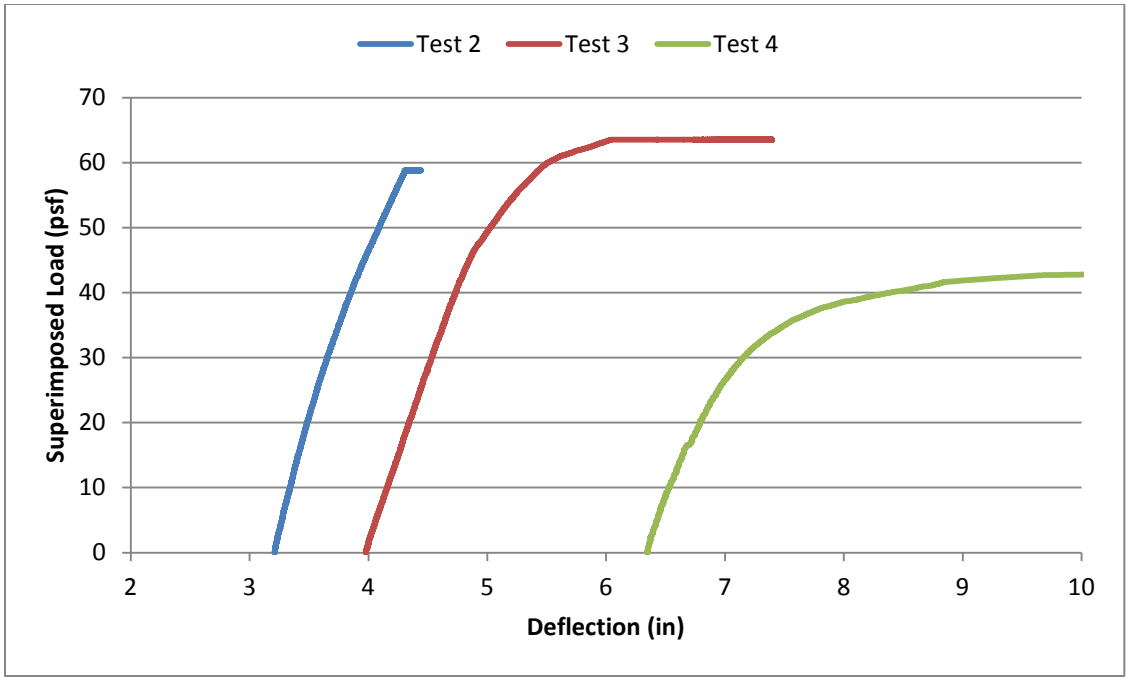

Figure 4-13: Comparison of Tests 2-4

Figure 4-13 presents the load-displacement relationship measured through Tests 2, 3, and 4. The plateaus observed in Test 2 and 3 do not depict ductile deformation, but the creep observed under the maximum applied load. The stiffness of the system reduces for each subsequent test due to the intentional weakening of the structural framing connections and likely also due to damage incurred by the specimen in the previous tests. These factors also likely contributed to the increasing initial deflection of each test. No displacement measurements could be collected during unloading of the test specimen.

4.3 STRAIN PROFILE IN GIRDERS

In this section, the measurements from the strain gages at the midpoints of each girder are examined to gain insight into the response of the girders during testing. The location of strain gages along the length of the girders and over the cross-section of the girder was described in Chapter 3. At each gaged cross-section, eight gages were attached to the girder: two on the top flange, two on the bottom flange, two near the top of the web, and two near the bottom of the web. Data from these eight strain gages are normalized to four strain locations over the depth of the cross-section by averaging the measurements on either side of the member. Curvature is calculated using the strain gradient between the measurements at the top and bottom flange. Positive strains correspond to tension and positive curvature corresponds to tension on the bottom flange of the girder. The accuracy of the assumption that plane sections remain plane can be assessed based on the plotted data for the strain at all four depths on the section.

All measurements of strain are taken relative to an initial position. The girders were instrumented after the concrete was cast but before the loading buckets were placed on the slab. Therefore, the strains measured in the first test are not an absolute measurement of strain in the section; some level of internal stress existed before the test began. In subsequent tests, the strain gages were re-zeroed at the beginning of superimposed water loading. There is no consistent reference point across tests. The primary function of the data presented in this section is the assessment of behavior during loading rather than the evaluation of the absolute stress in the girders at any time.

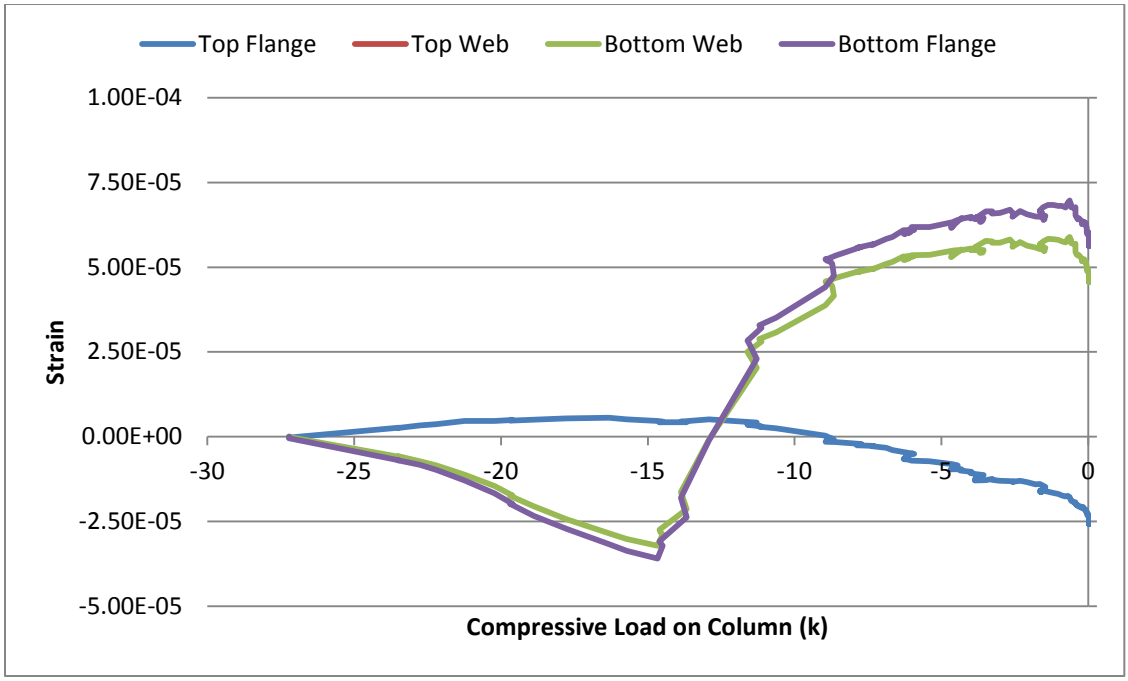

Figure 4-14: Strain in North Girder during Column Removal in Test 1

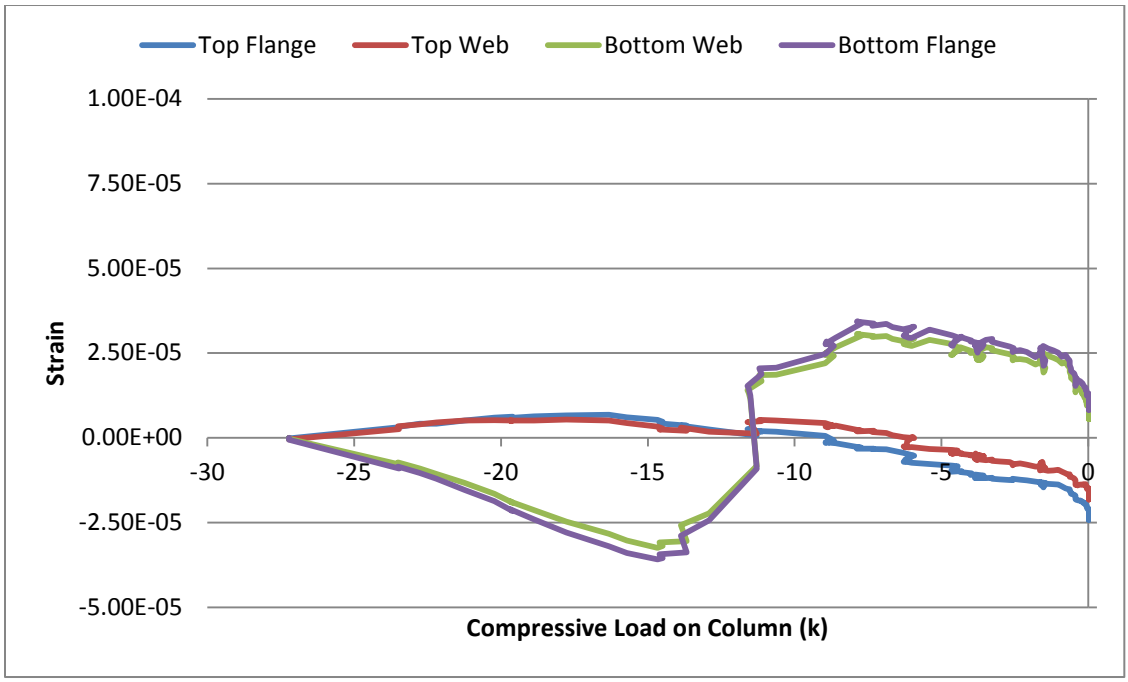

Figure 4-15: Strain in South Girder during Column Removal in Test 1

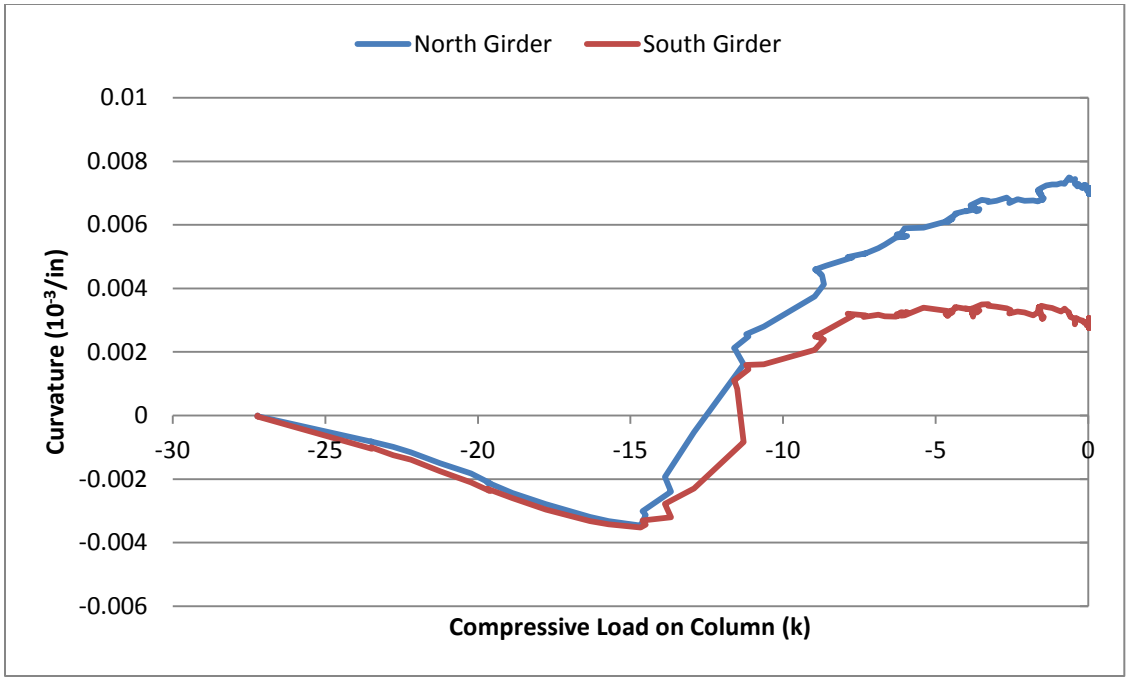

Figure 4-16: Curvature in Girders during Column Removal in Test 1

Figures 4-14 and 4-15 show the measured strains in the north and south girders respectively during the column removal procedure of Test 1. It can be noted that the measured strains are very small and well within the elastic range of behavior. The largest strain plotted in Figure 4-14 is approximately 7 x 10^{-5}. Taking a modulus of elasticity for steel of 29,000 ksi, this strain corresponds to a stress of about 2 ksi. Figure 4-16 shows the calculated curvature in each girder. The strain gages on the east and west sides of the north girder placed at the top of the web both failed during this test. Upon plotting the data, the author determined that the recorded measurements for the two strain gages were invalid due to excessive noise and unreasonable magnitudes and therefore this line has been eliminated from Figure 4-14.

In both girders, a distinct change in behavior can be observed at a load of 15 kips supported on the central column. When the column is being lowered, the girders initially shed flexural stress. Thus, the members appear to undergo reverse curvature with increasing compressive strain near the bottom of the section. After approximately 12 kips have been removed from the interior support, the girders abruptly regain stress to equilibrate the system. The north girder attracts significantly higher flexure during this procedure, indicating an asymmetrical distribution of stresses at this time.

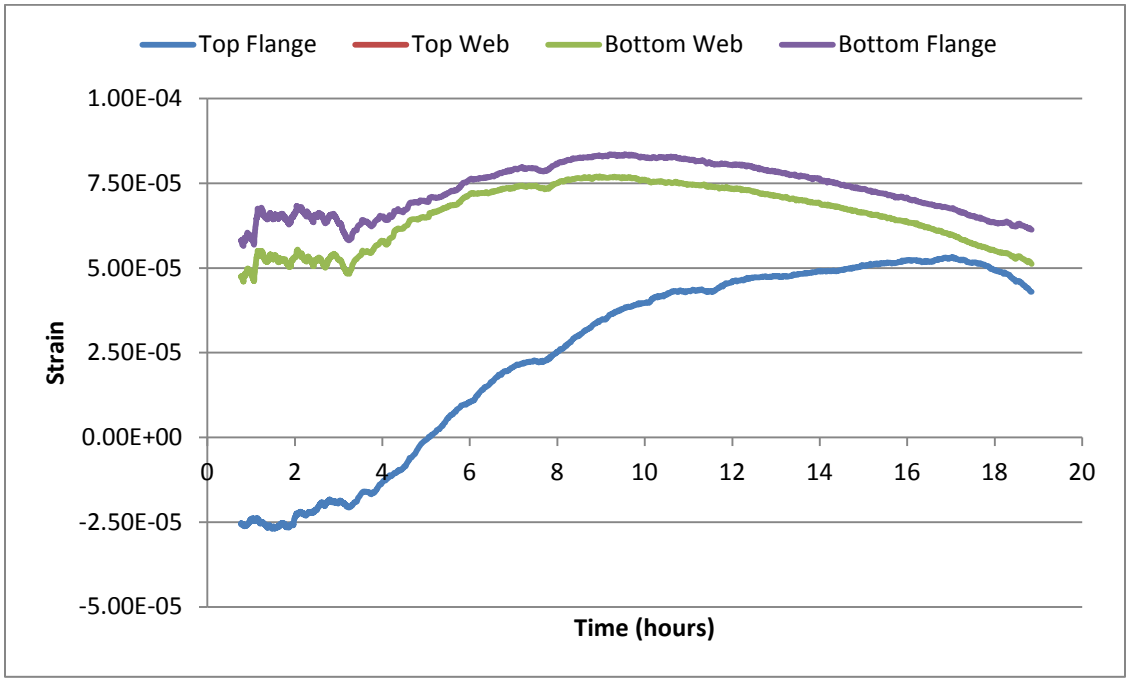

Figure 4-17: Strain in North Girder under Sustained Load

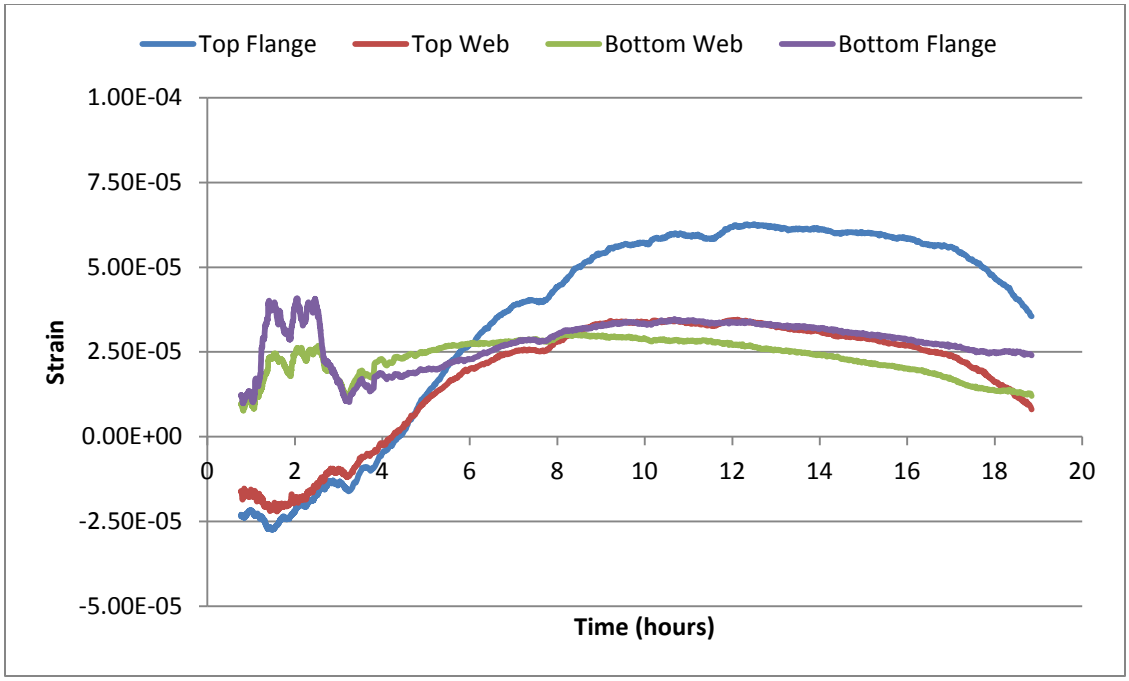

Figure 4-18: Strain in South Girder under Sustained Load

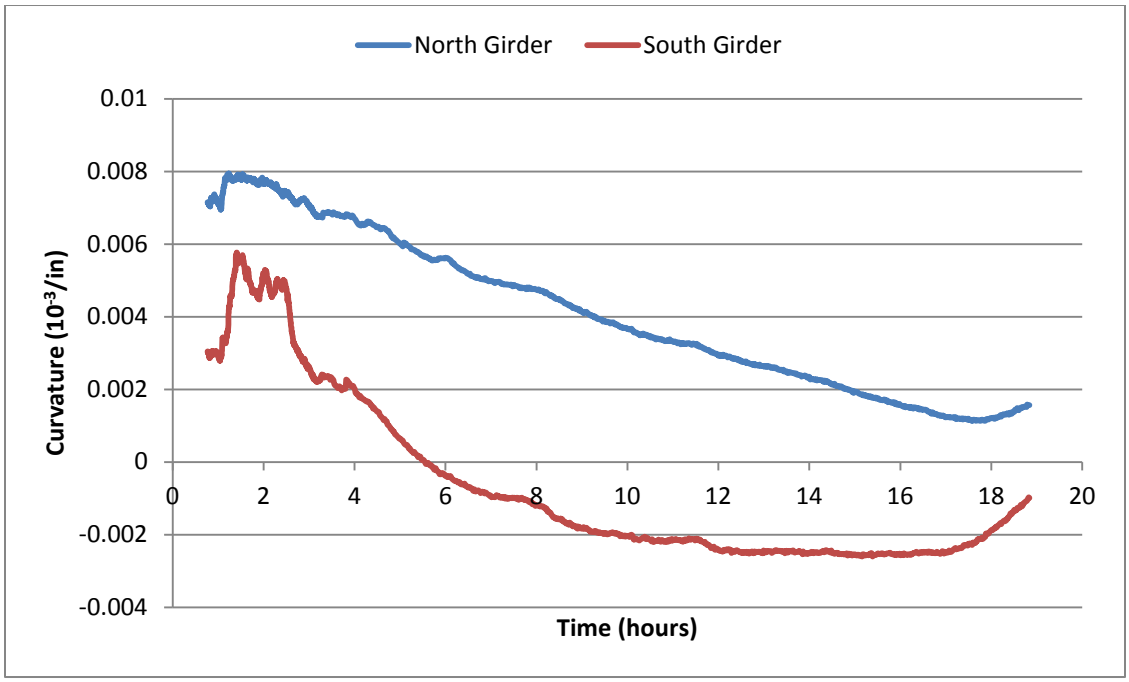

Figure 4-19: Curvature in Girders under Sustained Load

Figures 4-17 and 4-18 show the measured strains in the girder under sustained load while the structure was left unsupported overnight during Test 1. Figure 4-19 shows the calculated curvature in each girder during this period. As discussed earlier in this thesis, the floor slab continued to deform in the first three hours after column removal and then essentially stopped. Here, almost the opposite effect can be seen. The strain in the girders remained reasonably constant for the first three hours and then changed more significantly in the following hours. The strain throughout the depth of the section was primarily increasing during this time period. Although change in curvature is plotted in Figure 4-19, the strain profile does not appear to meet the requirement that plane sections remain plane. Figure 4-18 indicates that the deformation within the south girder section was not dominated by flexure.

The changes in strain observed here may be have been caused by thermal changes in the structure. The test took place outdoors on a summer day in Texas. At the end of the column removal, the temperature was approximately 100 degrees Fahrenheit. By the following morning, when superimposed loading began, the temperature had decreased to 75 degrees. The positive trend in the strains through the depth of both sections may have been caused by contraction of the steel in lowering temperatures. The high level of indeterminacy of the structure and temperature gradient throughout the structure itself makes it difficult to calculate theoretical stresses from thermal changes. However, the order of magnitude of thermal strains in this scenario is likely comparable to the small level of flexural strain measured during the test.

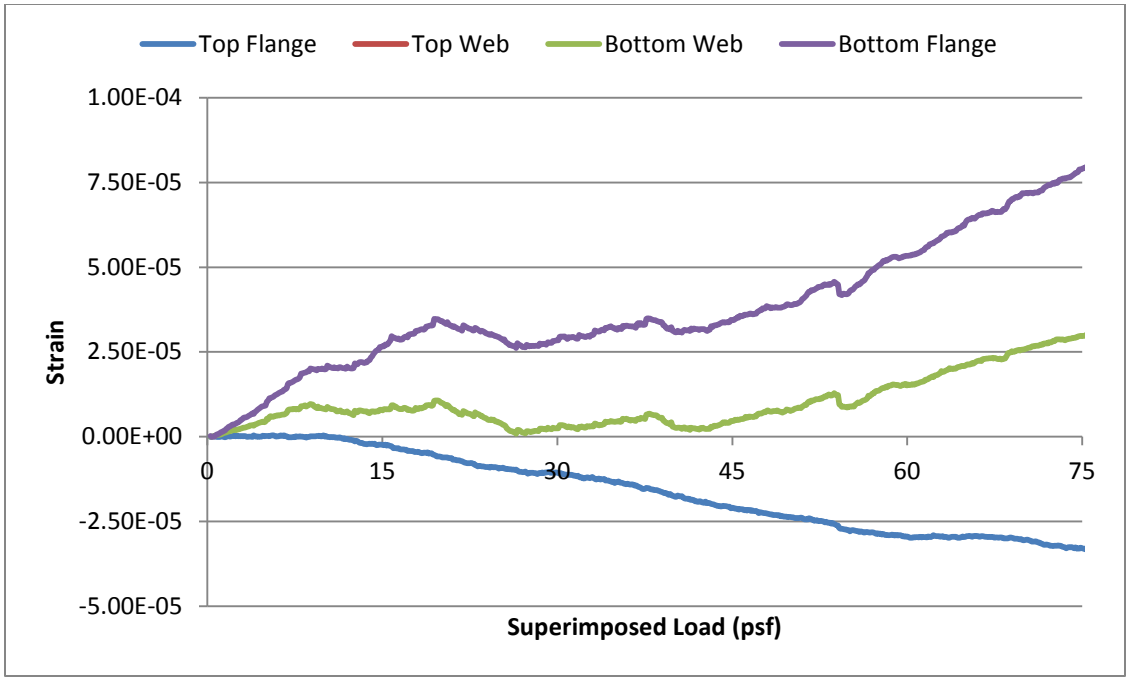

Figure 4-20: Strain in North Girder during Superimposed Loading

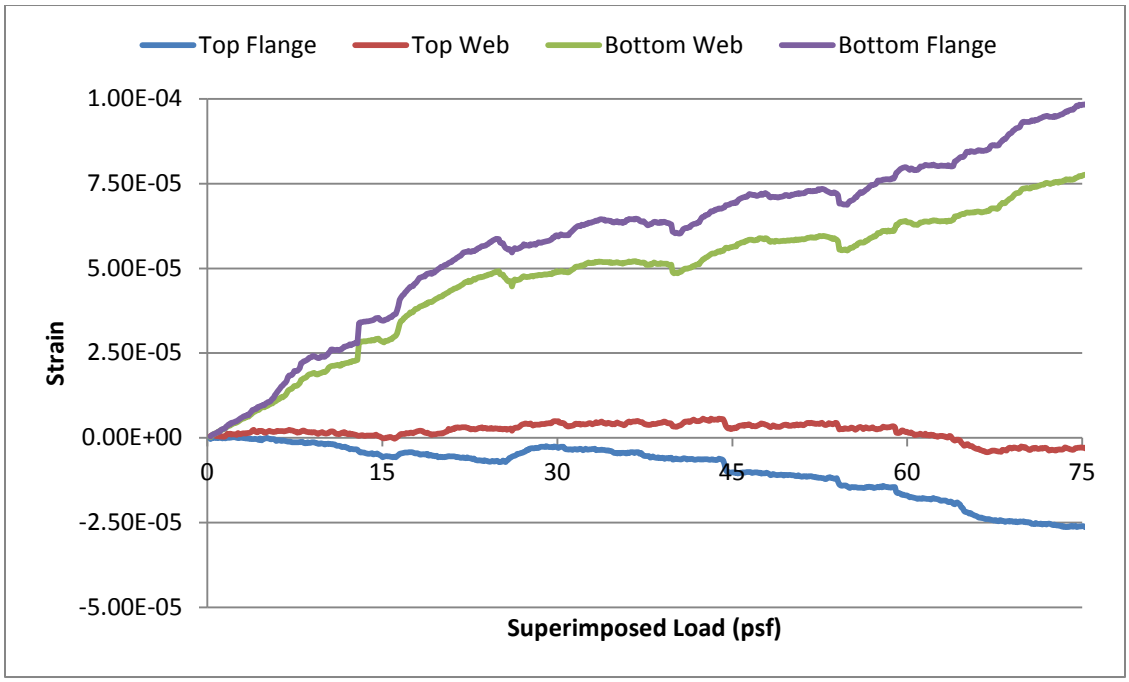

Figure 4-21: Strain in South Girder during Superimposed Loading

Figures 4-20 and 4-21 show the measured strain values during the water loading procedure of Test 1. The strain gage values have been reset to zero at the beginning of superimposed loading to show the trend during this stage of testing more clearly. The comparative strain in the top flange of both girders suggests that the neutral axis in the south girder is closer to the interface between the decking and the beam, which would be expected for a composite girder. The top flange of the north girder appears to be in the compression zone of the composite section.

In all three stages of testing, the change in strain in neither girder exceeds a value of 100 microstrain. Even with the inclusion of initial strain to approximate absolute strains in the section, it is clear that the girders did not approach their yielding capacity.

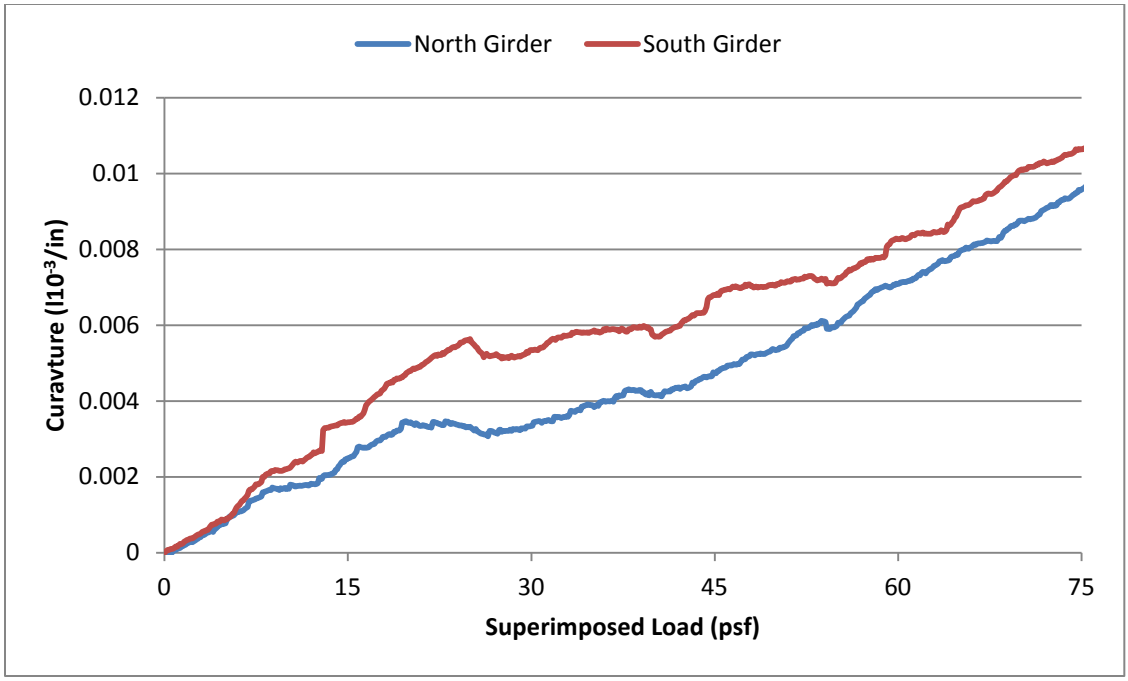

Figure 4-22: Curvature in Girders under Superimposed Load

Figure 4-22 shows the applied curvature in the girders during superimposed loading. While the north girder attracted more flexural stress during column removal, the south girder experiences higher flexure in this stage of loading. As previously stated, the relative stiffness of each girder is dependent on the level of cracking in the slab above. The distribution of load over the floor slab during this testing procedure was also uneven and may be responsible for this difference. The curvature induced in the girders under the maximum applied load of 75 psf is approximately $0.01 * 10^{-3}$/in.

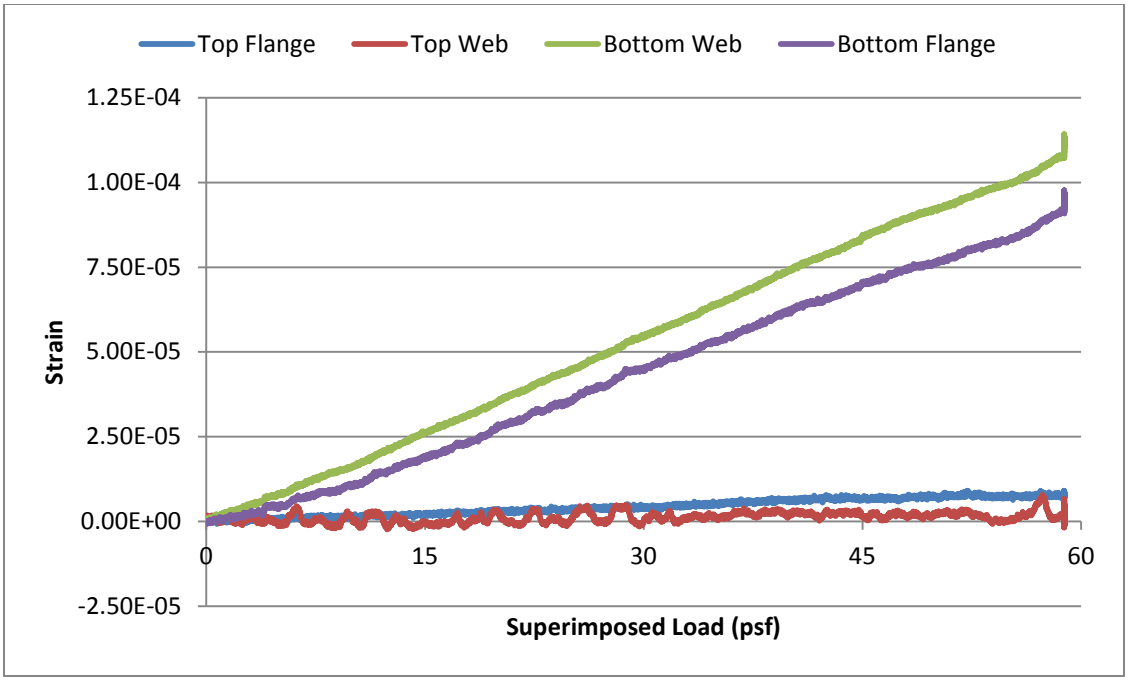

Figure 4-23: Strain in North Girder under Superimposed Load in Test 2

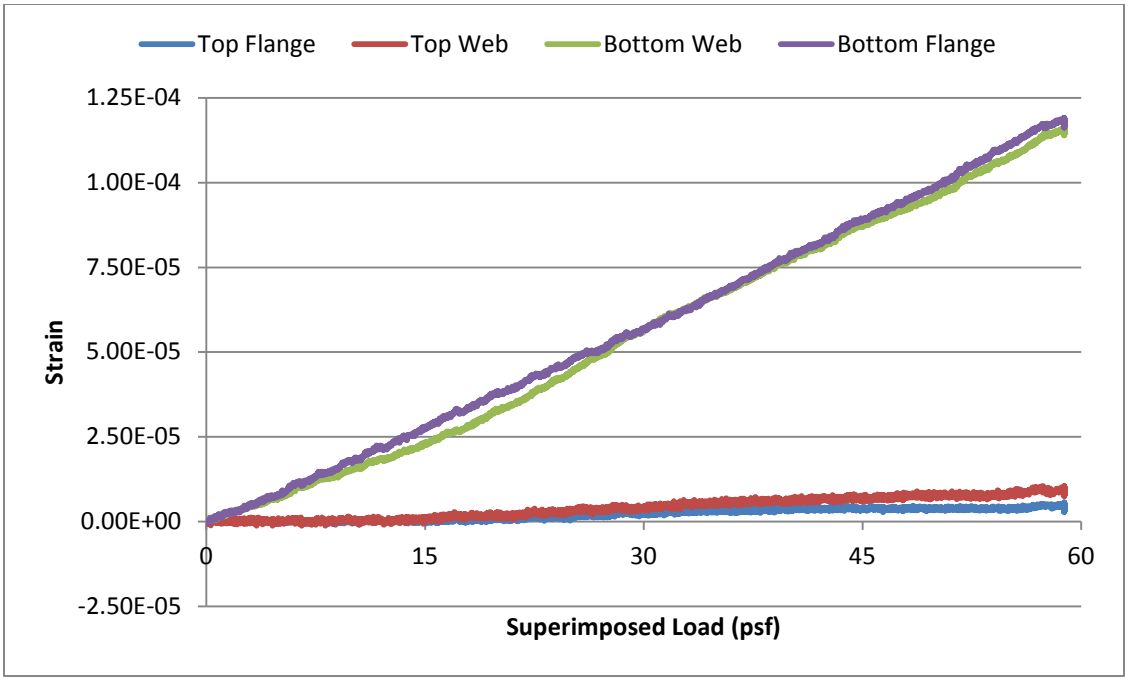

Figure 4-24: Strain in South Girder under Superimposed Load in Test 2

Figures 4-23 and 4-24 show the strains measured in each girder during Test 2. The strains were reset to zero at the beginning of superimposed loading because the absolute strain in the girder cannot be determined and the primary purpose of this data is to show the trend during loading. In Figure 4-23, the tensile strain in the bottom of the web is higher than the strain in the bottom of the flange. The strain gage on the west side of the bottom flange of the north girder was eliminated from the analysis because its measurements were excessively high. The strains measured at both the east and west sides of the bottom of the web were higher than the strain measured on the east side of the bottom flange. The reason for these trends is unclear. However, the strain values may have been too small for accurate measurements. Slight offsets in the horizontal orientation of the strain gages may have also caused error in the longitudinal strain measurements.

Unlike Test 1, where compressive strains were measured in the top flanges of each girder, the top flanges register almost zero strain throughout the course of testing in Test 2. This indicates that the neutral axis is near the interface between the decking and the girder. The concrete slab is functioning as the compressive zone of the composite section while the steel girder is in tension. Although the net axial force in the composite section cannot be calculated without more data, the tension in the girders may be contributing some resistance to the structure through catenary action.

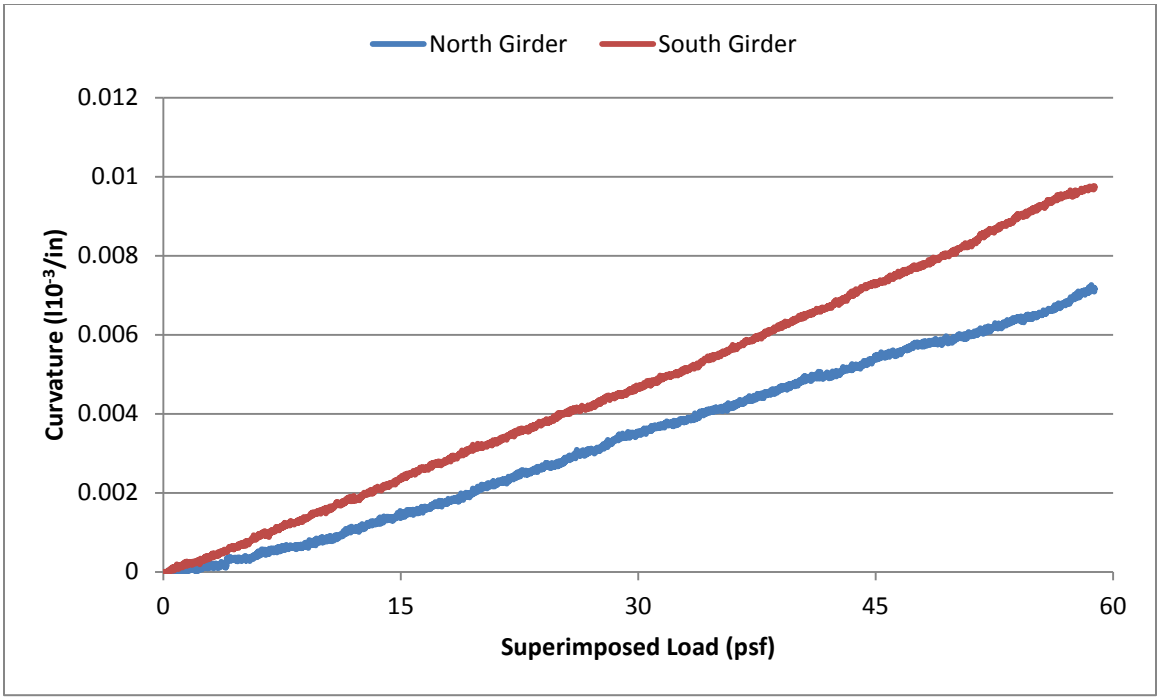

Figure 4-25: Curvature in Girders under Superimposed Load in Test 2

Figure 4-25 shows the calculated curvature in each girder during water loading in Test 2. The curvature for the north girder was determined using the curvature between the top and bottom flange as before, despite the irregularity with the strain profile given by the measurements. Figure 4-25 shows that the north girder experienced lower curvatures; if the strain gradient between the top flange and the bottom of the web is used instead, the separation between the two girders disappears.

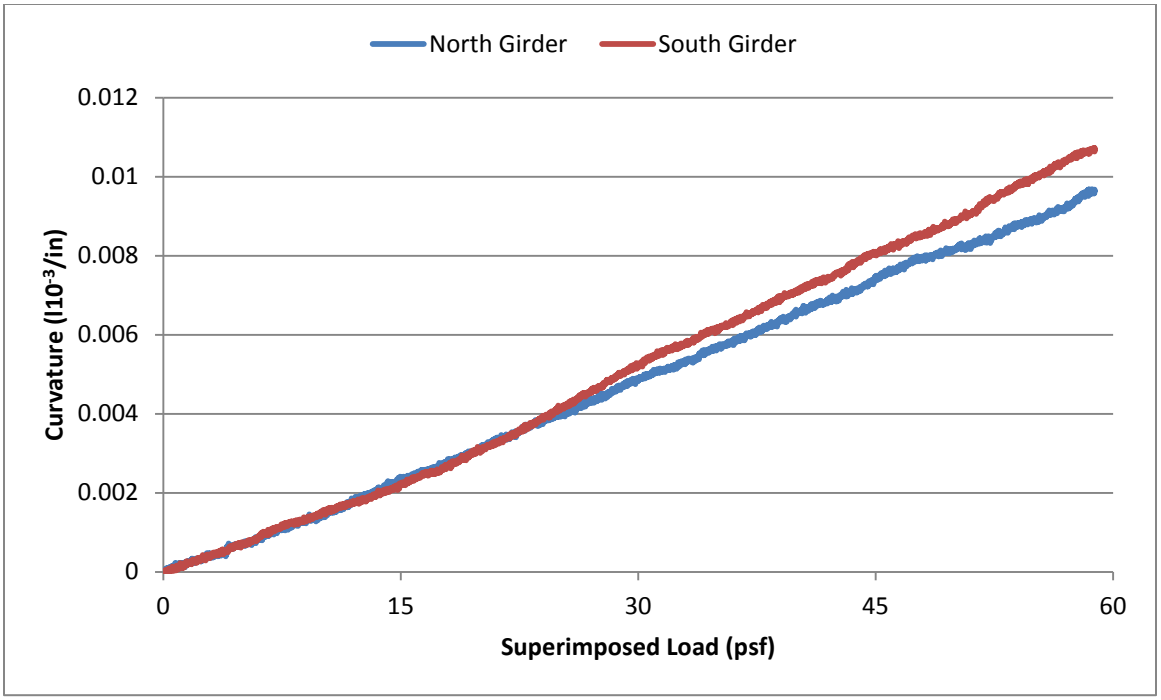

Figure 4-26: Modified Calculation of Curvature in Girders under Superimposed Load in Test 2

Figure 4-26 shows the curvature in the both girders calculated using the strain gradient between the top flange and the bottom of the web. This modification results in nearly identical strain gradients between the north and south girders under superimposed loading. The resulting curvature in the two girders at the maximum loading is approximately the same as seen in Test 1, 0.01 * 10^{-3}/in., but in this set of data there is a much clearer linear trend.

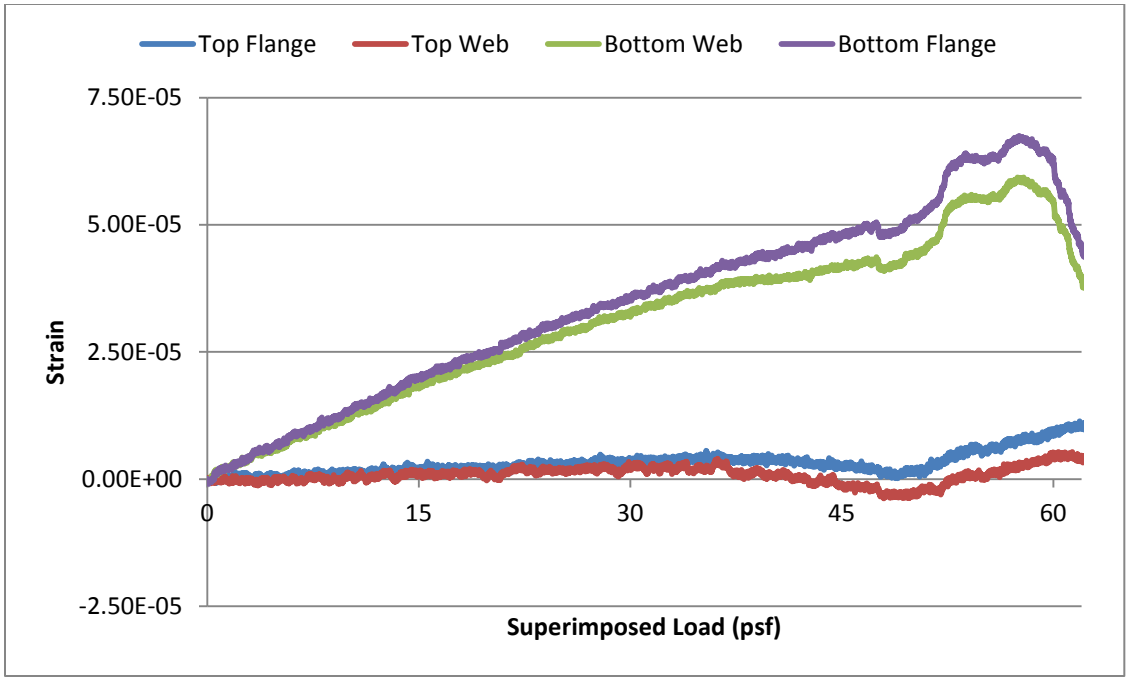

Figure 4-27: Strain in North Girder under Superimposed Load in Test 3

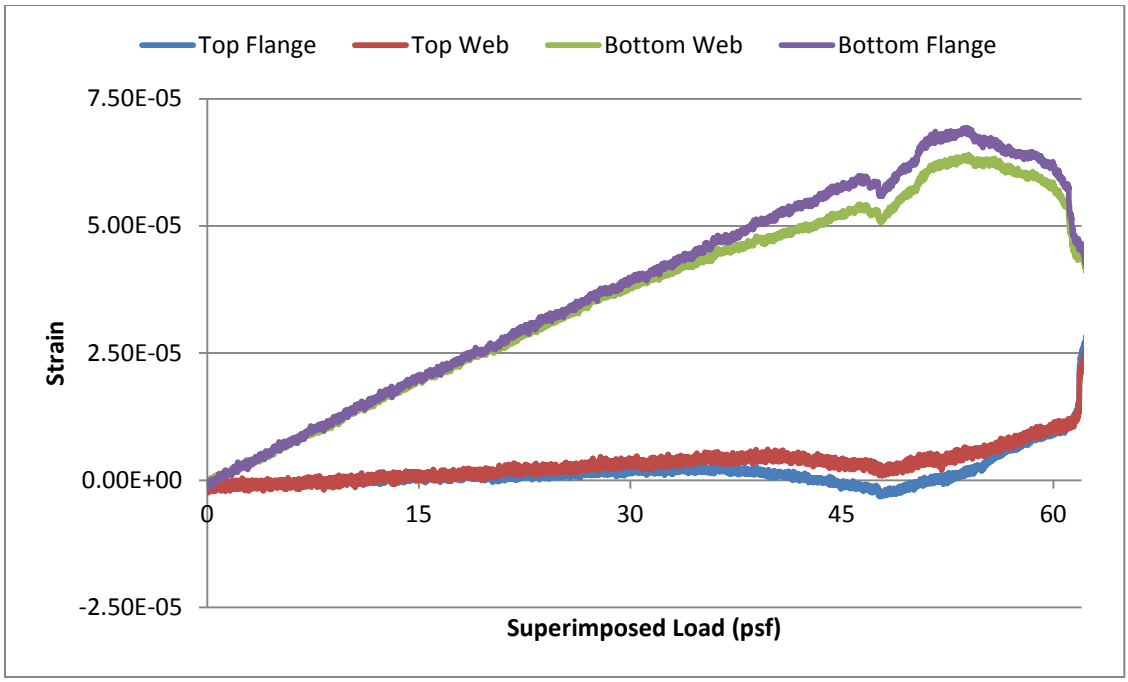

Figure 4-28: Strain in South Girder under Superimposed Load in Test 3

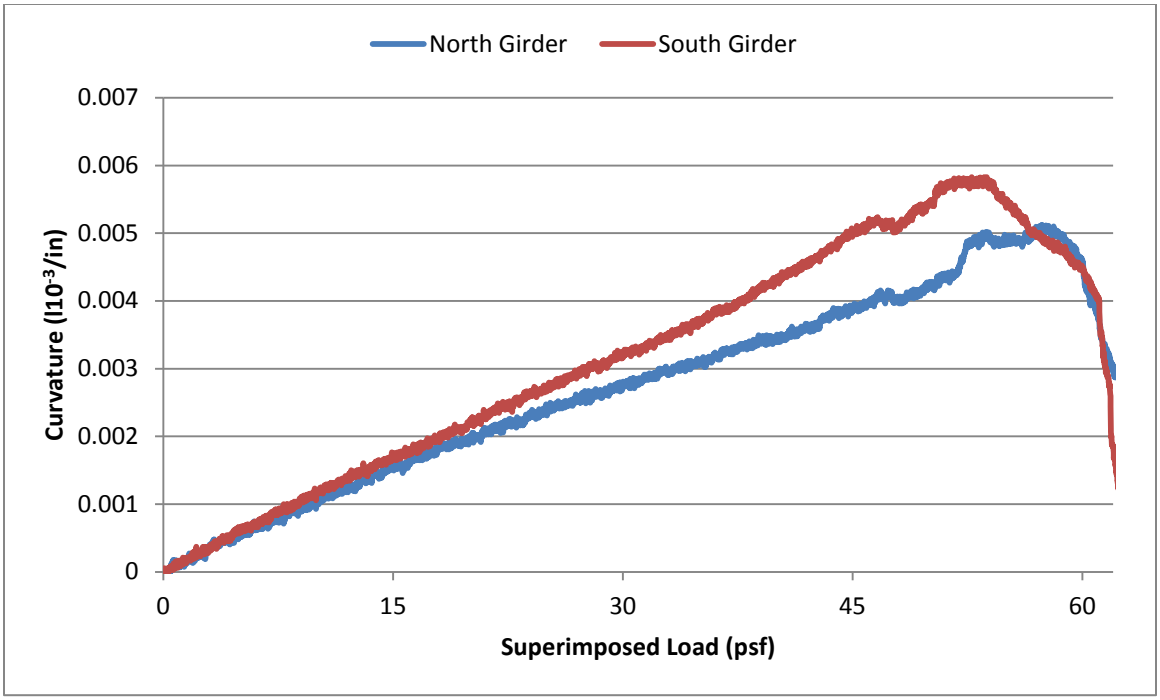

Figure 4-29: Curvature in Girders under Superimposed Load in Test 3

Figures 4-27 and 4-28 show the measured strains in the girders during Test 3. Figure 4-29 shows the calculated curvature in each girder. With the removal of the nuts from the bolts, the tensile and flexural resistance at the double angle connection to the interior column is significantly reduced. As a result, the behavior of each girder is between the response of a pinned-pinned beam and the response of a pinned-fixed beam, due to the rotational resistance at the connection to the restraining beams. Changing this boundary condition alone would increase the positive moment developed at midspan. However, this change reduced the stiffness of the girders. As the system reached higher deformation, a higher proportion of the load was carried by two-way action of the composite floor system. Therefore, the maximum curvature developed in the girders is only $0.006 * 10^{-3}$/in.

Softening was observed in the load-deflection plot around a load of 50 psf. In Figure 4-29, the curvature abruptly begins to drop off. When the curvature is plotted against time, the change in behavior is especially evident.

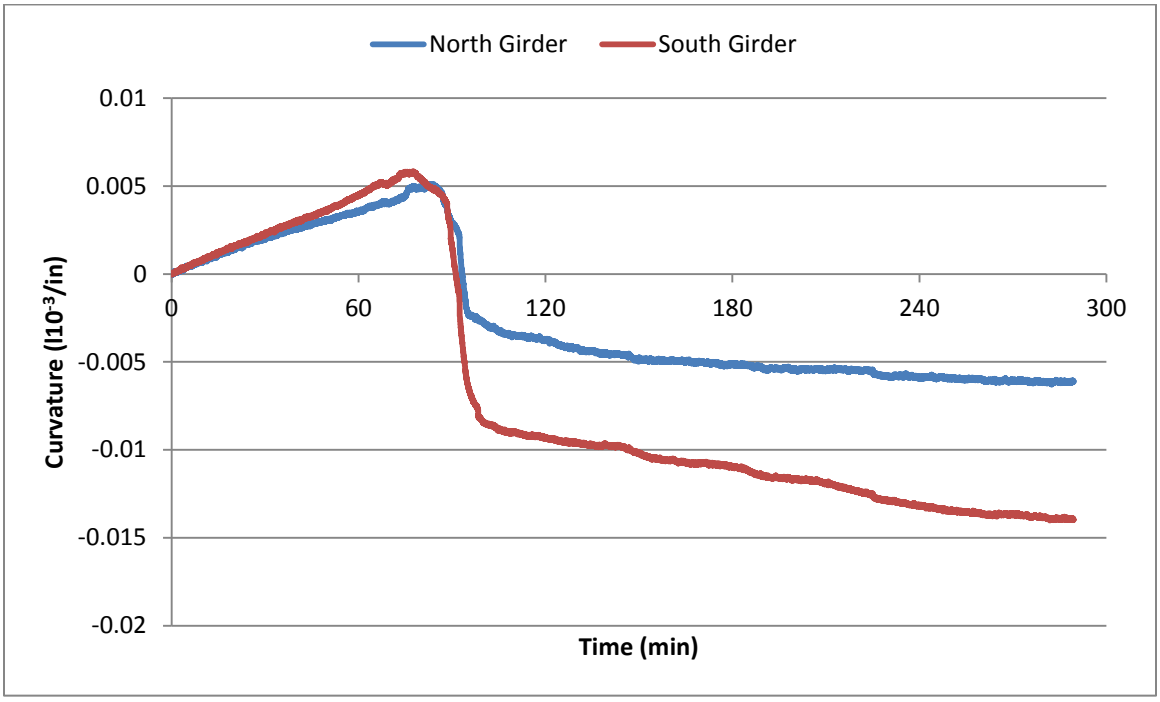

Figure 4-30: Curvature in Girders vs. Time in Test 3

Figure 4-30 depicts the change in curvature in the girders over time. The applied loading lasted approximately 90 minutes. During this period of time, the positive curvature in the girders gradually increased. Once the load reached a value of 50 psf, however, the curvature in the girders rapidly dropped off and changed sign. While deformation in the slab increased from 5 inches to 7 inches, the curvature in the south girder went from +0.005 * 10^{-3}/in. to -0.01 * 10^{-3}/in. over a period of only twenty minutes. The thermal changes in the girder are not sufficient to explain this magnitude of

change. It is possible that the floor system exhibited “snap-through” behavior. The sudden increase in negative curvature at the midpoint of the girders suggests that a hinge formed in the composite decking at the central connection. The rotational restraint at this point was lost, causing each girder to act independently as a cantilever. Only after undergoing substantial deformation was the structure able to reach equilibrium. The stability of the structure after “snap-through” may have been achieved through multiple resistance mechanisms, such as an increase in the reaction moment at the connection to the restraining beam and catenary action in both the girders and the floor.

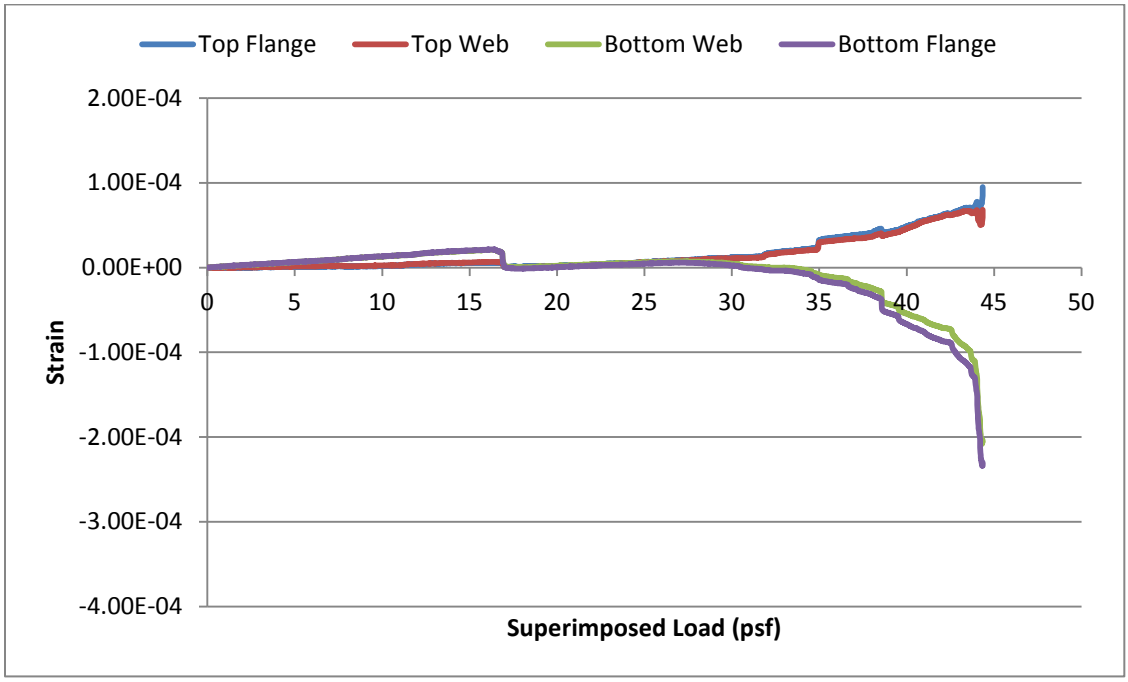

Figure 4-31: Strain in North Girder under Superimposed Load in Test 4

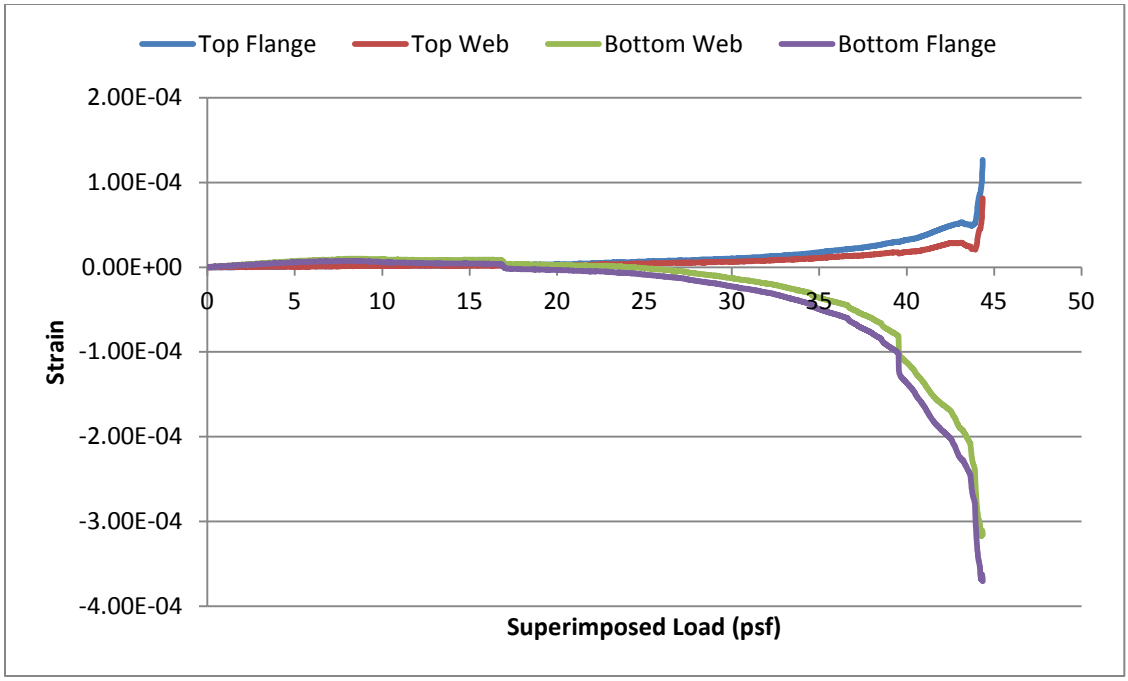

Figure 4-32: Strain in South Girder under Superimposed Load in Test 4

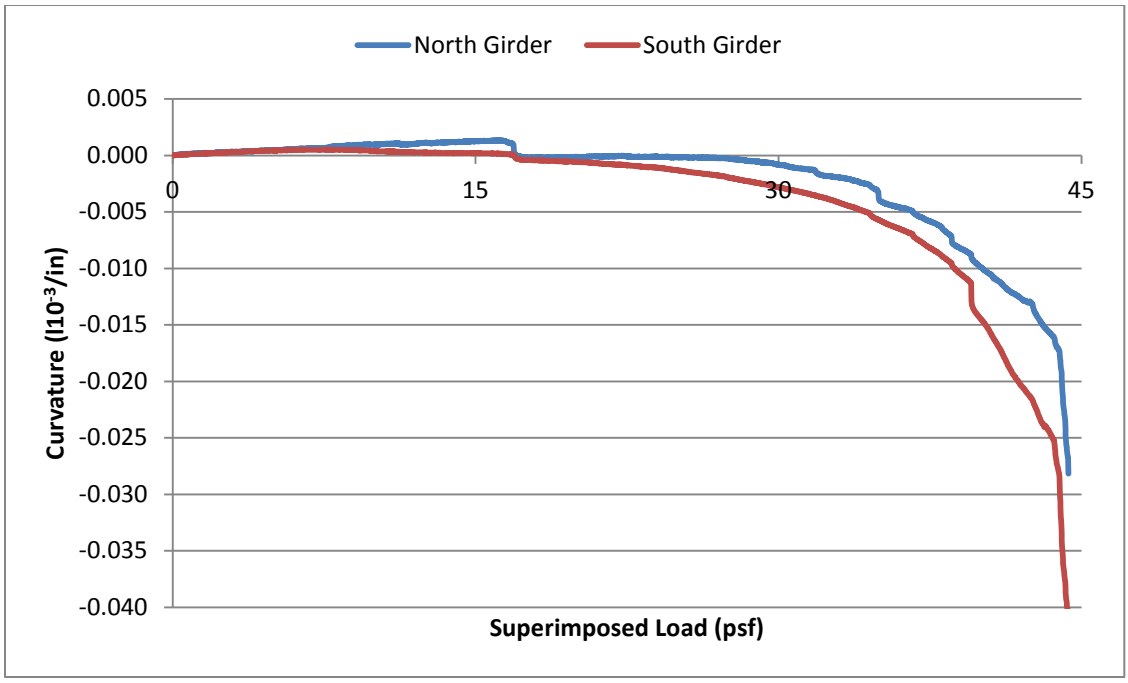

Figure 4-33: Curvature in Girders under Superimposed Load in Test 4

Figures 4-31 and 4-32 show the strains measured in each girder during Test 4. Figure 4-33 is a plot of the calculated curvature in each girder. The two girders experience very low levels of positive flexure in the beginning of the loading in Test 4. Due to the removal of the bolts from all connections, stresses are only being transferred into the members through the shear studs. As softening begins around a load of 35 psf, the girders develop substantial negative curvature. The magnitude of the stress in the girders leading up to collapse far exceeds the positive flexure developed in Tests 1-3, approaching -0.04 * 10^{-3}/in. in curvature at the time of collapse. The maximum strains in the girder, even during collapse, do not suggest that yielding occurred, even allowing a large margin of error for the inclusion of initial strain.

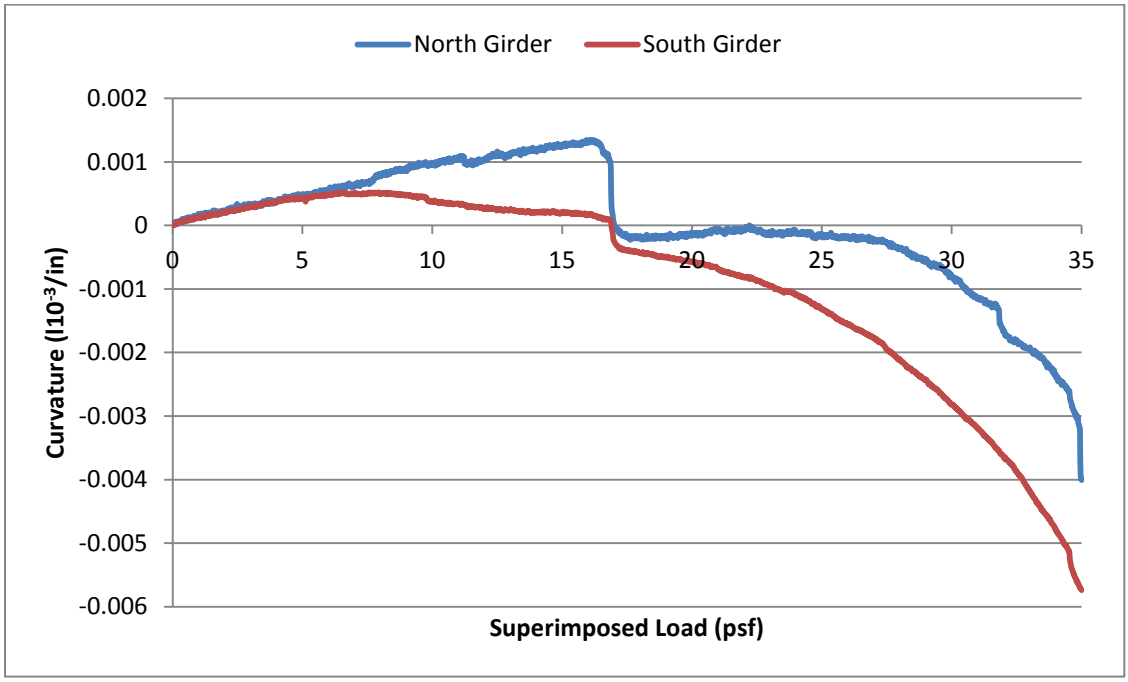

Figure 4-34: Curvature in Girders at Beginning of Test 4

Figure 4-34 shows the calculated curvature in the girders under the first 35 psf of loading. The snap-through point appears to occur at a load of 16 psf, when total deflection reached 6.65 inches. The change in deformation rate at this load is essentially undetectable, but the change in behavior is evident in the strain data. Up until this load point, the girders undergo increasing positive curvature. After snap-through, the girders begin to develop negative curvature.

4.4 BEAM AND GIRDER ROTATIONS AT INTERIOR COLUMN

The rotations at the central connection of both primary beams and girders were measured using the horizontal linear potentiometers described in Chapter 3. The difference between the average top displacement and average bottom displacement was divided by the vertical distance between the instruments to calculate the rotation in radians. The values calculated for the east and west primary beams were averaged, as were the values for the north and south girders. The horizontal potentiometers experienced significant signal noise and damage during the tests due to their exposure to water. Where certain instruments malfunctioned, their data was removed from the calculations.

The chord rotation of a beam or girder, as presented herein, was calculated using the total vertical deflection at the base of the interior column divided by the span length of 15 feet. The vertical displacement of the members at the restraining beam connections was assumed to be negligible compared to the vertical displacement of the column base.

The initial rotation in Tests 2-4 was approximated using the chord rotation for the initial displacement of the column at the beginning of each test.

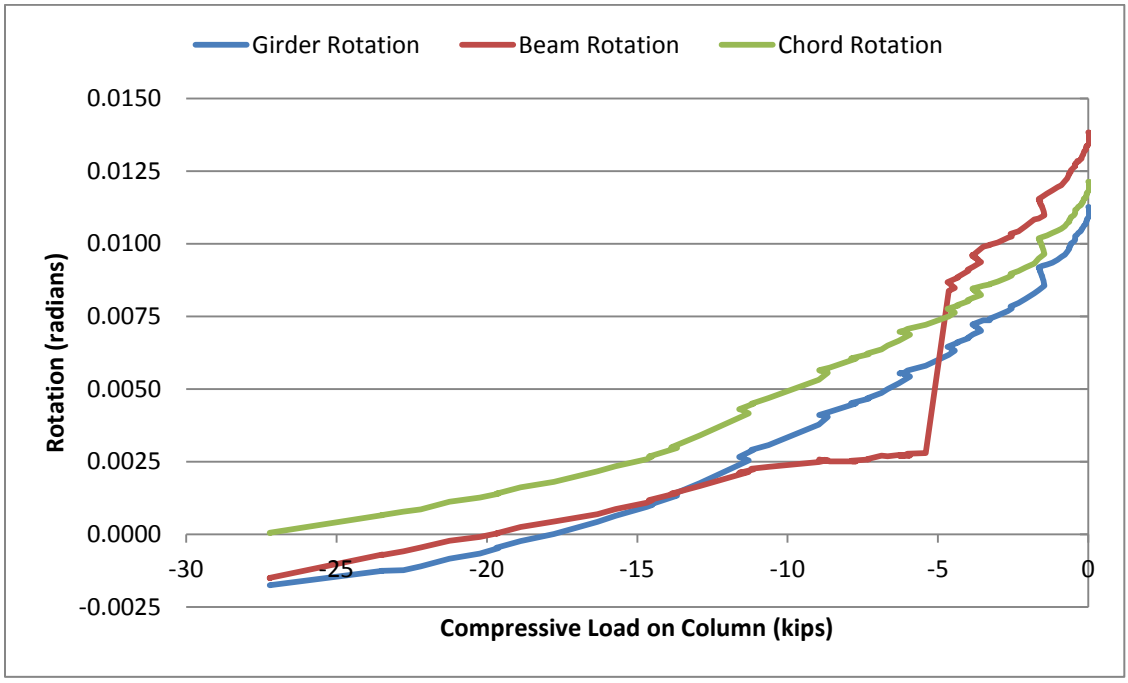

Figure 4-35: Rotation of Beams and Girders during Column Removal

The rotations of the beam and girder connections at the interior column during column removal in Test 1 are shown in Figure 4-35. The horizontal linear potentiometers were zeroed before the loading buckets were placed on top of the specimen. Based on the assumed deformed shape of a two-span continuous beam, the rotations at the central connection before column removal are expected to be negative. The rotation due to self-weight is not included in these measurements.

As the column was lowered, the rotation of the members at the central connection switched from negative to positive at a load of approximately 20 kips. The change in

flexural strain in the girders, as seen in Figure 4-25, occurred at a column load of 15 kips. Since the initial negative rotation is underestimated, it seems possible that the change in flexural stress coincided with the change in sign of the rotation. With the column in place, the flexural stiffness of the composite decking and the partial restraint of the double angle connections induce negative curvature in either end of the girders. As the column is lowered, the negative moment at the perimeter connection increases and the positive moment at the midpoint of the beams and girders decreases. After the rotation at the central connection becomes positive, the two girders begin to behave more like a continuous beam with a rotational spring at the center. Greater positive rotations at the central connection increase the positive moment developed at the midpoint.

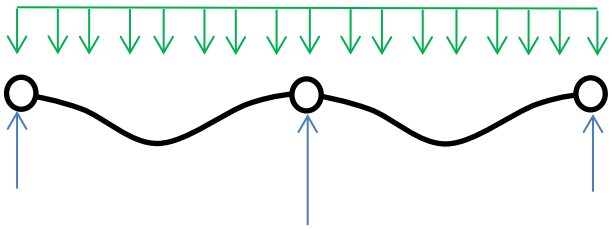

Girder deformed shape before column

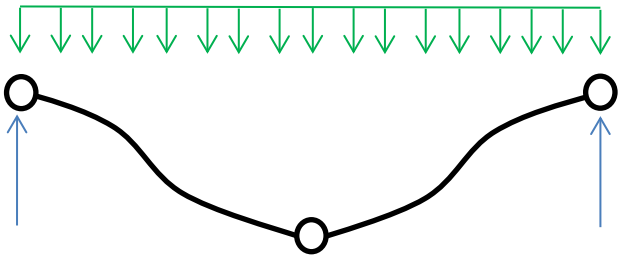

Girder deformed shape after column removal

Figure 4-36: Diagram of Change in Girder Deformed Shape

Figure 4-36 qualitatively illustrates the assumed deformed shape in the two girders before and after column removal as supported by the data described above. The circles in the diagram represent the rotational springs at each connection. When the rotation at the central connection switches from positive to negative, the area of negative curvature in the center of the span is eliminated.

There is much lower rotational fixity at either end of the primary beams because of the orientation of the steel decking. They behave more like simply supported spans. After the column is removed, they are supported by a shear reaction at the central connection from the girders due to their higher level of stiffness and by the development of axial tension. The rotation of the beams switches from negative to positive approximately when the chord rotation exceeds the flexural rotation at the central connection.

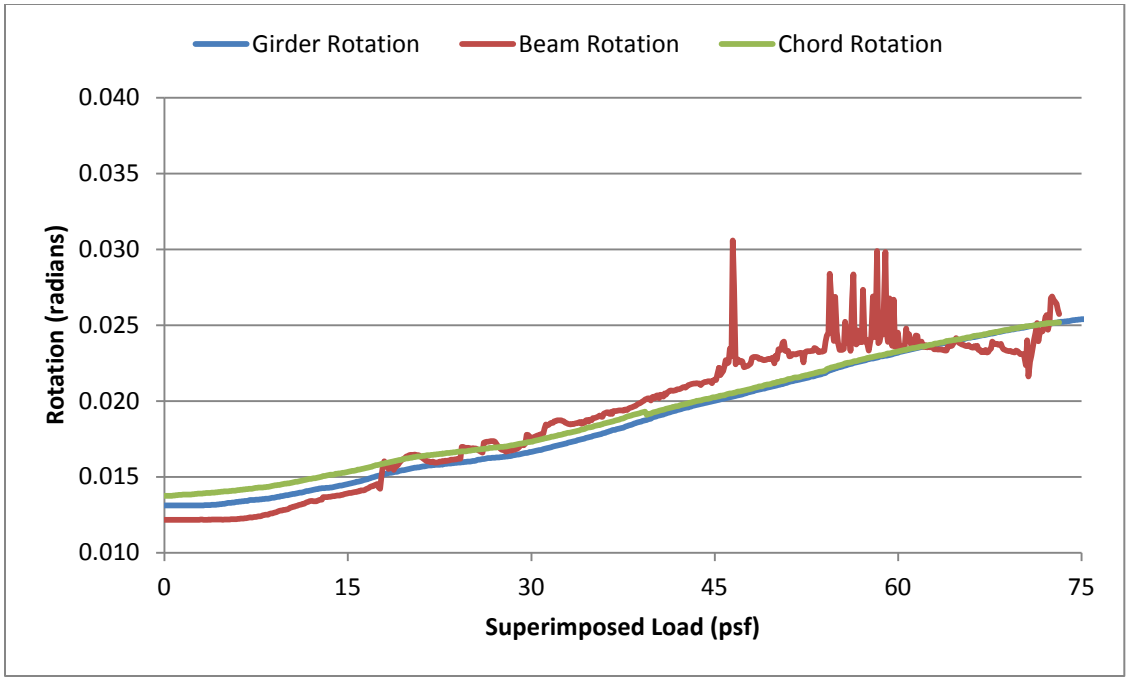

Figure 4-37: Rotation of Beams and Girders under Superimposed Load - Test 1

Figure 4-37 shows the change in rotation in the beams and girders under the superimposed water loading in Test 1. The data collected by the beam instrumentation is too uncertain to draw clear comparisons between the behavior of the beams and girders. The connections of the girders to the interior column undergo a rotation of 0.014 radians during the course of water loading. As the load on the specimen increases, the rotation at the end of the girder converges with the chord rotation. This suggests that the flexural deformation of the girder is decreasing and proportionally more load is being carried through catenary action at higher displacements.

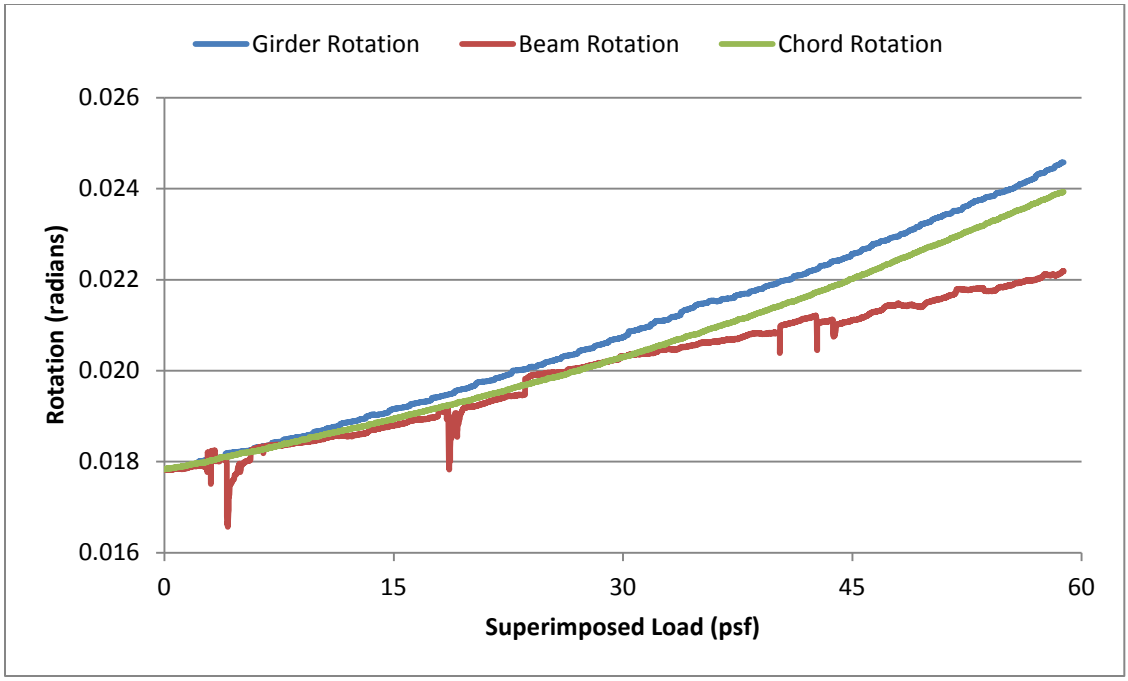

Figure 4-38: Rotation of Beams and Girders in Test 2

Figure 4-38 shows a plot of the measured rotation in the beams and girders experienced in Test 2 compared to the chord rotation calculated from the total displacement of the central connection. The girder rotation exceeds the chord rotation, indicating the development of negative curvature in the member. The beam rotation is lower than the chord rotation, suggesting that it is deforming as a simply supported beam between the restraining beam and the central connection. The maximum rotations measured at the end of Test 2 are approximately 0.024 radians in the girder and 0.022 radians in the beam.

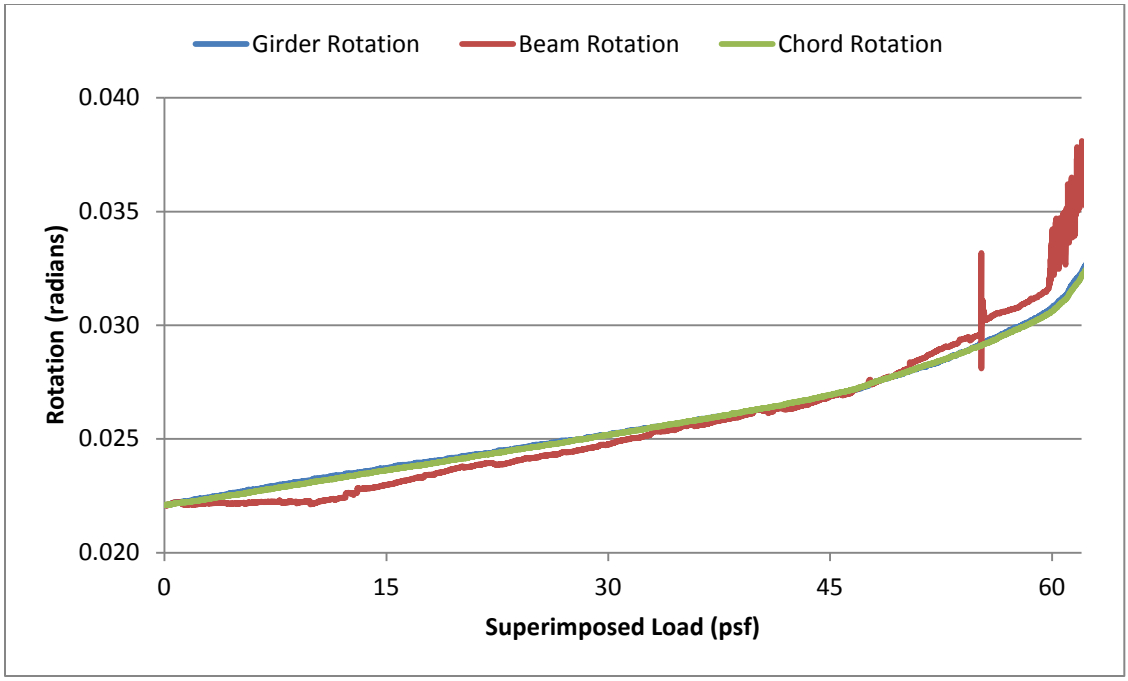

Figure 4-39: Rotation of Beams and Girders in Test 3

Figure 4-39 shows the rotation of the beams and girders along with the chord rotation measured during water loading in Test 3. The chord rotation and the girder rotation are very similar, suggesting that the beams and girders are rotating as rigid bodies.

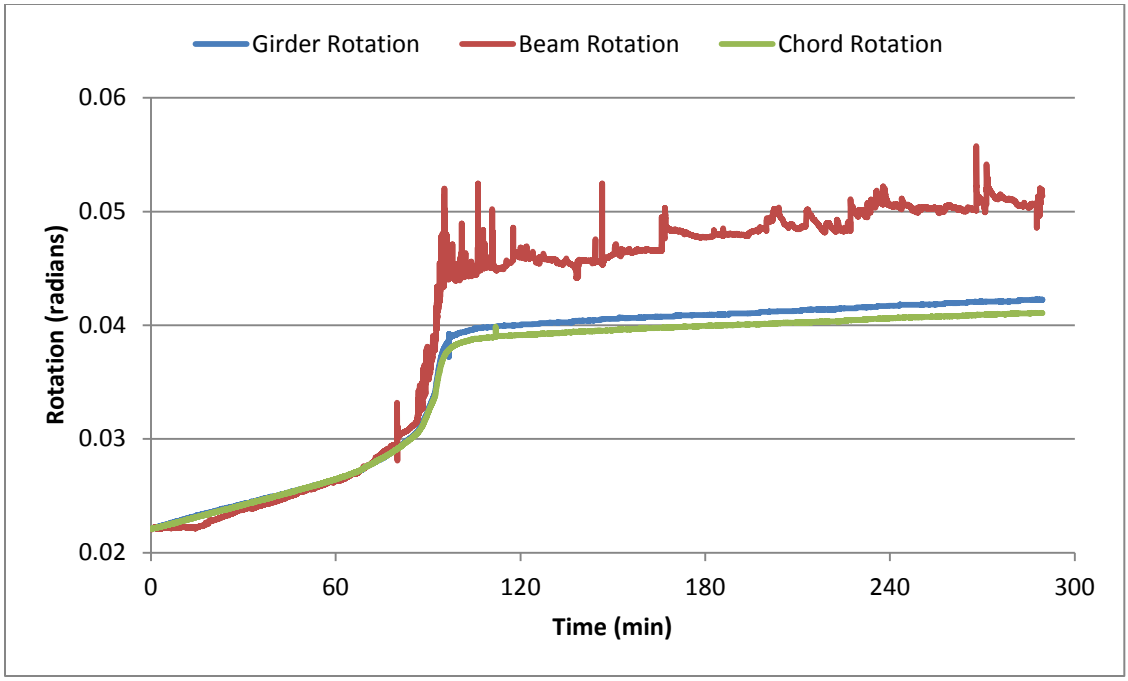

Figure 4-40: Rotation of Beams and Girders vs. Time in Test 3

Figure 4-40 shows the rotation measurements versus time in Test 3 to include the behavior observed after loading was completed. The same dramatic change in behavior starting at a load of 50 psf that was observed in the girder strain data can be seen in the rotation measurements. The large increase in rotation at the connections at this load supports the previous conclusion that the composite floor system may be undergoing plastic rotation in the central region.

The large increase in rotations begins at about 0.03 radians. The girder rotation continues to match the chord rotation closely during the sudden increase in deflection. After the hinge forms, however, the beam undergoes substantially more rotation. This behavior does not match the intuitive understanding of the deformation in the specimen. The measured rotation in the beam is higher than the calculated chord rotation for the

level of end displacement, suggesting that the beam is undergoing negative curvature while the girder rotates rigidly. Intuitively, there should be greater flexure in the girders because the composite decking should provide substantially more rotational restraint at the perimeter of the specimen along the axis of the girders.

This inconsistency may indicate some problems in the measurements or calculations of rotation. Slip in the decking system may also be contributing to unexpected deformation in the specimen. Figure 4-41 shows the connection of the girder to the ring beam after the completion of the third test. The slip at the top flange of the girder is visible. Further experimental research is necessary to investigate this behavior.

Figure 4-41: Girder to Ring Beam Connection after Test 3

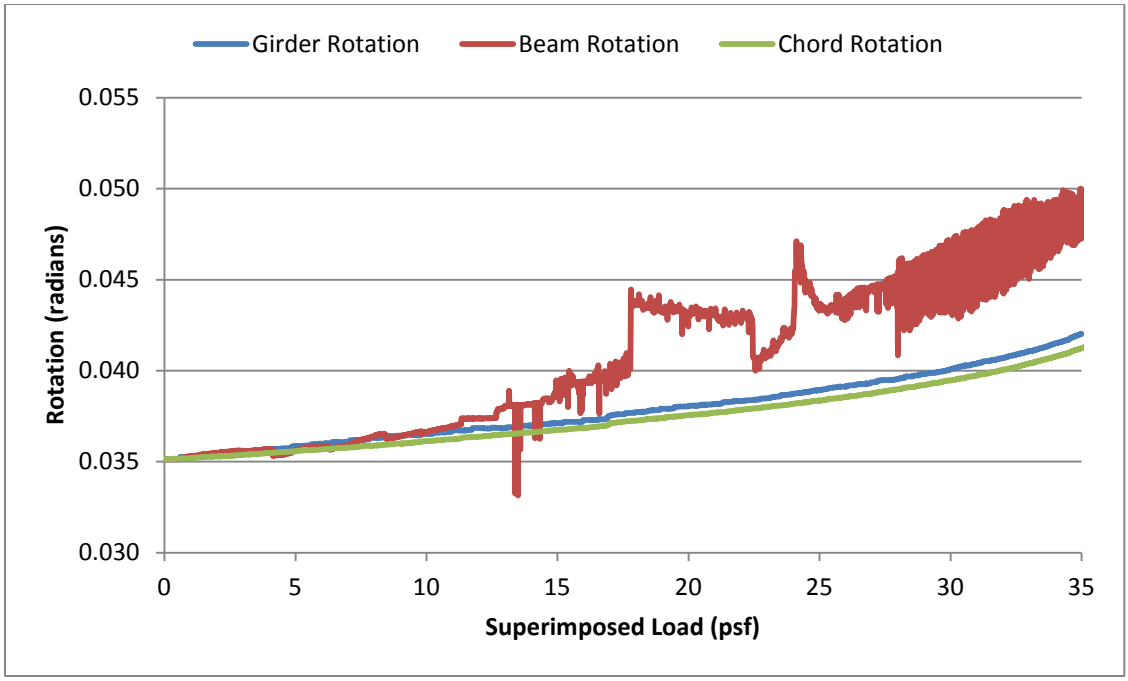

Figure 4-42: Rotation of Beams and Girders at Beginning of Test 4

Figure 4-42 shows the rotation versus superimposed load using the data that was collected for the first 35 psf of loading, before collapse was initiated. A significant proportion of the horizontal potentiometers malfunctioned during the fourth test, reducing the data available for analysis.

As seen in Figure 4-42, the beam rotation measurements are particularly unreliable in this test, but the data indicates that the beam rotation is higher than the chord rotation. As previously discussed, this trend does not coincide with current understanding of the specimen behavior. The girders appear to be rotating rigidly throughout this test.

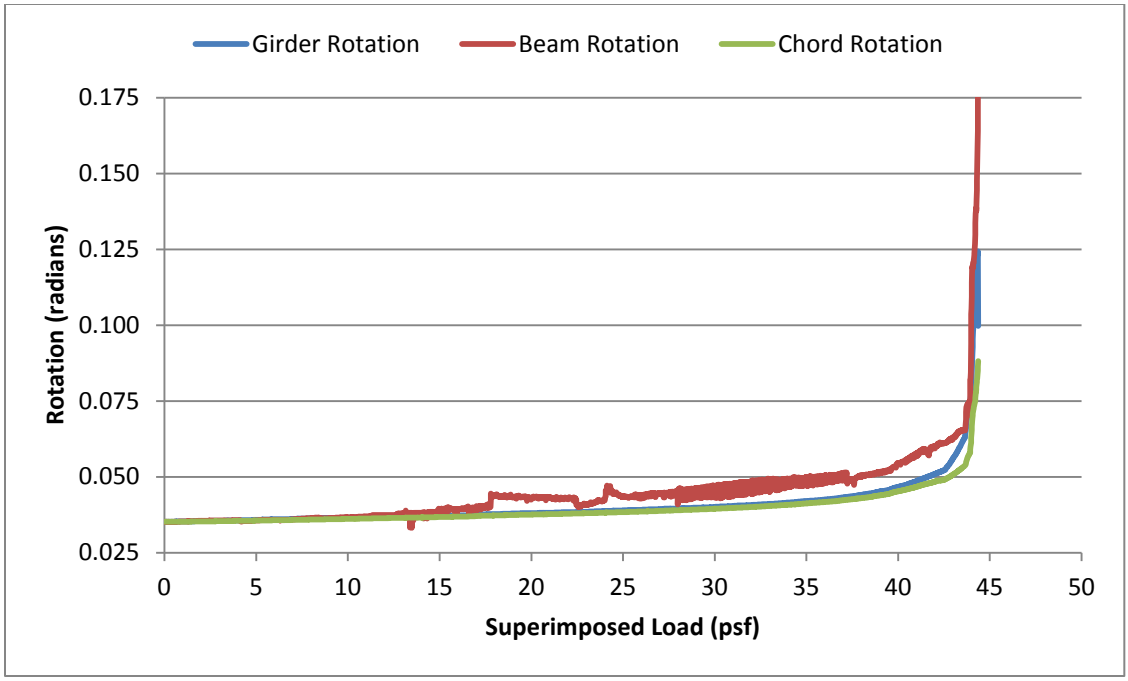

Figure 4-43: Rotation of Beams and Girders in Test 4

Figure 4-43 shows the relationship of beam and girder rotations to superimposed load through the collapse point in Test 4. As expected, the rotations increase dramatically in both the beams and girders as the structure moves towards collapse in the final minutes of loading. The highest measured rotation before total collapse was approximately 0.12 radians in the girders and 0.17 radians in the beams. Without the nuts and bolts in place, the steel framing connections did not contribute any flexural resistance to this rotation. The rotation observed at the ends of the beams and girders may be considered an upper bound on the required deformation capacity of these connections to prevent failure at a lower load.

4.5 RESTRAINING BEAM FLEXURE

The data from the strain gages on the restraining beams was used to measure an approximation of flexural stress and bending moment in the restraining beams over the course of testing. The location of strain gages on the restraining beams was described in Chapter 3. The average strain at the top and average strain at the bottom were used to calculate vertical curvature. “Vertical” curvature corresponds to bending of the restraining beam in a vertical direction that is perpendicular to the plane of the undeflected floor slab. The average strain on the inside and average strain on the outside were used to calculate lateral curvature. “Lateral” curvature corresponds to bending of the restraining beam in a horizontal direction, i.e., in the plane of the undeflected floor slab. Positive curvatures and moments correspond to tension on the bottom and inside edges of the beams. The moment of inertia on each axis of the restraining beam was calculated including the half inch plates welded to the top and bottom of the section. The modulus of elasticity of steel was taken as 29,000 ksi. The restraining beams were considered non-composite due to their proportionally high stiffness, so stresses in the floor slab were neglected in the calculation of moment.

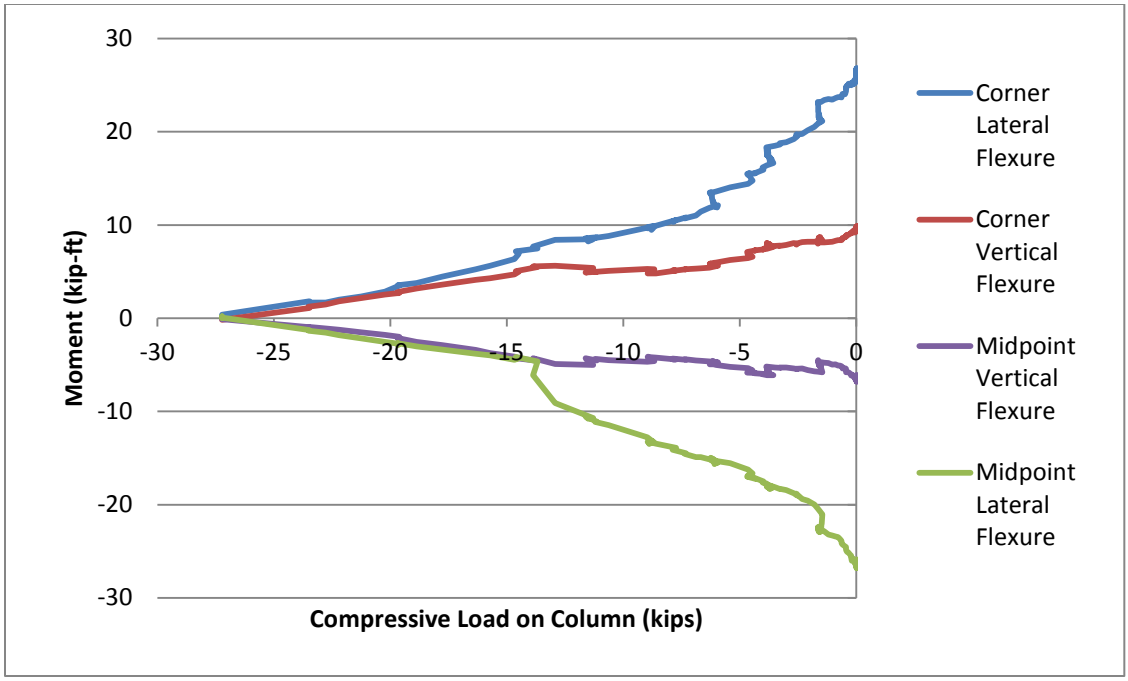

Figure 4-44: Moments in East and West Restraining Beams during Column Removal in Test 1

Figure 4-44 shows the lateral and vertical moments measured at the midpoint and at either end of the east and west restraining beams. The midpoint of the restraining beams where the strain gages were placed is actually an intermediate support point. The strain gages are only offset from the centerline of the intermediate columns by less than a foot. As a result, the midpoint sections experienced negative moment while the corner sections experienced positive moment. The magnitude of the lateral flexure during column removal is significantly higher than the vertical moments, suggesting that the restraining beams were seeing significant in-plane forces.

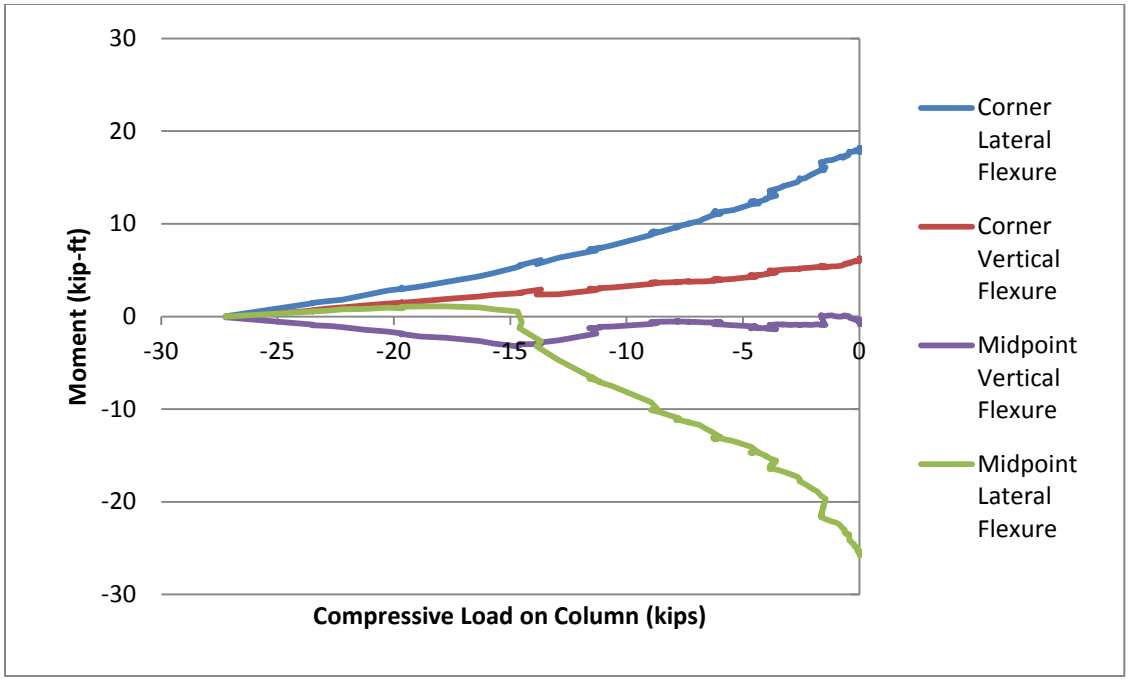

Figure 4-45: Moments in North and South Restraining Beams during Column Removal in Test 1

Figure 4-45 shows the lateral and vertical moments measured in the north and south restraining beams during the column removal in Test 1. At a column load of 15 kips, the curvature in the girder switched from increasingly negative to increasingly positive (see Figures 4-14 and 4-15). The effect of this behavior can be seen in the flexure at the midpoint of the north and south restraining beams. The lateral moment increases from essentially zero to -25 kip-ft. during the removal of the final 15 kips from the interior support. After the change in flexural behavior in the girders, they began to apply significantly lateral (in-plane) force to the restraining beams. This may indicate the development of catenary action as a significant source of resistance.

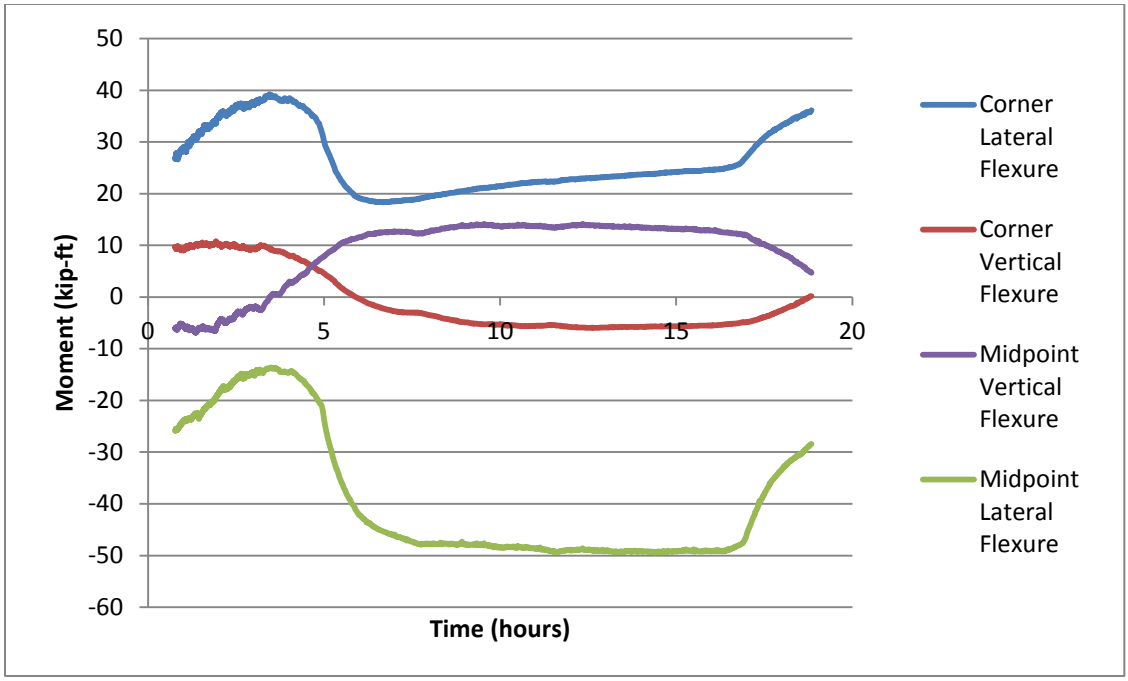

Figure 4-46: Moments in East and West Restraining Beams under Sustained Load in Test 1

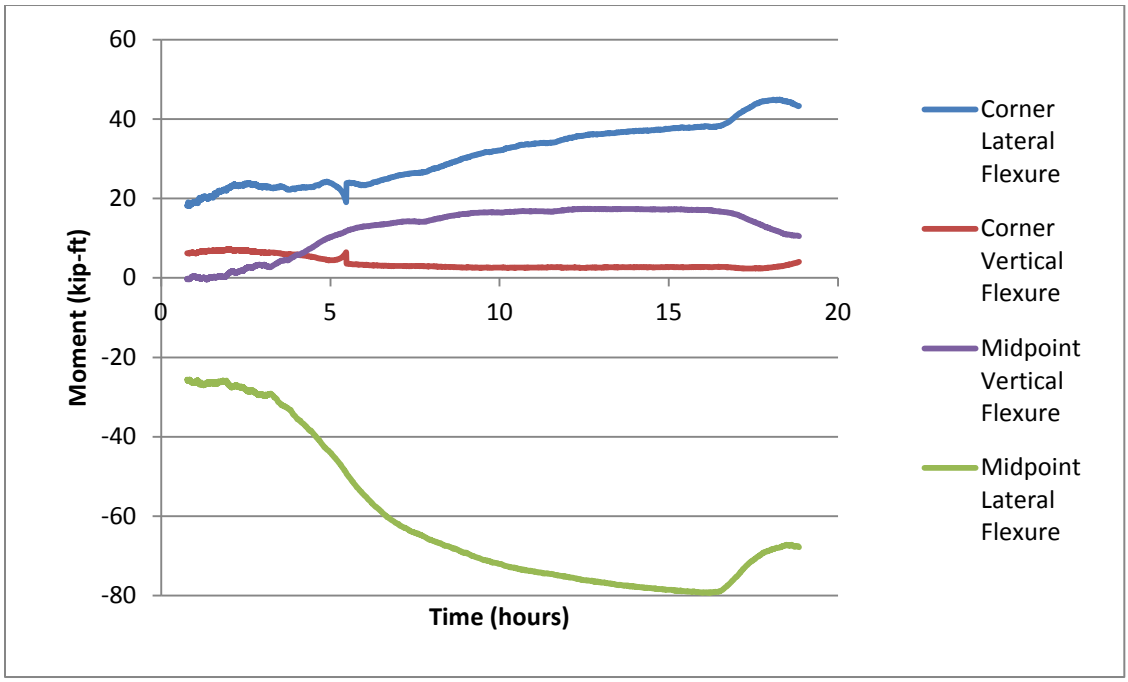

Figure 4-47: Moments in the North and South Restraining Beams under Sustained Load in Test 1

Figures 4-46 and 4-47 show the calculated lateral and vertical moments in the restraining beams while the structure was left unsupported. Overnight, the strains in the restraining beam changed significantly. In all four beams, the vertical curvature essentially inverted during this time period. The calculated lateral flexure experienced changes in magnitude as large as the deformation experienced during the column removal. The tension in the outer face of the restraining beams increased significantly overnight, resulting in large negative curvature. This was most likely caused by thermal contraction as the air cooled. Since the strains in the restraining beam caused by structural loading were so small, they were prone to significant temperature effects.

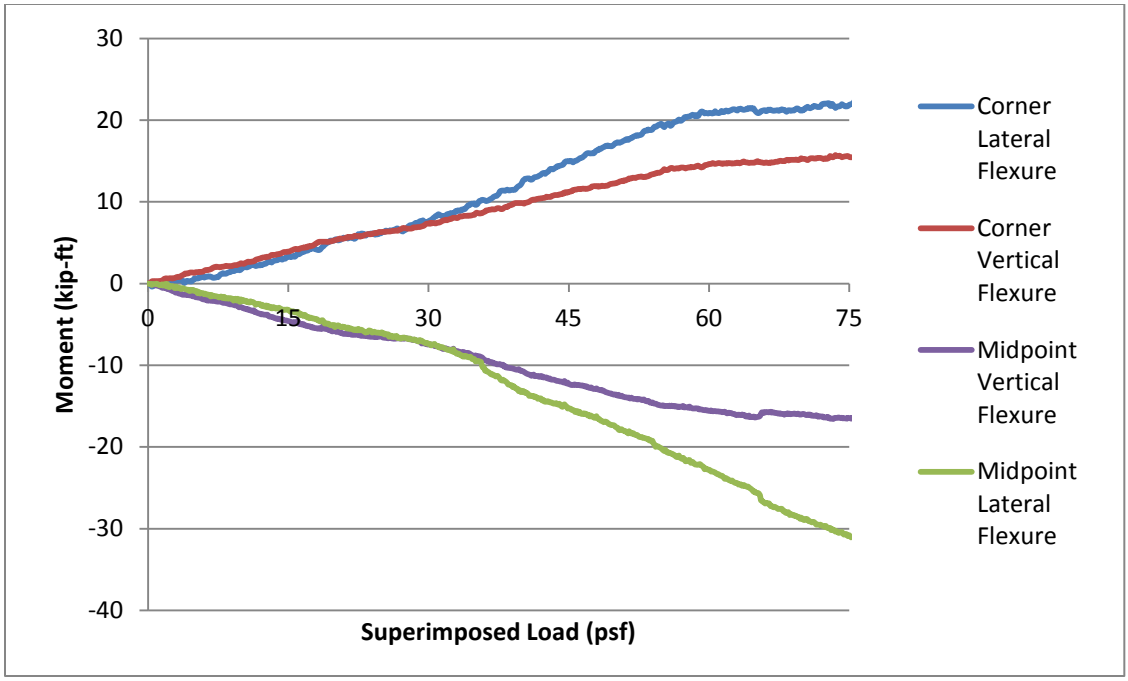

Figure 4-48: Moments in East and West Restraining Beams under Superimposed Loading - Test 1

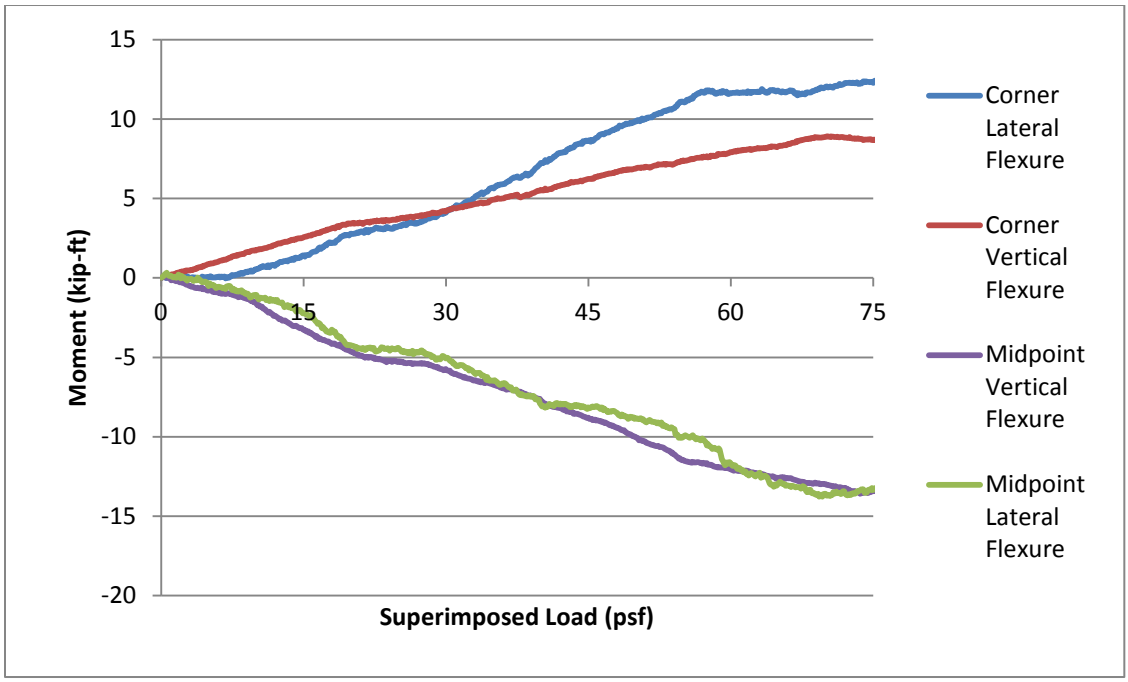

Figure 4-49: Moments in North and South Restraining Beams under Superimposed Load - Test 1

Figures 4-48 and 4-49 show the measured flexure in the restraining beams during water loading in Test 1. The strain gage readings were reset to zero at the beginning of this stage of the test to provide a standard point of comparison between Tests 1 through 4. Negative moment is developed at the midpoint of all four beams due to the intermediate vertical support provided by the column. The lateral moment measurements indicate that the structural steel framing and the composite floor system are applying substantial lateral forces to the restraining beam as deflection increases. The difference in moments between the north and south beams and the east and west beams may have several causes. The ribs of the composite decking apply force directly to the north and south beams. The primary and secondary beams apply load at three points along the length of the east and west beams. The rotational fixity at the corners is different due to the construction detail seen in Figure 2-9.

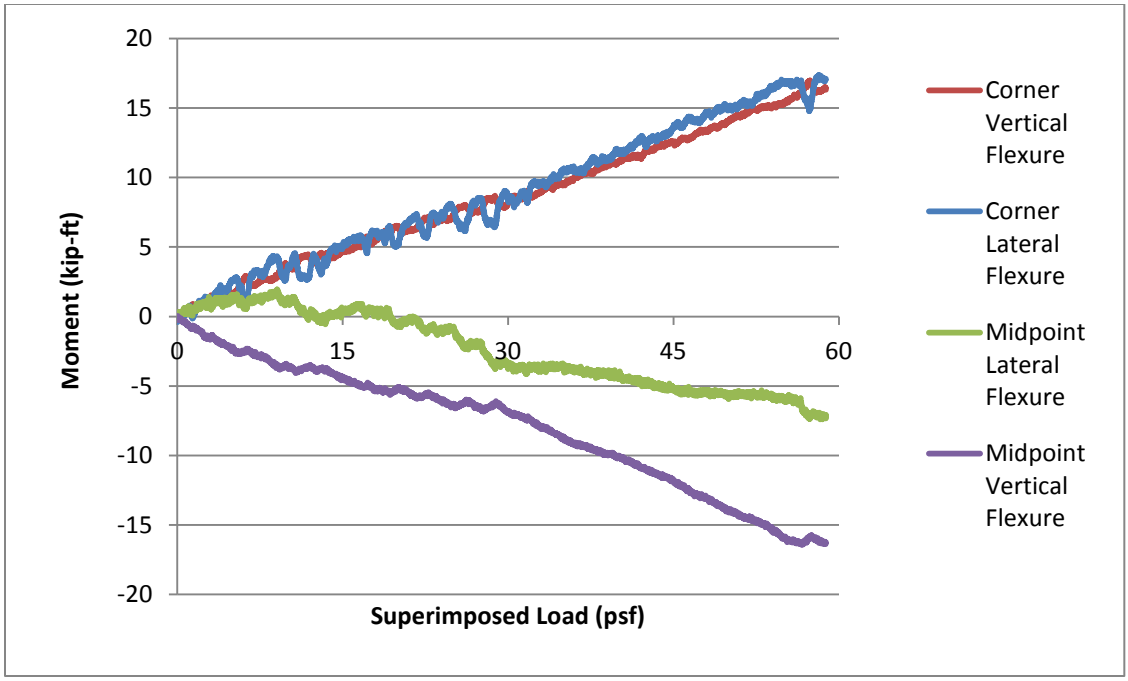

Figure 4-50: Moments in East and West Restraining Beams under Superimposed Load - Test 2

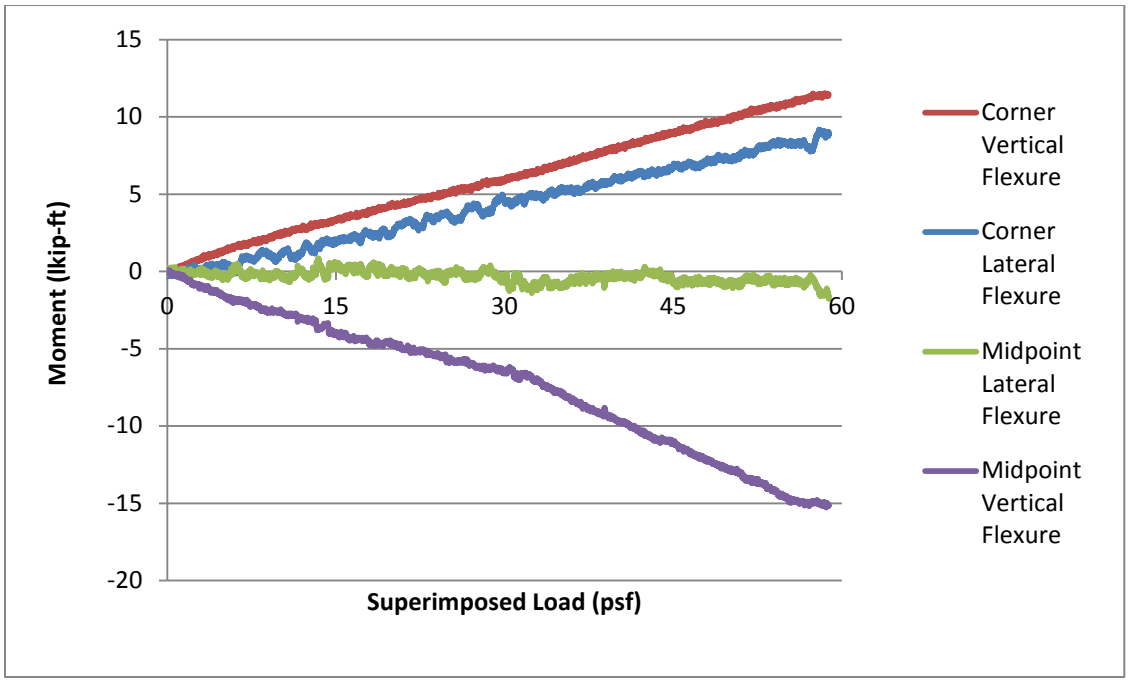

Figure 4-51: Moments in North and South Restraining Beams under Superimposed Load - Test 2

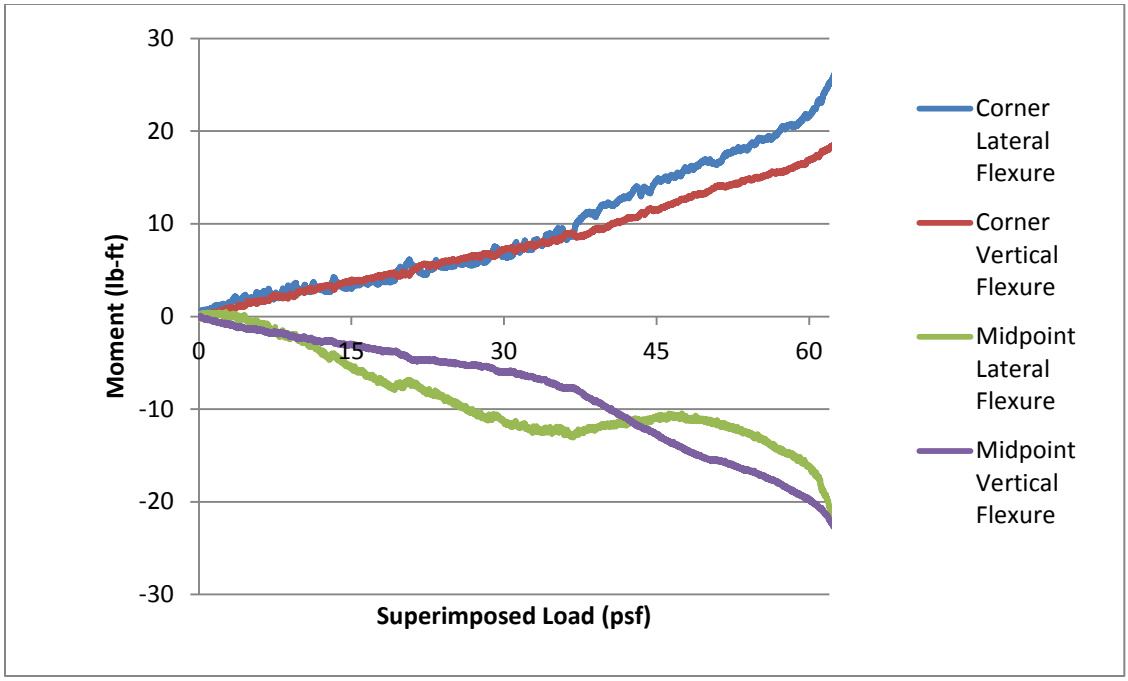

Figure 4-52: Moments in East and West Restraining Beams under Superimposed Load- Test 3

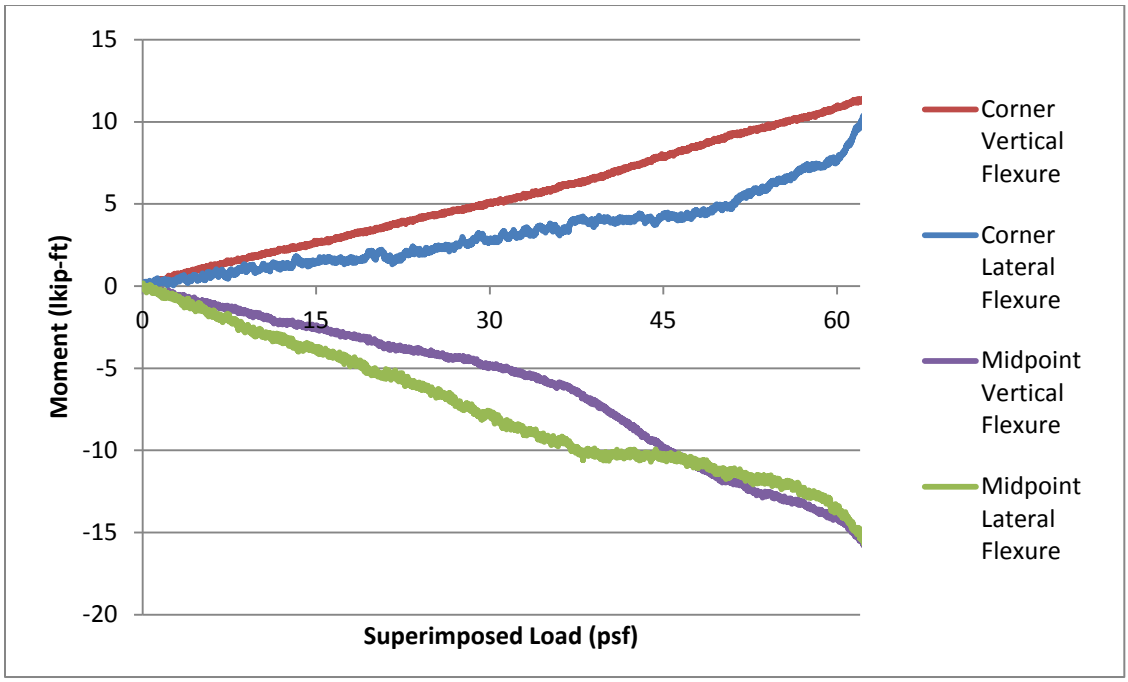

Figure 4-53: Moments in North and South Restraining Beams under Superimposed Load - Test 3

Figures 4-50 and 4-51 show the calculated flexural moments in the restraining beams under water loading during Test 2. Figures 4-52 and 4-53 show the calculated flexural moments during Test 3. Similar trends can be observed in both tests. The data in Tests 2 and 3 continues to demonstrate that higher flexural forces developed in the east and west restraining beams. The north and south restraining beams were expected to experience higher demand from tension in the composite decking ribs. However, this does correspond to the behavior observed in the beam and girder rotation measurements.

One factor that may contribute to the observed load distribution was the use of extra steel reinforcement placed transverse to the girders. As stated in Chapter 2, this reinforcement was intended to reduce cracking in negative moment zones. Although it might be assumed is that the majority of load will be carried along the ribs in a corrugated floor deck, the data in this test seems to indicate that greater loads were carried perpendicular to the ribs. The ratio of measured rotation to chord rotation at the ends of the beams indicates substantial flexural deformation. The measured deformation in the east and west perimeter beams indicates that higher forces are being carried in the beams than the girders.

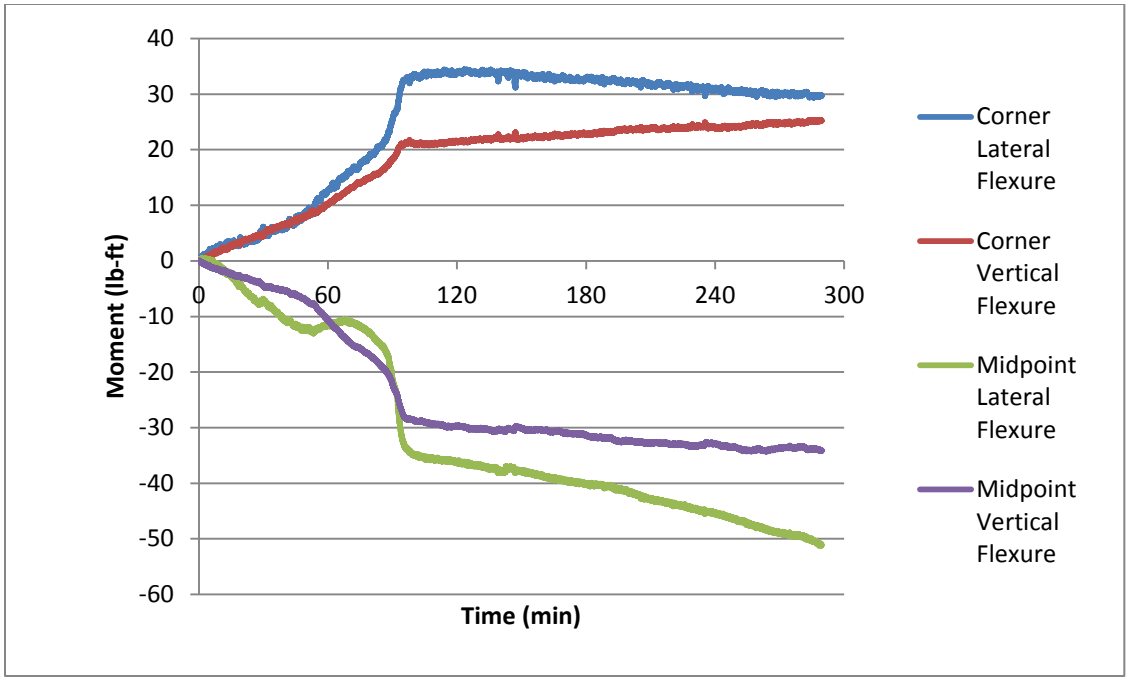

Figure 4-54: Moments in East and West Restraining Beams vs. Time - Test 3

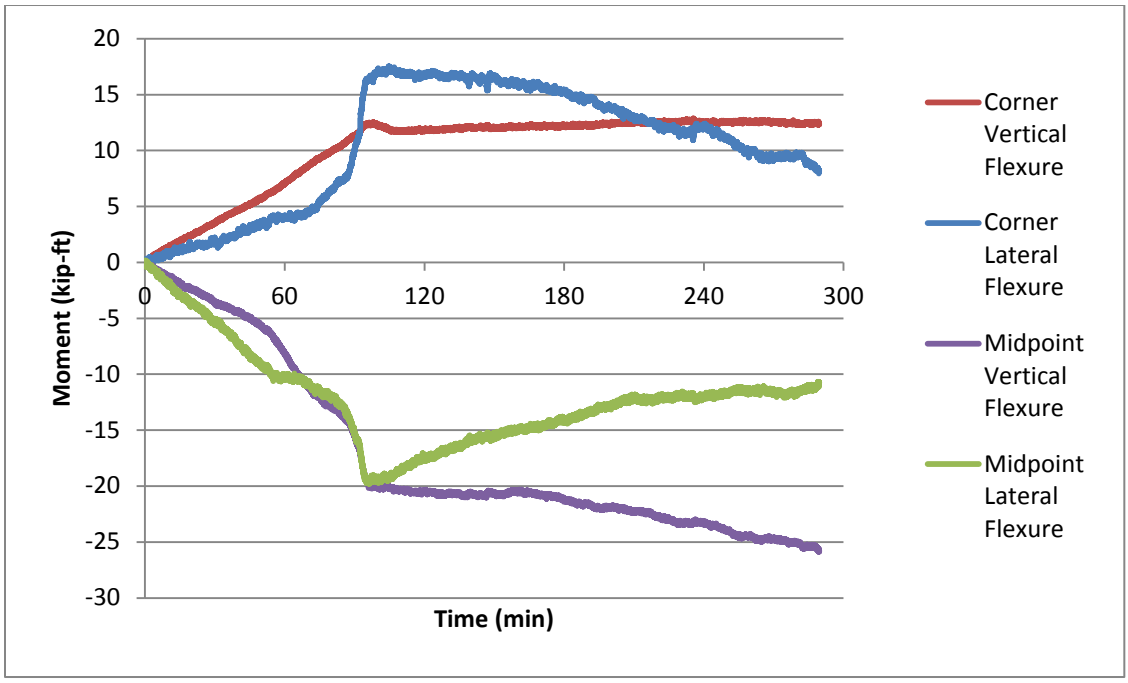

Figure 4-55: Moments in North and South Restraining Beams vs. Time - Test 3

Figures 4-54 and 4-55 show the measured moment in the restraining beams versus time in Test 3. During the period of time where a high deformation rate was observed, the lateral moment in all four beams increases significantly. This supports the possibility that the structure reached a snap-through point at a load of approximately 50 psf. The rate of vertical moment does not undergo the same sudden increase, indicating that the mechanism that allowed the structure to equilibrate at high displacement was the formation of a tension membrane with lateral restraint.

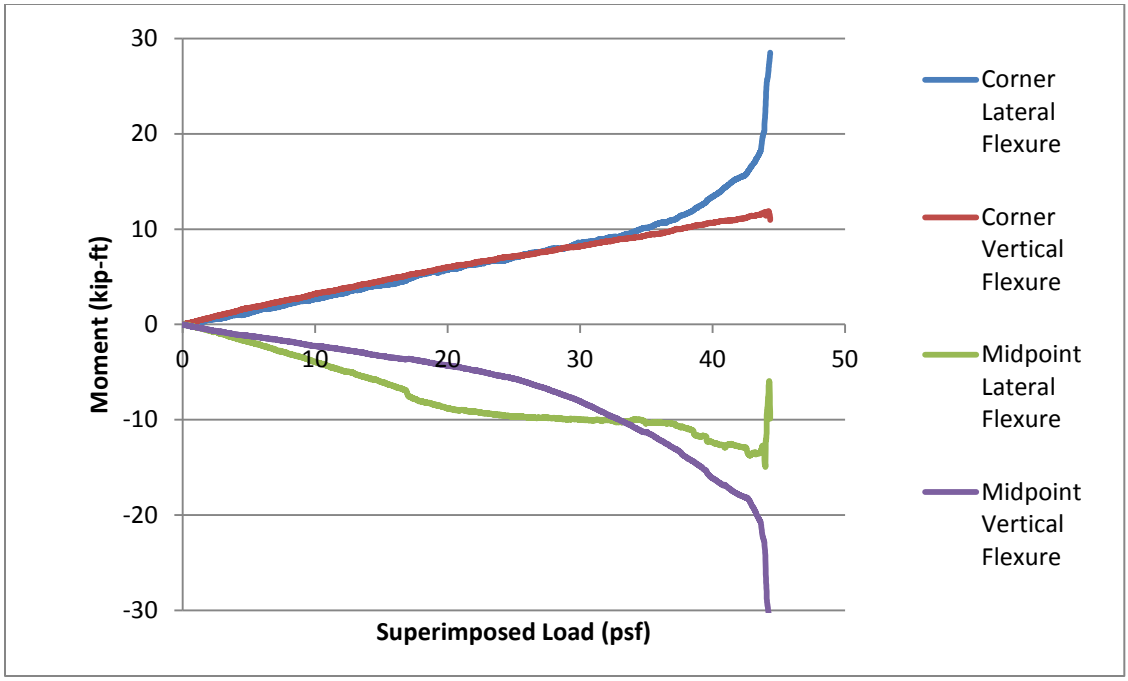

Figure 4-56: Moments in East and West Restraining Beams under Superimposed Load - Test 4

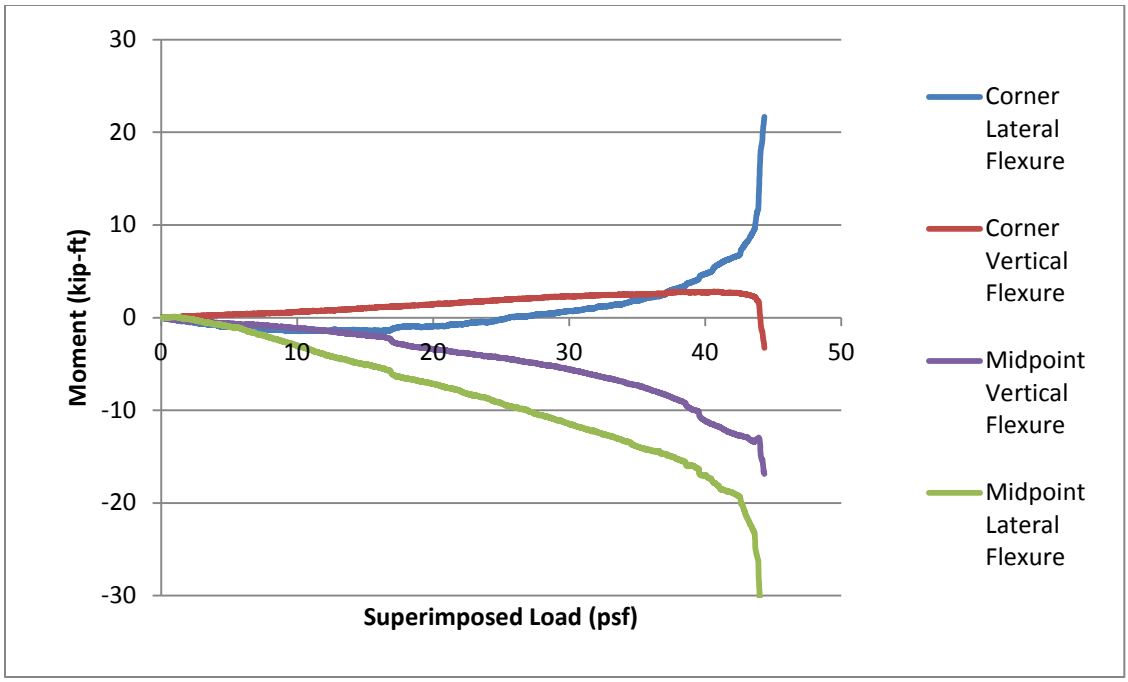

Figure 4-57: Moments in North and South Restraining Beams under Superimposed Load - Test 4

Figures 4-56 and 4-57 show the measured flexure in the restraining beams in Test 4 up until collapse. Without any tensile capacity in the beam and girder connections, the only lateral forces applied to the restraining beams must be transferred through the shear studs. The lateral flexure at the midpoint of the north and south restraining beams spikes right before collapse, indicating the development of large tensile forces along the ribs of the corrugated decking. This supports the observation that the collapse was initiated by the failure of the longitudinal seam in the decking. Tension along the north-south axis of the decking likely exceeded the capacity of the seam, causing tear-out.

4.6 TEST SPECIMEN AFTER COLLAPSE

As stated in Chapter 3, visual observations made during testing suggest that the collapse was initiated by the failure of the longitudinal seam in the corrugated decking. The remainder of this section presents photographs documenting the condition of the test specimen after collapse. These photos are in Figures 4-58 to 4-64.

The yellow paint seen along the end of the corrugated decking in Figures 4-58 and 4-59 marks the placement of the longitudinal seam. The two sheets of corrugated decking were attached with a 4 inch overlap and welded to the primary beams with a single row of shear studs. The tear out of the shear studs is clearly visible in Figures 4-58 and 4-59.

Figures 4-60 and 4-61 show that the secondary beams remained mostly undamaged by the collapse. Since the bolts and nuts were removed from the shear tab connections, the beams were simply hanging from the composite floor system.

Along the length of each member, different failures were observed in the composite floor. In some cases, the shear stud tore out of the concrete and remained attached to the beams. In other locations, the shear stud was torn off of the beam. Figure 4-62 shows the condition of the shear stud attachment along the length of one beam. Along the east and west perimeter of the floor system, the side lap attachments failed and the sheets of corrugated decking separated during collapse, as seen in Figure 4-63. However, the failure of the side lap connections in the decking appears to be a consequence of collapse and not a cause.

The girders remained attached to the composite floor slab. The force of the collapse crushed the ends of the girders into the face of the restraining beam. Figure 4-64 shows the bottom flange of one girder sheared from the rest of the section along the bottom edge of the restraining beam.

The damage that was incurred during the course of collapse does not appear to have contributed to the failure of the structure. However, it does provide information on weak areas in the test specimen. The floor system failed along the side laps of the corrugated decking. The attachment of the composite decking to the north and south restraining beams was strong enough to survive the impact of the girders crushing against the face of the restraining beam.

Figure 4-58: Corrugated Decking after Collapse

Figure 4-59: Corrugated Decking Tear-Out at Longitudinal Seam

Figure 4-60: View of Collapsed Specimen from North

Figure 4-61: Secondary Beam after Collapse

Figure 4-62: Shear Studs after Collapse

Figure 4-63: Side-Lap Failure after Collapse

Figure 4-64: Crushing at Girder End after Collapse

CHAPTER 5

Summary, Conclusions, and Recommendations

5.1 SUMMARY AND CONCLUSIONS

This chapter summarizes the most significant findings from the experimental testing of a 2-bay by 2-bay steel gravity frame structure with a composite floor system under interior column removal.

The deflection at the base of the interior column after the actuator was fully disengaged from the specimen was 2.15 inches. The load on the specimen at this time was approximately 120 psf, which is slightly higher than the progressive collapse design load mandated by the Unified Facilities Criteria. After the specimen was left unsupported for several hours under this load, deflection stabilized at 2.45 inches.

The maximum deflection of the fully intact specimen from the initial, supported position was 4.5 inches under an approximate total load of 180 psf. No structural damage or significant changes in stiffness were observed at this point.

The approximate collapse load for the structure after the removal of the nuts and bolts from all structural framing connections was 155 psf. This load is estimated using the point at which significant softening was initiated rather than the load at the point of failure. The total deflection at the interior column base was 15.6 inches at the time of collapse.

The flexural deformation at the midpoint of the girders in the specimen changed direction twice during the sequence of tests. Assuming that the initial curvature at the midpoint of the girders was positive when column removal began, the flexural stress initially decreased. After approximately half the reaction force had been removed from the interior column, the positive moment at the midpoint of the girders began to increase. In Tests 3 and 4, significant increases in negative curvature in the girders were observed coinciding with substantial increases in specimen deformation.

The strains measured in the restraining beams during the tests indicate that the deformation of the floor system after column removal applied significant in-plane lateral forces to the restraining beam. Because of the indeterminacy of the system, the magnitude of these loads is dependent on the stiffness of the lateral restraint provided. The magnitude of the flexural moments developed in the restraining beams is unlikely to accurately represent the demand on neighboring bays in the case of interior column removal in a multi-bay structure. However, the measurements taken in this test indicate that such demand does exist. Especially high lateral moments were observed at high displacements in Tests 3 and 4, when plastic deformation began to develop in the specimen. This suggests that tension membrane action in the decking and wire mesh reinforcement provides resistance at high displacements.

The results of this testing program suggest that steel gravity frame structures may have significant reserve strength that can be mobilized in cases of interior column loss. The test specimen was able to resist the ultimate gravity load of 1.2DL + 1.6LL after

interior column removal with a maximum deflection of 1/80 of the total, two-bay span length. The experimental data also supports the observation that the floor system can support significant load even after failure of the structural steel framing connections. The test specimen carried substantial load after all nuts and bolts were removed from all beam and girder end connections.

5.2 RECOMMENDATIONS

The following recommendations may be derived from the observed behavior in this test:

Based on the available data and the video observation of the testing, the collapse of the test specimen appeared to be initiated by failure of the longitudinal seam of the steel decking. As previously discussed, the longitudinal seams in this specimen were attached with a 4-inch overlap and shear studs welded directly through both sheets to the top flange of the primary beams. This observation suggests that the longitudinal seams in the decking play an important role in collapse resistance. Further research is necessary to better define the role of these seams in the structural system behavior and to evaluate the capacity of different longitudinal seam details.

The data collected in this test raises some questions that may be assessed in future testing. Instrumentation of the decking to measure strain on each axis may help to resolve the questions of stress distribution through the floor system. Measuring the rotation at the steel framing connections to the restraining beam would provide further insight into the flexural deformation of the girders and beams at increasing levels of load and deflection.

The rotation measurements at the central connection and the strain gages on the girders established the changing flexural modes of the girders, but there were some inconsistencies observed in the data. Strain gages in the transverse beams may also clarify some of these inconsistencies.

Data collected in this test series showed that once the column was removed and substantial load was placed on the specimen, deflections of the floor systems would continue for minutes or sometimes hours under constant load. Such creep-type deformations may be a significant factor in understanding resistance to progressive collapse. It is recommended that more data be collected on the deflection of the floor system under constant load in future tests. Additional work is needed to better understand the sources of these time dependent deformations and to allow inclusions of these effects in computational models. In realistic progressive collapse scenarios, the behavior of the structure in the hours after column loss is significant to the preservation of public safety.

Computational modeling must account for the capacity of the structure after the failure of the steel framing connections. The results of Test 4 indicate that the structure is able to bear substantial additional load after the capacity of the connections is significantly reduced. The system failure criteria for computational models should be based on failure in the floor system. Longitudinal seams should also be included in models; in most previous work the corrugated steel decking has been modeled as continuous. The changes in flexural behavior of the girders at different levels of loading

and deflection provide benchmarks that may be valuable for use in matching the computational analysis to the experimental data.

5.3 FUTURE WORK

As described in Chapter 1, this thesis is part of a larger research project investigating the progressive collapse resistance of steel gravity framing. Additional tests are planned and will be reported in subsequent theses and dissertations.

In addition, as part of this project, predictions of structural response from detailed finite element models of the test specimens will be compared to the experimental data. Work is also underway to develop simpler models that predict the observed structural response with reasonable. Simplified modeling will be assessed to provide guidance for progressive collapse analysis in professional practice.

References

Alashker, Y.;El-Tawil, S.;Sadek, F. (2010). "Progressive collapse resistance of steel-concrete composite floors." *J. Struct. Eng.*, 136, 1187-1196.

ASCE. (2010). ASCE 7-10, *Minimum Design Loads for Buildings and Other Structures*, American Society of Civil Engineers, Reston, VA,

Astaneh-Asl, A., Madsen, E., McCallen, D., and Noble, C. (2001). *Study of catenary mechanism of cables and floor to prevent progressive collapse of buildings subjected to blast loads.* Dep. of Civil and Env., Eng., Univ. of California, Berkeley.

Chen, J.; Huang, X.; Ma, R.; He, M. (2012). "Experimental study on the progressive collapse resistance of a two-story steel moment frame." *J. Perform. Constr. Facili.***,** 26 (5), 567-575.

Corley, W. G., Mlaker, P. F., Sozen, M. A., and Thornton, C. H. (1998). "The Oklahoma City bombing: summary and recommendations for multihazard mitigation." *J. Perform. Constr. Facil.*, 12(4), 100-112.

Department of Defense, (2009). Unified Facilities Criteria (UFC) 4-023-03, *Design of Buildings to Resist Progressive Collapse,* Washington, D.C.

Department of Defense, (2005). Unified Facilities Criteria (UFC) 4-023-03, *Design of Buildings to Resist Progressive Collapse,* Washington, D.C.

Donahue, S. (expected 2013). *Design of an Experimental System for Progressive Collapse Testing of Steel Gravity Framing* (*tentative title).* M.S. Thesis, Department of Civil, Architectural and Environmental Engineering, University of Texas at Austin.

Foley, C.M., Martin, K. and Schneeman, C. (2007). *Robustness in structural steel framing systems.* Report to American Institute of Steel Construction, Chicago, IL.

General Services Administration, (2003). *Progressive collapse analysis and design guidelines for new federal office buildings and major modernization projects*, Washington, D.C.

Izzuddin, B.A., Vlassis, A.G., Elghazouli, A.Y., and Nethercot, D.A. (2008). "Progressive Collapse of Multi-Storey Buildings due to Sudden Column Loss - Part I: Simplified Assessment Framework," *Engineering Structures*, 30(5), 1308-1318.

Main, J.A.; Sadek, F. (2012). Robustness of steel gravity frame systems with single-plate shear connectors, National Institute of Standards and Technology (NIST) Technical Note 1749. Gaithersburg, MD.

Newland, D. E. and Cebon, D. (2002). "Could the World Trade Center have been modified to prevent its collapse?" *J. Eng. Mech.*, 128(7), 795-800.

Pearson, C. and Delatte, N. (2005). "Ronan Point Apartment tower collapse and its effect on building codes." *J. Perform. Constr. Facil.*, 19(2), 172-177.

Sadek, F.;El-Tawil, S.;Lew, H. (2008). "Robustness of composite floor systems with shear connections: modeling, simulation, and evaluation." *J. Struct. Eng.*, 134(11), 1717-1725.

Song, B.; Sezen, H. (2009). "Evaluation of an existing steel frame building against progressive collapse." Structures Congress 2009.

Vlassis, A.G., Izzuddin, B.A., Elghazouli, A.Y., and Nethercot, D.A. (2008). "Progressive Collapse of Multi-Storey Buildings due to Sudden Column Loss - Part II: Application," *Engineering Structures*, 30(5), 1424-1438.

Vita

Lindsay Hull was born on January 27, 1989 to Tom and Julie Hull. She grew up in Seattle, Washington, with her older brother, Sandy, and younger sister, Maggie. After graduating from Lakeside School in 2007, she attended Tufts University in Boston, receiving a Bachelor of Science in Civil Engineering in 2011.

Lindsay enrolled at The University of Texas at Austin as a master's student in structural engineering in the fall of 2011. At UT, she worked as a teaching assistant for the first year civil engineering course for four semesters. She obtained her Master of Science in Engineering in May of 2013 and returned to Seattle to begin her career in structural design.